CELLULAR FRAGMENTATION-MEDIATED CHROMOSOME ELIMINATION AND BLASTOMERE EXCLUSION: MECHANISMS FOR OVERCOMING CHROMOSOME MISSEGREGATION IN THE RHESUS MACAQUE PREIMPLANTATION EMBRYO.

By

Brittany L. Daughtry

A DISSERTATION

Presented to the Department of Cell, Developmental, and Cancer Biology

and the Oregon Health & Science University

School of Medicine

In partial fulfillment of

the requirements for the degree of

Doctor of Philosophy

September 2017

OREGON HEALTH & SCIENCE UNIVERSITY

SCHOOL OF MEDICINE

CERTIFICATE OF APPROVAL

_____

This is to certify that the PhD dissertation of

Brittany L. Daughtry

has been approved.

_____
Shawn L. Chavez, PhD, Mentor

_____
Susan B. Olson, PhD, Co-Mentor/Member

_____
Soren Impey, PhD, Member

_____
Jon D. Hennebold, PhD, Member

_____
Matthew Thayer, PhD, Member

_____
Lucia Carbone, PhD, Member

TABLE OF CONTENTS:

FIGURES:

Introduction

Chapter 1: Aneuploidy and ploidy errors in the rhesus macaque embryo

Tables:

ABBREVIATIONS:

aCGH	Array comparative genomic hybridization
CBS	Circular binary segmentation
CCF	Chromosome-containing cellular fragment
CHI	CBS/HMM intersect
CNV	Copy number variation
DNA-FISH	DNA-fluorescent *in situ* hybridization
DNA-Seq	DNA sequencing
EGA	Embryonic genome activation
ExB	Excluded blastomere
γ-H2A.X	Gamma-(serine 139 phosphorylated) H2A histone family, member X
HMM	Hidden Markov model
ICM	Inner cell mass
IVF	*In vitro* fertilization
MDA	Multiple displacement amplification
mRNA	Messenger RNA
mtDNA	Mitochondrial DNA
MTOC	Microtubule organizing center
PBS	Phosphate buffered saline
PBST	PBS with Tween-20
PCR	Polymerase chain reaction
PGS	Preimplantation genetic screening
RTqPCR	Real-time quantitative polymerase chain reaction
SNP	Single nucleotide polymorphism

TLM	Time-lapse monitoring
VNOWC	Variable non-overlapping window CBS
WGA	Whole genome amplification

Acknowledgments

This dissertation would not be possible without the support of numerous people. First and foremost, I owe a tremendous amount of gratitude to my mentor Dr. Shawn Chavez. Shawn has not only given me a copious amount of her time molding me into a better researcher but she gave me a second chance to do science in an area I love. Restarting my dissertation after three years of graduate school was one of my biggest challenges but I would do it again to have Shawn as my mentor. The members of the Chavez lab also played a big role in my success and the open and supportive environment has allowed me to thrive. Many thanks are given to Nash Redmayne, the first person to join Shawn's lab who helped me get started and offered a hand in many IVF cycles and confocal experiments. I am also grateful to Jimi Rosenkrantz for her work with developing the whole genome amplification protocol and serving as the sequencing guru in the lab. Sweta Ravisankar has also been very supportive, offering feedback on my presentations and sharing gametes from IVF cycles. Postdoc Dr. Kelsey Brooks is owed thanks as well, especially for zygote microinjections of mRNAs and scientific discussions. Members of Dr. Lucia Carbone's lab have been instrumental in my training as well, from coaching me through presentations to major bioinformatics analyses required for my dissertation. Generous feedback from Lucia Carbone, Nathan Lazar, Kimmi Nevonen and Suzi Fei addressing my naïve questions about genomic and sequencing questions have been immensely appreciated and I am thankful for their commitments to this dissertation. I am also thankful for members of my dissertation committee, Drs. Soren Impey, Matt Thayer, Jon Hennebold, and Susan Olson for their guidance and helping me focus my research track to maintain momentum for a timely graduation. Dr. Susan Olson has served as my co-mentor and has been a wonderful advocate. Without her I would have never had the opportunity to become a PEO scholar and for this I will always be grateful. Finally, this

acknowledgement would not be complete without giving thanks to the PMCB and CDCB programs for recruiting me here and supporting me despite the ups and downs. Knowing there were people in my corner really kept me going. My time here in Portland has given me some of my best life experiences and friendships. I will always reflect fondly on my time here.

Dedications

This dissertation is dedicated to the women in my family who valued education, especially my grandmother, Peggy Creech Daughtry, my aunts, Connie Daughtry Nance and Leslie "Gabby" Gabriel Tishler, and my mother, Minda Tishler Daughtry. My grandmother was an educator and helped raise my brothers and I. She taught us many lessons early on which helped us excel beyond our grade levels. Grandma made learning fun and I wanted nothing more than to make her proud because she made me feel special and loved. My Aunt Connie has also been an inspiration, being the first Daughtry to receive a doctorate degree. She would always remind me that perseverance and hard work will get you farther than intelligence and I remind myself of this every time I reach a roadblock. Aunt Connie passed away from an aggressive lung cancer in 2016 at the age of 55 and before she died she told me how proud she was that I going after my PhD. I am very grateful that I can continue to make her proud with this achievement. Aunt Gabby is an accomplished lawyer in NYC and has always been there for me. She never sugarcoated the necessary advice that I needed to hear. My brothers and I are indebted to her dedication to ensure investments were well managed for our educations. This dissertation is also dedicated to my mother who earned her bachelor's degree after having three children and a master's degree after my brothers and I had finished our own degrees. Not only did my mother delay many of her own dreams so that I could have mine but she had the courage to go after them later on in life. I hope that I too will have the courage to always go after what I want, even if there are setbacks.

Technical Acknowledgements

Many people helped make this dissertation possible through technical contributions. Special thanks to Nathan Lazar for his work developing and implementing the single-cell VNOWC copy number variation pipeline and Suzi Fei of the Biostatistics and Bioinformatics Unit for the single-cell single nucleotide polymorphism pipeline and Lina Gao for biostatistics analyses and suggestions. Further thanks are given to Jimi Rosenkrantz who contributed to development of the single-cell whole genome amplification, quantification, pooling, and sequencing workflow protocols. Much of the sequencing was performed in the lab of Dr. Andrew Adey where Kristof Torkenczy performed CHI copy number variation analysis and Sarah Vitak and Andrew fields permed NEXTSeq runs. The level of support they provided was beyond compare and I am grateful for their help. Nash Redmayne also contributed significantly by serving as the third reviewer for measuring cell division parameters for over 100 embryos. I am also especially grateful to Drs. Cecily Bishop, Carrie Hanna, and Jon Hennebold as well as Cathy Ramsey for rhesus monkey samples and/or embryology expertise. Special thanks also go to the Colony Genetics Resource Core for providing the parental DNA samples, the Molecular & Cellular Biology Core for the MiSeq runs, and Imaging & Morphology Core for confocal microscopy support. The time lapse monitoring part of the study would not be possible without the generosity and support from Auxogyn, Inc.

Dissertation Abstract

Whole and segmental chromosomal abnormalities, or aneuploidy, are a key determinant of whether embryos will arrest or form a normal blastocyst capable of implanting and growing into healthy offspring. Despite the implementation of preimplantation genetic screening and other advanced IVF techniques, the identification of aneuploid embryos remains complicated by high rates of mosaicism, atypical cell divisions, cellular fragmentation, sub-chromosomal instability, and micronucleation. Recent technological achievements in genetic and non-invasive imaging have provided additional embryo assessment approaches, particularly at the single-cell level, but fertility clinics are slow to adopt these practices. Despite these advances, basic research for embryonic aneuploidy is limited because of restrictions placed on human embryos and the cost associated with recruiting young donors for invasive medical procedures. The mouse has always been a powerhouse model for embryology, but it is not ideal for the study of aneuploidy since 1-4% of embryos experience aneuploidy whereas 50–80% of cleavage-stage human embryos will carry abnormal chromosome number(s).

In this dissertation, the rhesus macaque embryo was evaluated for aneuploidy frequency to determine if it is a suitable translation model to study human embryology. Using single-cell DNA-Sequencing, chromosome instability was established in the rhesus macaque monkey model and found to occur in 74% of embryos at a nearly identical rate to human embryos. Additional findings of reciprocal sub-chromosomal deletions and duplications support previous reports that chromosome breakage is common in human embryos. Pairing sequencing technology with non-invasive live-cell time-lapse imaging revealed that multipolar divisions were present as well and often resulted in chaotic aneuploidy,

which is defined as greater than five whole or segmental chromosomes affected in at least one blastomere where chromosome distribution amongst cells appeared unconstrained and random [1]. Furthermore, measuring cell cycle division intervals to the four-cell stage, was predictive of whether an embryo would reach the blastocyst stage or arrest. When the cellular fragments of embryos were also sequenced, ~20% of rhesus macaque embryos contain cellular fragments that encapsulate whole or partial chromosomes, either maternal or paternal origin. Confocal microscopy revealed that indeed, micronuclei containing missegregated chromosomes are found within the cellular fragments of cleavage stage embryos. These ejected micronuclei experienced extensive DNA damage which may indicate their expulsion for this reason. Despite frequent chromosomal errors, rhesus macaque embryos were also found that prevented cellular fragments and non-dividing blastomeres from incorporating at the blastocyst stage. The findings from this study propose that embryos respond to segregation errors by eliminating micronuclei via cellular fragmentation and select against and exclude aneuploid blastomeres to overcome chromosome instability. Overall, the rhesus macaque embryo is an excellent model for translational studies for human embryonic aneuploidy and measuring morphokinetic parameters for developing time-lapse imaging technology. Furthermore, the rhesus macaque embryo exhibits two potential mechanisms for overcoming aneuploidy through cellular fragmentation and blastomere exclusion, mechanisms that might explain how aneuploidy is tolerated in the embryo to yield viable pregnancies and healthy offspring.

Introduction and Literature Review

Overview of aneuploidy in human embryos

The formation of a blastocyst is one of first major landmarks in early mammalian development and yet, only ~30-50% of preimplantation embryos will typically reach this stage following IVF [2]. In contrast, approximately 80% of mouse embryos will form blastocysts when cultured *in vitro*. Although the cause(s) of embryo arrest may differ between species, an abnormal number of whole chromosomes, or aneuploidy, is thought to be a primary determinant of whether a human embryo will progress in development [3]. To complicate matters, despite the higher probability that aneuploid embryos will arrest at the cleavage-stage, embryos with chromosomal abnormalities still form blastocysts, where embryos with viable trisomies (e.g., trisomy 21) are morphologically indistinguishable from euploid embryos, especially when evaluated by static observations [4, 5].

In vitro fertilization success rates hover around ~30-35% (cdc.gov/art) when all patient age groups are combined. These low rates are mainly due to whole and sub-chromosomal abnormalities that arise during preimplantation development [3]. Over the past decades, implementation of more advanced, yet invasive, IVF techniques such as intracytoplasmic sperm injection, preimplantation genetic screening (PGS), and assisted hatching has not dramatically changed the percentage of live births [6-8]. These odds only continue to worsen as it is well documented that meiotic chromosome segregation errors increase in the oocyte with age [9]. For instance, it is estimated that for women 40 years and older, 30% of recognized conceptions will be trisomic [10]. These numbers are cause for concern

as the use of IVF has created over 5 million children worldwide, has more than doubled in the past decade, and is expected to continue to increase as reproductive-age couples delay childbirth [11]. With the exception of trisomy 13, 18, 21, and abnormalities in the X- or Y-chromosome, the vast majority of human embryonic aneuploidies involving whole chromosomes are incompatible with live birth. It should also be noted that there are high infant mortality rates associated with trisomy 13 (Patau syndrome) and trisomy 18 (Edwards syndrome), with only a small number of infants surviving past one year. For IVF-derived embryos, those with aneuploidy will likely arrest either prior to transfer to the mother, fail to implant if transferred, or spontaneously abort early in gestation [12]. In the case of *in vivo* human conceptions, an aneuploid embryo may undergo arrest before a pregnancy is detected and thus go unnoticed. Although distinctions between *in vitro* and *in vivo* conceptions are difficult to ascertain, studies estimate that ~30-35% of natural conceptions lead to human pregnancies and up to 70% of spontaneous miscarriages are diagnosed as chromosomally abnormal [13-16].

Aneuploidy is not unique to human preimplantation development as other mammals are prone to chromosome missegregation in embryos [17]. For animal species that are often used for embryology, the numbers vary. Mouse embryos exhibit aneuploidy at ~1-4%, depending on the strain [18-20]. In the bovine model, one study determined that up to 74% of cleavage stage embryos derived from in vitro matured oocytes are abnormal, containing at least one aneuploid blastomere [21]. However, all of the oocytes collected for this bovine study were immature and *in vitro* maturation (IVM) increases aneuploidy by itself[22]. More importantly, this is not the procedure used in >98% of human IVF cycles, whereby oocytes are matured *in vivo* for aspiration and then undergo IVF (cdc.art/gov). Previous studies with rhesus macaque embryos using DNA-fluorescent *in situ* hybridization (DNA-FISH) probes to human chromosomes 13, 16, 18, X, and Y indicated

that the level of aneuploidy in rhesus macaque embryos is 35-50% [23-25]. However, it does appear that humans are affected by a higher incidence than most other mammalian species, whereby it is estimated via high-resolution techniques that 50-80% of cleavage stage embryos, including those from both young and fertile women, will have aneuploidy [26-31]. With this to consider, it is important to address causes of aneuploidy in human embryos with appropriate models. Although aneuploidy can be chemically induced in the mouse [20], determining the mechanisms that drive the high incidence of meiotic or mitotic aneuploidy will require animal models that are affected by a similar degree of aneuploidy to human embryos. Given that aneuploidy can affect human embryos even from young and otherwise fertile individuals, aneuploidy in the embryo appears to be a common [32, 33]. With the increased demand for IVF for a spectrum of patients, it is paramount that further research continues to elucidate the causes of chromosome missegregation, understand how the embryo responds to aneuploidy, and finally improve our ability to detect these events.

Aneuploidy detection approaches for embryo biopsies

The introduction of preimplantation genetic screening has provided a sufficient means for aneuploidy detection in IVF embryos. However, there are several challenges with implementing these methodologies and interpreting results, including the assumed risk of detriment to the embryo during biopsy [34], chromosomal mosaicism between different cells or cell lineages [33, 35-37], the effects of sub-chromosomal aberrations [26-29] on subsequent development, and the mathematical improbability that a trophectoderm biopsy of 5-7 cells accurately reflects the chromosomal composition of a ~300 cell blastocyst [38]. Recent identification of common genetic variants in patients that are at high-risk for

producing aneuploid embryos adds further complexity to the pathways involved in preimplantation chromosomal instability [39].

Methods for PGS have changed rapidly since the first clinical report in 1988 by Elena Kontogianna where single-blastomeres were biopsied for sexing by polymerase chain reaction that targeted a repeat dense region of the Y chromosome [40]. Previously in this field, PGS has included DNA-FISH or array comparative genomic hybridization analysis of polar bodies and blastomeres to detect meiotic and mitotic aneuploidy [41-45]. Now, the most common type of PGS is array comparative genomic hybridization of trophectoderm biopsies that contain ~5-7 cells. While the blastocyst stage is a better indicator of implantation potential, mosaicism is still problematic [46]. Discussed below are five PGS approaches: DNA-FISH, array comparative genomic hybridization (aCGH), single nucleotide polymorphism (SNP) arrays, real-time quantitative polymerase chain reaction (RTqPCR), and next-generation whole genome DNA sequencing (DNA-Seq).

In the past, the most frequently used method for diagnosing aneuploidy was PGS of day 3 biopsied blastomeres via DNA-FISH [47]. Briefly, DNA-FISH is a cytogenetic technique that involves using fluorescent probes that are complementary to specific regions of chromosomes, often centromere-specific or locus-specific. For PGS of day 3 blastomeres, DNA-FISH is performed on cells that are spread, lysed, and fixed at interphase. Probes are selected for sex determination, ploidy, chromosomal rearrangements, or sporadic chromosome aneuploidy. Since chromosome copy number is determined by fluorescence signals, typically two rounds of hybridization are needed for one nucleus to detect more than three chromosomes [48]. DNA-FISH for PGS of blastomeres has two significant challenges compared to using this technique in other cell types. First, only one or two cells are available for analysis, so it is necessary that DNA-FISH is performed by a highly skilled

cytogeneticist since there is no room for error. Secondly, the turnaround time for results must be within one or two days for a fresh day five transfer so the protocol must be efficient [49]. Unfortunately, DNA-FISH can result in false positives or negatives due to procedural artifacts and is limited to the simultaneous analysis of only a select number of chromosomes, typically between five and twelve of the most frequently affected like chromosomes 21, X, and Y [33, 35-37]. Thus, several studies initially underreported the incidence of human embryonic aneuploidy since all 24 chromosomes can potentially be affected, particularly in cases of mitotic errors [27, 29]. Considering these shortcomings, DNA-FISH has been replaced by more comprehensive karyotyping methods that are described below.

When whole genome amplification technology became available, the PGS field shifted from DNA-FISH to aCGH and SNP microarrays to evaluate all 24 human chromosomes. Studies using aCGH or SNP microarrays to examine blastomere biopsies from high-quality whole human embryos have demonstrated that 50-80% of human embryos at the cleavage-stage have one or more blastomeres that are aneuploid. Both microarray platforms amplification of embryo biopsies to produce enough DNA for hybridizing to millions of oligonucleotide probes on a microarray. For the purpose of detecting copy number variations, combination pre-amplification and PCR-based amplification methods (e.g., PicoPlex by Rubicon Genomics and MALBAC by Yikon Genomics) are more reliable for uniform CNV detection because of reduced amplification bias [50]. However, for SNP arrays, accurate allele representation is crucial and therefore multiple displacement amplification WGA is preferred since there is less allele drop-out [51].

The principle behind “two-color” aCGH is competitive hybridization to the microarray between the DNA of the sample and normal euploid reference DNA. The reference DNA

is labeled with one color probe, and the experimental sample has a separate color probe. Both the reference and sample DNA are fragmented and loaded onto the microarray in equal quantities. The DNA is allowed to hybridize for several hours to oligonucleotide probes that represent thousands of unique regions throughout the genome. After hybridization, the aCGH microarray is scanned to record a digital image for CNV analysis. The intensity of these different probes is compared using a Log2 ratio calculation to determine copy number changes [52]. Since aCGH covers approximately 30% of the genome and can only detect gross chromosomal abnormalities due to a lower threshold of approximately 1-10 MB [53], sub-chromosomal aberrations smaller than this resolution are missed by aCGH.

Unlike aCGH where there is competitive hybridization between the sample and the reference DNA, SNP arrays only require hybridization of the sample DNA, but the same principle is maintained because the probes represent the normal diploid reference. The SNP array differs in that it contains allele-specific oligonucleotide probes for various single nucleotides across the genome that vary in the population. These probes come in pairs, one for each allele set. Software can then be used to align the SNPs in chromosomal order and determine their copy number based on allele frequency as determined by the signal ratio of SNP-specific probes. Blocks of the genome where there is change in allele frequency can be interpreted as CNVs for partial or whole chromosomes. There are several advantages to performing SNP arrays including the detection of allelic imbalances which can reveal triploidy and mosaicism or uniparental disomies, gynogenesis, or androgenesis if copy-neutral Loss of Heterozygosity is found. Therefore, the added benefit of utilizing SNP arrays is the detection of ploidy errors in addition to CNVs [52]. Furthermore, if the disease-causing genes from the parents are known then haplotyping can determine if the embryo acquired pathogenic genes that are embedded among SNPs

detected by the array. Furthermore, because less sample DNA is needed for a SNP array, a single gene mutation can be validated by PCR with the remainder of the sample [54]. The field of PGS is quickly shifting to next-generation DNA-Seq for CNV detection now that costs have improved, and preimplantation diagnostics corporations like Igenomix and CooperGenomics (formerly Reprogenetics) have stopped offering aCGH. Next-generation whole genome DNA-Seq comprehensively assess aneuploidy in human embryos, including at the single-cell level with much less sample input [55-57]. These samples also undergo WGA, preferably with combination pre-amplification and PCR-based amplification methods. During WGA of each sample, short fragments of DNA are amplified, and unique indices are ligated. These indices have adapter sequences that allow single-stranded DNA fragments to anneal to probes on the surface of flow cells. From there, the DNA fragment undergoes clustering by solid-phase bridge amplification so that each DNA fragment is clonally expanded. After clusters are formed, DNA sequencing begins on the forward strand where fluorescently tagged nucleotides complimentary the DNA fragment are added to the single strand. For each nucleotide added, a fluorescent signal is captured to determine the base pair call. This process is repeated for 50-300 base pairs, depending on the sequencing platform used. Using this approach, hundreds of millions of DNA fragments can be sequenced in one run. These sequences are then groomed so that only high-quality reads are aligned to the genome (https://www.illumina.com). Downstream CNV analysis only requires about 1 million unique reads after mapping so in a few hundred barcoded samples can be simultaneously sequenced with low coverage by multiplexing if high output kits are used [58]. Lastly, next-generation sequencing also allows for the analysis of repetitive DNA sequences [59], balanced chromosomal rearrangements when paired-end sequencing is used in single-cells, as well as an initial map of insertion and deletion variation in the genome [60].

To counter the time consuming methods of DNA-FISH and whole genome amplification for aCGH and SNP microarrays, fluorescent RTqPCR was developed as an alternative for PGS [61]. The protocol for rapid PGS in four hours involves embryo biopsy lysis, multiplex preamplification PCR of four loci per chromosome, RTqPCR, and analysis [61]. While RTqPCR provides a more rapid method for ploidy assessment, the multiplex amplification and relative quantitation of only 96 presumably single copy loci (four on each chromosome) does not allow for the identification of all potential segmental aneuploidy in embryos. Given that certain sub-chromosomal aberrations, such as homozygous or hemizygous deletions, large duplications or amplifications, and regions of *de novo* uniparental isodisomy may induce embryonic/fetal lethality and are one of the major causes of developmental disorders in offspring that survive to birth [62, 63], it is important to evaluate both whole and sub-chromosomal instability in embryos. Moreover, as this technology is still impacted by mosaicism and has only been applied to trophectoderm biopsies [64-66], which generally consist of between 5 and 10 cells, it remains unknown if RTqPCR can reliably detect aneuploidy in single cells.

Time-lapse monitoring for non-invasive assessment of embryo quality

Despite the prevalence and advantages for using PGS to select euploid embryos for transfer, biopsies are invasive and the slightest mechanical error may hinder subsequent development. Considering this, the limitations and risks associated with PGS illustrate the need for alternative approaches for embryo selection. One such approach has been the implementation of time-lapse imaging to monitor embryos throughout development rather than at specific time points that may not reveal subtle differences in embryo behavior (**Fig. 1b**). While initial studies focused on the utility and safety of time-lapse monitoring (TLM) [67-71], once it was determined that TLM was not detrimental to embryo development,

several groups began to investigate whether there were morphological, spatial and/or temporal correlates between imaging behavior and embryo quality [17, 72, 73] (**Fig. 2**). In 2010, Wong and colleagues demonstrated that TLM could be used to predict blastocyst fate prior to embryonic genome activation (EGA) by measuring the duration of the first cytokinesis and time between the second and third mitotic divisions [72]. Since this initial report, other studies have confirmed the importance of early cleavage divisions as well as identified additional imaging parameters predictive of developmental success [73-84] (**Fig. 2**). Whether the first three mitotic divisions are similarly prognostic for other mammalian species besides the human remains to be determined, but an examination of early mitotic timing in murine, bovine, and rhesus monkeys has suggested that this may be the case [85-87].

In a follow-up study, Chavez *et al.* determined that the timing of the first three mitotic divisions, in conjunction with assessment of a dynamic process called cellular fragmentation, might also be used to largely distinguish euploid from aneuploid human embryos at the cleavage-stage [27]. It is important to note, however, that approximately 12% of aneuploid embryos from this study exhibited normal parameter timing and no cellular fragmentation, indicating that certain embryos can appear euploid at least up to the 4-cell stage. Upon further examination, these embryos all had incurred mitotic errors with 4 chromosomes or less affected to suggest that if they were allowed to progress in development, perhaps additional later imaging parameters might be used to distinguish chromosomally normal and abnormal embryos. Indeed, other imaging parameters such as pronuclear disappearance, time to 5th cell, initiation of cavitation, and completion of blastulation may also differentiate between euploid and aneuploid cleavage-stage human embryos as well as blastocysts [64, 88-91] (**Fig. 2**). Although it is known that aneuploidy often results in the absence of or delayed blastulation [92, 93], no study has yet observed

a direct correlation between the first cell division in aneuploid embryos and blastocyst formation either because this parameter was not evaluated or it was not measured from a shared start point such as time from insemination [94-96]. This is imperative since meiotic errors are likely to cause a delay in the first mitotic division. In addition, cellular fragmentation, which frequently occurs at the 1- to 2-cell stage, appears to be associated with spindle formation and progression through meiosis and mitosis [97] [27]. Recently, Rodriguez and colleagues demonstrated that the duration of the first mitotic division is predictive of embryo chromosomal status up to approximately the 8-cell stage, but whether this imaging parameter is similarly predictive beyond 8-cells is unknown [98]. Additional studies have also reported a significant difference in the duration of, or synchrony between, the second and subsequent mitotic divisions in euploid versus aneuploid embryos that reach the blastocyst stage, however others have observed no such correlation [92, 94-96]. Taken together, this suggests that aneuploidy can have differential effects on preimplantation development, depending on the number of abnormal chromosomes and at which stage the error(s) occurred. Perhaps future studies using high-resolution live-cell imaging of chromosome dynamics will more precisely determine how chromosomal missegregation impacts embryo cell division behavior.

Clinical validation of these findings is required and recent retrospective or prospective registered clinical trials of patient embryos have confirmed the importance of certain cell cycle parameters in predicting blastocyst formation and/or aneuploidy risk [99-101] (**Fig. 2**). While there currently is some debate as to whether TLM is actually beneficial for embryo selection [102] and the assessment of ploidy status [64] the first randomized control trial evaluating implantation rates, ongoing pregnancy, and early pregnancy loss suggests that TLM is more effective than conventional IVF techniques [103]. It remains to be determined, however, if dynamic imaging analysis can also positively impact live birth

rates, particularly in cases of single embryo transfers. It is also important to note that when comparing these time-lapse studies, any discrepancy in findings may be due to differences in the stage of preimplantation development evaluated, whether only a portion of or whole embryos were analyzed, and how the imaging parameters were measured. Moreover, the use of a common procedural start point such as the time of intra-cytoplasmic sperm injection can have confounding effects on the measurement of other overlapping parameters as recently shown by a study that implemented a biological start point instead [104]. Lastly, which method(s) of ploidy assessment used is also a consideration since array-based and sequencing approaches are far more comprehensive than RTqPCR and DNA-FISH, which may influence the interpretation of results. Nevertheless, despite evidence that the measurement of developmental kinetics can differentiate a large proportion of aneuploid embryos from those that are euploid, chromosomally normal and abnormal embryos that appear and behave similarly may be indistinguishable and still require PGS and/or additional screening [27, 90].

Based on observations that the measurement of imaging parameters can be diverse, subjective, and rather time-consuming especially in cases of abnormal cell divisions, several studies have investigated the use of computer-assisted technologies for embryo selection [89, 100, 105-107] (**Fig. 2**). The initial focus of these reports was on the implementation of algorithms for automated cell tracking and/or aneuploidy risk models for embryo classification. In addition, Conaghan and colleagues also demonstrated that morphology plus automated cell tracking improved embryo selection particularly among high quality embryos and reduced inter-individual variability when used adjunctively [100]. Additional studies have concentrated on the correlation between computer-derived embryo scoring and clinical pregnancy rate with promising results as well as other algorithms for the classification of embryo potential or ploidy status [89, 105-107]. Given

the inherent diversity in embryo kinetics and vast differences in IVF routine between clinics, it will be important to determine if clinic-specific or even patient-specific algorithms are necessary for embryo classification.

Current knowledge for causes of chromosome missegregation in embryos

Chromosomal missegregation in oocytes during meiosis has long been considered the primary reason for aneuploidy, especially in cases of advanced maternal age. However, recent studies using comprehensive chromosome screening of all blastomeres in cleavage-stage human embryos have established that mitotic errors occur at an equal or greater frequency than meiotic errors in embryos from women of average maternal age [26, 39, 46, 108-110]. Mitotic nondisjunction and/or lagging chromosomes during anaphase may not only lead to aneuploidy, but can also give rise to a mosaic embryo with different chromosomal copy number amongst cells. To determine the possible causes of aneuploidy in preimplantation embryos, research has primarily focused on the cellular and molecular players involved in the fidelity of correct chromosome segregation during meiosis and/or mitosis.

Given the complexity of meiosis during oogenesis and the age of oocytes upon maturation, it is not surprising that the majority of meiotic errors can be traced back to the maternal chromosomes [111]. Oocytes remain in meiotic arrest from fetal life until meiosis is resumed, in some cases several decades after puberty. The lack of or improper placement of chiasmata increases with maternal age which in turn increases the risk for non-disjunction due to altered patterns of recombination [112, 113]. Cytogenetic analyses of spontaneous miscarriages, stillbirths, and newborns determined that up to 70% of meiotic

aneuploidies originated from the oocyte, depending on which chromosome(s) was affected [114-116]. This percentage, of course, does not take into account pregnancies that miscarried during the first few weeks of gestation and were not detected. *In vitro* fertilization and other artificial reproductive technology procedures have suggested that meiotic error rates in women are relatively high in comparison to other mammalian species, with approximately 20-25% of human oocytes identified as aneuploid [111]. The incidence of human aneuploidy also increases with maternal age since as many as 50% of pregnancies are diagnosed as aneuploid in women over the age of 40 [117, 118]. However, mosaic aneuploidies, which are mitotically derived, are generally not correlated with advanced maternal age [119-121], except in cases of mitotic non-disjunction [122].

Although meiotic errors can occur during either fetal oogenesis or the resumption of meiosis several decades later, the considerable time between the initiation and the completion of meiosis is likely to contribute to the alteration or degradation of factors important for chromosome segregation fidelity. Since the major wave of EGA does not occur until approximately the 4- to 8- cell stage in human embryos, the first cell divisions are highly dependent on the large pool of maternal messenger RNAs (mRNAs) and proteins provided by the oocyte [123]. This is supported by findings that the oocyte cytoplasm alone is sufficient to reprogram a somatic cell capable of development to the blastocyst stage [124]. Thus, defective maternal resources from the oocyte, along with relaxation or absence of cell cycle checkpoints, may contribute to aneuploidy and allow embryos to proceed in mitosis [125-127]. By definition, these factors are termed maternal-effect genes since they are initially transcribed during oogenesis. In the mouse, several maternal-effect genes have been identified (for review see Li *et al*., 2010) and include factors associated with remodeling sperm chromatin, EGA, and *de novo* DNA methylation [128] (**Fig. 1c**). For example, remodeling of the male genome can lead to DNA breaks

[129], and the maternally-derived ubiquitin-conjugating enzyme, UBE2A [130], repairs sperm chromatin in preparation for EGA. Other maternal-effect genes such as ZFP36L2 ring finger protein-like 2 [131] and autophagy protein ATG5 [132] are involved in maternal messenger RNA (mRNA) and protein degradation, respectively.

The expression of certain maternal RNAs and proteins can persist beyond the oocyte-to-embryo transition. To complicate matters, particular maternal effect genes may not be expressed until after EGA, making it difficult to differentiate between maternal and embryonic effects [128]. Multi-protein complexes of maternal origin, such as the subcortical maternal complex, have also been shown to be important for embryonic progression beyond the 2-cell stage in mouse embryos [133] (**Fig. 1c**). The subcortical maternal complex is a group of at least five proteins, including *FLOPED/Ooep, MATER/Nlrp5, TLE6, Padi6,* and *FILIA/Khdc3*, which localize to cytoplasmic lattices in mouse oocytes [134]. Interestingly, depletion of *FILIA* leads to mitotic aneuploidies. This is most likely due to the role of *FILIA* in assembling key spindle components such as *AURKA, PLK1*, and γ-tubulin to the microtubule organizing center (MTOC) as well as *MAD2* to kinetochores [135]. In a study by Yu *et al*. [136], the subcortical maternal complex was also shown to control symmetrical divisions in mouse zygotes by influencing the central position of the mitotic spindle via Cofilin, a key regulator of F-actin assembly. These observations may be explained by evidence that *Tle6* null mice exhibit unequal sized blastomeres and cellular fragmentation, a phenotype more often observed in higher mammals such as cattle, rhesus monkeys, and human. So far, only a few maternal-effect genes have been studied in relation to mitotic aneuploidy in humans even though subcortical maternal complex members appear to be conserved across mammalian species [128];[137-139]. Since subcortical maternal complex proteins play a role both in maintaining euploidy [135] and symmetrical divisions [136] in mouse preimplantation

embryos, it will be important to determine if they have analogous functions in other mammalian species [127]. In addition to the potential inheritance of aberrant maternal RNA and proteins, there is also evidence that suboptimal maternal genetic variants and mutations within meiosis or mitosis associated genes may also lead to abnormal chromosome segregation and cell division. Recently, McCoy and colleagues identified a genetic variant of *polo-like kinase 4*, a gene known to cause aneuploidy upon disruption of the centrosome cycle [140], that occurred at higher frequency in women who produced aneuploid embryos solely due to mitotic errors. Whether there are other genetic variants associated with mitotic errors remains to be determined.

Another potential maternal source of aneuploidy is oocyte mitochondria (**Fig. 1c**). Accumulation of maternal mitochondrial DNA (mtDNA) mutations over the years between fetal oogenesis and meiotic resumption may also lead to defective mitochondria and possible aneuploidy generation. Women of advanced maternal age have been shown to exhibit increased rates of mtDNA mutations [141] and less ATP production [142]. Moreover, a significant decrease in mitochondrial activity has been documented in mosaic human embryos with chaotic profiles in comparison to euploid or mosaic embryos with non-chaotic profiles [143] as well as in individual aneuploid versus euploid blastomeres from the same embryo [144]. A study found that enzymes responsible for ubiquinone production of the electron transport chain, *Pdss2* and *Coq6,* were diminished in oocytes of older females in both mouse and human. This age-related decline could be reversed in old mice that were treated with ubiquinone 10 for a period of 15 weeks as demonstrated by a significantly higher number of resting primordial and growing secondary follicles in ovaries and improved mitochondrial function in oocytes. Additionally, mitotic spindle and chromosome misalignment defects in aging oocytes were comparable to “young” oocyte morphology after ubiquinone administration [145], further supporting the notion that

healthy oocyte mitochondria are required for proper chromosome segregation. Since ATP production is required for the movement of microtubules during anaphase and cytoskeletal actin filament contraction during cytokinesis [143, 146], it is plausible that maternal mtDNA mutations could indirectly impact chromosome segregation and cell division. Thus, the replacement of dysfunctional mitochondria with healthy mitochondria by nuclear transfer into an enucleated oocyte may provide an alternative means, especially for women of advanced maternal age, to successfully conceive as previously shown in both mice and cow [147];[148].

Although maternal meiotic errors are far more frequent that those of paternal origin and increase with age, mitotically derived mosaic aneuploidies in embryos are generally not associated with advanced maternal age. This is supported by studies that determined mitotic errors are just as frequent, if not more frequent, than meiotic errors in embryos from women of average maternal age [27, 29, 149]. Thus, when mitotic mosaicism is detected in embryos, it may be due to defects in the sperm used for fertilization [119-121]. Aside from providing the paternal genome and phospholipase C-zeta to release the oocyte from MII arrest through calcium oscillations [150, 151], the sperm also contributes its centrosome in the majority of mammalian species (**Fig. 1c**). The sperm centrosome, consisting of two centrioles, duplicates and separates around the time of pronuclear syngamy in zygotes to generate spindle microtubules that pull the chromosomes apart during the first embryonic divisions [152, 153]. In contrast to all mammalian species studied to date, rodents do not have centrosomes deposited from the sperm but rather oocyte MTOCs set up the first divisions [154, 155] and may help explain the relatively low aneuploidy rates observed in mouse embryos [156].

Palermo *et al*. [153] demonstrated that the presence of two sperm in human zygotes led to mosaicism in embryos, whereas monospermic embryos and those that inherited an extra haploid set of chromosomes from the mother were euploid. Moreover, dispermic embryos also exhibit multipolar mitotic spindles and disruption of the sperm centrosome induces mosaicism in embryos (reviewed in [157]). As further proof that the centrosome is paternally derived, it has been shown that the spindle complex in mature human oocytes lacks both centrioles and asters at the poles [158]. Studies have found that certain forms of male infertility are due to centriole abnormalities [159] and may contribute to mosaicism in embryos [160]. Additional evidence is provided by observations of increased mitotic mosaicism in embryos fertilized by testicular sperm extraction from men with non-obstructive azoospermia to suggest that non-ejaculated spermatozoa may be immature and less effective in organizing the first mitotic spindle [121]. Despite substantial evidence that the centrosome is paternally contributed in the majority of mammalian species, an apparent contradiction to this notion are findings of mitotic divisions following parthenogenetic activation. Parthenotes and gynogenotes can develop to the blastocyst stage and are a source of highly proliferative parthenogenetic embryonic stem cells (reviewed in [161-166]). Data from Brevini *et al*. [167, 168] demonstrated that porcine parthenotes do indeed contain centrioles, but at an excessive number, to suggest that *de novo* centriole generation is dysregulated. Similar findings were observed in both porcine and human parthenogenetic embryonic stem cells where multipolar spindles were observed as well as a high degree of aneuploidy. Furthermore, studies in parthenogenetic embryos have found that blastomeres are predominately aneuploid [169, 170]. This suggests that although there appears to be a maternal source of centrioles in parthenotes, paternally inherited centrosomes are more proficient in early mitotic divisions. Altogether, these studies suggest that further consideration should be given to paternal age and the

potential inheritance of an age-related dysfunctional centrosome similar to how an association between advanced maternal age and meiotic errors is regarded [118].

Even with the presence of parental factors for the maintenance of euploidy, meiosis and mitosis are complex cellular processes with several key events where errors can arise and impact subsequent development. Regardless of whether meiotic or mitotic in origin, it is thought that the majority of missegregation errors are the result of two different mechanisms, either lagging chromosomes during anaphase or non-disjunction (**Fig. 1d**). Anaphase lagging occurs when a chromatid fails to connect or is dissociated from the spindle apparatus and is lost upon karyokinesis and cytokinesis, which can result in a monosomy or trisomy in one of the two daughter cells during meiosis or mitosis. For meiosis, this might occur as early as the MI stage if the spindle assembly checkpoint is bypassed, leading to precocious division and abnormal chromatid allocation to the first polar body and MII oocyte [171]. Lagging chromosomes in anaphase may be due to the depletion and/or reduced stringency of the spindle assembly complex in oocytes and early preimplantation embryos, which rely on maternally supplied spindle assembly complex mRNAs and proteins until EGA. Evidence for this is provided by RNA interference studies in mouse embryos that showed that knockdown of the spindle assembly complex components, Bub3, BubR1, and Mad2 led to improper chromosome segregation, micronuclei formation, and aneuploidy generation [172]. Furthermore, additional studies have demonstrated that chromosome lagging commonly arises from the formation of merotelic attachments in mitosis, whereby a single kinetochore on one side of the chromosome is attached to microtubules emanating from both spindle poles (reviewed in [173]). While lagging chromosomes arising from the formation of merotelic attachments has been show to occur in oocytes during meiosis [174, 175], the exact mechanisms of chromosomal missegregation during early mitotic divisions in mammalian embryos

remains an enigma. Unlike other mitotic cell types, the cleavage-stage embryo undergoes mitosis to produce cells of decreasing cell size with each subsequent division, which can impact spindle length and symmetric versus asymmetric division [176].

The other major source of chromosome missegregation errors is non-disjunction where there is the failure of the sister chromatids to separate at the centromere during metaphase, resulting in the loss of a chromosome in one daughter cell and a reciprocal gain in the other. This event can be recognized as 3:1 chromosomal ratios between daughter cells and will give rise to an aneuploid zygote or mosaic aneuploid embryo depending on whether it occurs during meiosis or mitosis, respectively [35, 42, 177-179]. Although non-disjunction and anaphase lagging may have the same consequences, aneuploidy due to a single chromatid loss in MII oocytes far exceeds the prevalence of non-disjunction at least during meiosis [180, 181]. Mitotic errors, however, appear to be equally distributed between chromosome lagging during anaphase and chromosomal non-disjunction [26-29]. To complicate matters, human preimplantation embryos have also been shown to express both heightened cell cycle drivers and diminished cell cycle checkpoints, which might make blastomeres more vulnerable to chromosome lagging during early mitotic divisions [125, 182] (**Fig. 1d**). It is only after EGA, from approximately the 4- to 8-cell stage onwards [123, 183], that cell cycle control becomes activated in human embryos. Thus, permissive cycle checkpoints allow aneuploid embryos to proceed through mitosis even if chromosomes are not yet properly aligned on the mitotic spindle at the completion of metaphase [125, 126].

Potential mechanisms for overcoming aneuploidy

In light of the lack of cell cycle control and frequent findings of euploid-aneuploid mosaicism [33, 36] as well as chaotic aneuploidy, it is not surprising that the majority of chromosomal errors are unlikely to be corrected [26, 27]. Nevertheless, there is some evidence to suggest that "embryo self-corrective" mechanisms do exist based on PGS biopsy of aneuploid blastomeres at the cleavage-stage followed by biopsies of euploid trophectoderm cells from the same embryo a few days later [184, 185]. While thought to occur only occasionally, the so-called embryo self-correction phenomenon may be explained by other processes such as blastomere exclusion and cellular fragmentation that are observed in embryos (**Fig. 1e**). Cellular fragmentation is relatively common in humans, with approximately 50% of human embryos or more exhibiting fragmentation to some degree [186, 187]. Preimplantation embryos from other mammalian species, including cattle and equine undergo cellular fragmentation, although to a lesser extent than humans and non-human primates [188, 189]. Notably, cellular fragments are also detected in embryos conceived *in vivo* [190, 191], indicating that fragmentation is not an artifact of *in vitro* culture. It is also important to note that cellular fragmentation is distinct from the cell death-induced DNA fragmentation that can occur late in mammalian preimplantation development during the morula and blastocyst stages [192-194]. Cellular fragments can vary in size, temporal and spatial distribution, as well as organelle content [195-197], making them sometimes difficult to differentiate from small blastomeres. High levels of fragmentation is associated with an increased incidence of aneuploidy [119, 198] and depending on the timing of fragmentation, can be used to distinguish embryos with meiotic and/or mitotic errors [27]. Although extensive fragmentation may correlate with low implantation and clinical pregnancy potential [186, 192, 199-201], by itself it is not a clear indicator of poor embryo quality as live births have resulted from the transfer of fragmented

embryos [186, 187, 202-204]. Rather, it is the pattern and degree of cellular fragmentation, along with the stage that it initially occurs, which are better predictors of embryo viability [186, 187].

Recent evidence presented by Chavez and colleagues suggest that cellular fragments can also encapsulate missegregated chromosomes following extrusion from the embryo [27], but exactly how this occurs remains unknown. Given that fragmentation was originally thought to represent membrane-bound extracellular cytoplasm, the idea that cellular fragments might contain nuclear DNA was intriguing especially since microsurgical removal of fragments was once promoted [205, 206]. Nonetheless, the authors also reported frequent findings of micronuclei in cleavage-stage human embryos to suggest that the formation of micronuclei might provide a mechanism by which chromosomes are sequestered into cellular fragments after missegregation [27]. Since cellular fragmentation is a dynamic process, whereby chromosome-containing cellular fragments (CCFs) can remain as either discrete units or be reabsorbed by the embryo [27];[68, 70], it may also allow corrective means to overcome aneuploidy generation. More specifically, if a CCF fuses with the blastomere from which it originated or a neighboring blastomere that lacked the encapsulated chromosome(s), euploidy could potentially be restored in an embryo following breakdown of the nuclear envelope. However, not all cellular fragments necessarily contain DNA and thus, fragment resorption may have no impact on ploidy status or it may even increase genotypic complexity in embryos upon fusion with a euploid blastomere [27]. Regardless of the potential consequences, little is still known about what leads to cellular fragmentation and thus, it will be important to determine the precise mechanism(s) by which it occurs and how the timing, degree and/or resorption of fragments contributes to the generation and potential correction of embryonic aneuploidy.

Chromosomes within micronuclei are highly unstable and can undergo DNA damage in the form of double stranded breaks [207]. Recently, studies have proposed a direct link between micronuclei formation and the incidence of "chromosome pulverization," or chromothripsis [207-210] (**Fig. 1e**). First described in cancer genomes [211], chromothripsis is a phenomenon through which one or a few chromosomal segments are "pulverized" into many pieces and randomly reassembled in one unique cellular event over the course of one cell division [212]. Chromothripsis has also been suggested to occur during preimplantation development [212, 213] based on frequent observations of micronuclei formation, cellular fragmentation, segmental rearrangements, and abnormal mitotic divisions in cleavage-stage embryos. This pulverization and random reassembly can lead to chromosomal duplications, deletions, translocations, and inversions, which are often detrimental, resulting in subfertility or congenital abnormalities depending on when the event occurred [214, 215]. It is important to note that there are no studies at the moment that have examined if preimplantation embryo micronuclei undergo chromothripsis. Cellular fragmentation-mediated elimination of micronuclei with damaged chromosomes may be a corrective mechanism, especially in euploid-aneuploid mosaic embryos whereby euploid blastomeres can out compete aneuploid cells once EGA has occurred. As cancer cells also sequester missegregated chromosomes and chromatid fragments within micronuclei [216-219], micronuclei research in preimplantation development may also be translatable to somatic tissues.

While the cellular fragmentation-mediated elimination of missegregated chromosomes might occur at the earliest stages of preimplantation development, there appears to be other means for the resolution of aneuploidy later in embryogenesis during the transition from the cleavage to the blastocyst stage (**Fig. 1e**). In particular, the complete exclusion of large fragments and blastomeres has been observed in both compact morulas and

blastocysts from several mammalian species, including humans, rhesus macaques, cattle, and mice homozygous for the yellow allele (A^y) of the agouti locus [186, 192, 220-225]. Although the frequency of blastomere exclusion is unknown since it is not a well-documented process, it is generally accepted that preimplantation embryos can tolerate the loss of one or more blastomeres based on blastomere biopsy for PGS. Given that lower aneuploidy rates are observed in blastocysts as compared to cleavage-stage embryos [226], one possible explanation for this may be the exclusion of aneuploid blastomeres from the rest of the embryo (**Fig. 1e)**. However, the chromosomal and/or genetic analysis of extruded blastomeres or cellular fragments is still lacking and may be due to the limitations of aCGH and other microarray-based methods for the detection of complex or polyploid genotypes. Nevertheless, it seems plausible that the extrusion rather than the reincorporation of micronuclei-containing blastomeres may be beneficial for embryo genomic integrity since DNA damage can occur in the micronuclear environment [207, 216, 227, 228]. Future work should focus on the precise frequency of this process and how blastomere exclusion might relate to the "embryo self-correction" phenomenon as a whole.

Another mechanism termed confined placental mosaicism (**Fig. 1e**) may explain embryo correction and the reduced incidence of aneuploidy at the blastocyst stage [226]. In this scenario, aneuploid cells would be deliberately confined to the trophectoderm layer, whereas euploid cells could incorporate into the inner cell mass (ICM) and give rise to a chromosomally normal fetus [229]. Studies have identified the presence of two or more cell populations with different chromosomal make-up at the blastocyst stage and this appears to be more prevalent in embryos from women of advanced maternal age [230, 231]. After careful separation of ICM and trophectoderm cells, however, several studies demonstrated that chromosomally abnormal cells detected at the 8-cell stage are not

preferentially allocated to the trophectoderm compartment, but rather evenly distributed throughout the blastocyst [232-238]. Johnson and colleagues disaggregated over 50 blastocysts from mothers of average maternal age and observed discordance between trophectoderm and ICM samples in approximately 4% of the embryos for structural chromosome aberrations [237]. It is important to note that this study evaluated ploidy status in multiple cells of the same cell type at once rather than single cells, which may mask discordance between the trophectoderm and ICM. Yet there are other reports showing the preferential allocation of aneuploid cells in chorionic villi samples as compared to fetal tissues to suggest that confined placental mosaicism may play a role later in post-implantation development [229, 231, 239-243]. Furthermore, while classified as aneuploid, aneuploid-euploid mosaic embryos may still result in the birth of healthy offspring upon transfer, which suggests that corrective mechanisms exist to overcome chromosomal instability during preimplantation development [20, 244, 245]. There is still disagreement on whether the trophectoderm layer of blastocysts preferentially contain chromosomally abnormal cells. For future studies, it will be necessary to use more comprehensive PGS methods at the single cell level in whole blastocysts.

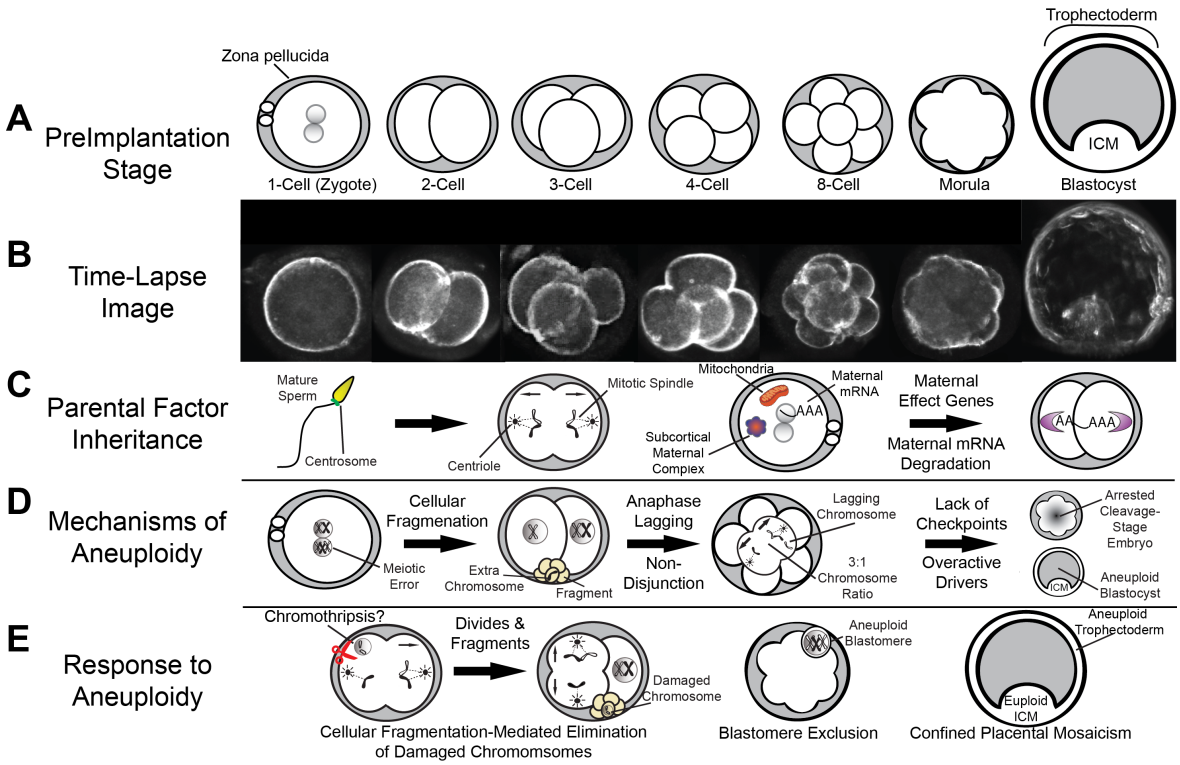

Figure 1. *Cause and responses to aneuploidy in the mammalian preimplantation embryo.* Recent advances in mammalian embryology from the (**A**) zygote to blastocyst stage, including but not limited to (**B**) time-lapse image analysis, have greatly contributed to our knowledge of the key chromosomal and genetic characteristics impacting each major stage of preimplantation development. (**C**) Embryo chromosomal integrity may be influenced by the lack of and/or inheritance of aberrant paternal contribution of the centrosome, which mediates the first mitotic divisions. Select maternal mRNAs termed maternal effect genes are recruited for translation following fertilization, whereas the remaining maternal mRNAs are degraded. Besides individual maternal proteins, multi-protein complexes such as the subcortical maternal complex, are important for embryonic progression beyond the 2-cell stage and potential prevention of mitotic aneuploidy. Oocyte mitochondria dysfunction also plays a role in the integrity of chromosome missegregation. (**D**) There are several additional factors that can contribute to the generation of

chromosome instability, particularly in human embryos, including cellular fragmentation, anaphase lagging, chromosomal non-disjunction, as well as the lack of cell cycle checkpoints and overexpression of cell cycle drivers. (**E**) If and how the embryo responds to aneuploidy may include the elimination of damaged chromosomes contained within a micronucleus through cellular fragmentation. Aneuploid blastomeres may also fail to divide and become eliminated from the embryo in the compacting morula and blastocyst. Furthermore, aneuploid-euploid mosaic embryos are able to produce healthy offspring and this may be due to allocation of aneuploid cells to the trophectoderm while euploid cells remain in the ICM.

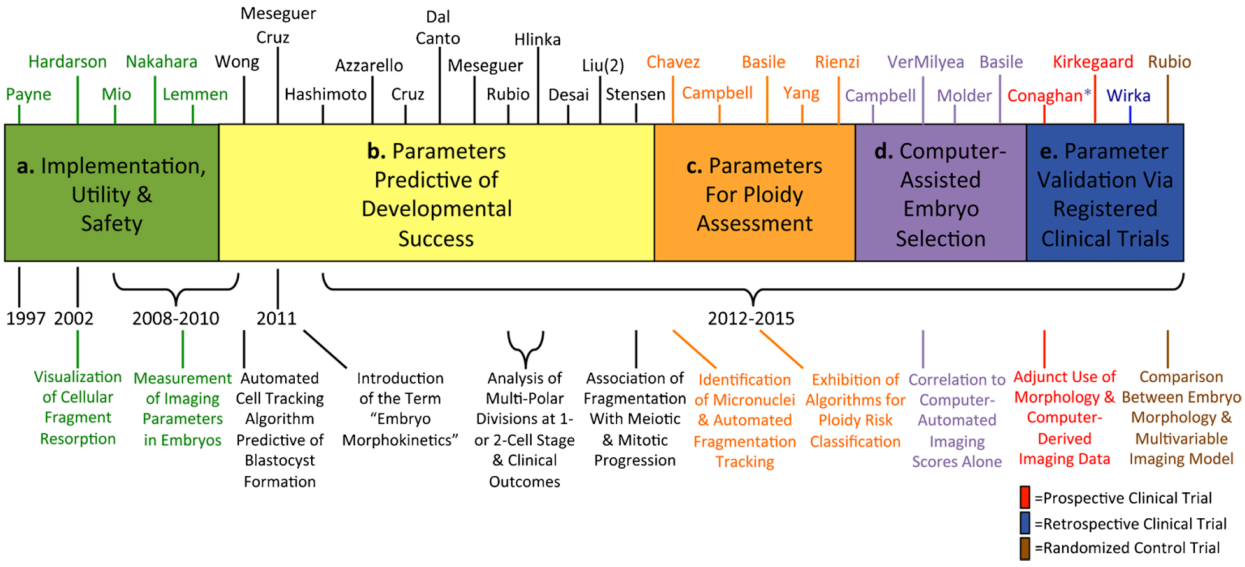

Figure 2. *An evolutionary timeline of time-lapse imaging for embryo assessment.* A timeline from 1997 to present day showing the different "eras" of time-lapse image analysis with relevant references for the evaluation of embryo viability. The first time-lapse publications examined the implementation, utility and safety of this technology to monitor embryo development. After safety validation, studies began identifying cellular parameters predictive of success to the blastocyst stage, followed by the identification of parameters predictive of embryo ploidy status. More recent reports have focused on clinically applying and validating these parameters or newly identified parameters in either retrospective or prospective registered clinical trials. The first randomized control trial evaluating time-lapse image analysis versus traditional IVF techniques was recently published with others likely to follow and additional studies have concentrated on the development of computer-assisted algorithms for automatic embryo assessment and classification.

Preface: Chapter 1

The introduction of this dissertation provided an overview of the current landscape for the investigation of aneuploidy in mammalian preimplantation embryos. Although ideally human embryos would be the subject of study, federal and ethical restrictions as well as cost limit our ability to obtain fresh embryos from otherwise fertile and young individuals and perform mechanistic studies and embryo transfers. Over the decades, the mouse has been the primary model to study embryology. However as described above, murine preimplantation embryos not only have a low incidence of aneuploidy, but they also rarely exhibit micronucleation and cellular fragmentation during development [27, 156, 246]. Whether other mammalian species more closely related to humans such as non-human primates have similar aneuploidy fragmentation frequencies has not been investigated in detail and directly addressing this question is necessary for translation to human embryogenesis. As mentioned above, previous studies with rhesus macaque embryos using DNA-FISH probes to human chromosomes 13, 16, 18, X, and Y indicated that the level of aneuploidy in rhesus macaque embryos is more comparable to human than mouse [23-25]. Given that only a few chromosomes were analyzed by low-resolution techniques, however, the actual percentage of rhesus macaque embryos carrying whole or sub-chromosomal aberrations remains unknown. In this chapter, methods and findings are described for the incidence of aneuploidy and ploidy errors in the IVF-derived rhesus macaque preimplantation embryo. This work sets up the basis for further translational studies in the monkey model that can provide insight into mechanism of and responses to aneuploidy in human embryos.

Chapter 1: Aneuploidy and ploidy errors in the rhesus macaque embryo.

Abstract

A major contributor to *in vitro* fertilization failure and loss of human embryos is abnormal chromosome number, or aneuploidy. Considering the research limitations surrounding human embryos, there is need to establish a relevant animal model that inherently recapitulates the high incidence of aneuploidy observed in human embryos. The rhesus monkey shares many key reproductive characteristics with humans, including mono-ovulation and similar live birth rates following periovulatory timed intercourse. Previous studies have examined the aneuploidy frequency in rhesus macaque embryos but not comprehensively for all chromosomes. Given the detection of an increased incidence of aneuploidy in the rhesus macaque embryo with DNA-FISH and the reproductive similarities shared between human and rhesus macaques, the hypothesis of this part of the study is that rhesus macaque embryos from IVF will have a similar aneuploidy frequency to human embryos when all chromosomes are examined with DNA-Seq. Thus, the objective is to determine if the rhesus macaque embryo is a suitable substitute for the investigation of aneuploidy in human embryos. Rhesus macaque preimplantation embryos (N=43) from average reproductive aged males and females (9.4 $\pm$ 1.5 and 9.2 $\pm$ 2.3 years old, respectively) were monitored by time-lapse imaging and later disassembled at the 2-14 cell stage into individual blastomeres and polar bodies. The DNA of these single cells was subjected to PCR-based whole genome amplification, barcoding for Illumina sequencing platforms, and low coverage DNA-sequencing. In-house pipelines for CNV and SNP analyses were built to determine the copy number and parent-of-origin of each chromosome, respectively. While 28.6% of the cleavage-stage embryos were completely

euploid, the other 71.4% contained aneuploid blastomeres. When polar bodies were detected in aneuploid embryos, it was determined that mitotic origins of aneuploidy were just as frequent meiotic errors. As anticipated, the gender ratio was split nearly equal as 46.8% of embryos had a Y chromosome. Additional findings of reciprocal sub-chromosomal deletions and duplications demonstrate that chromosome breakage also occurs. Although only confirmed zygotes with two visible pronuclei and/or two polar bodies were used in this study, 40.8% of embryos displayed abnormal ploidy profiles instead of the expected biparental distribution of maternal and paternal chromosomes throughout the embryo. This surprisingly high percentage of embryos with abnormal ploidy demonstrate that detection of 2 pronuclei and 2 polar bodies may not always be indicative a diploid, biparental zygote. Paternal contribution to mitotic aneuploidy was also evident as multipolar divisions and chaotic aneuploidy were prevalent in embryos produced by the same male donor, suggesting inheritance and formation of a faulty centrosome from the sperm. Overall, these findings support the hypothesis that the aneuploidy frequency in cleavage-stage embryos is conserved between humans and rhesus macaques. Therefore, this study proposes that the monkey is an appropriate model for investigating mechanisms of embryonic aneuploidy generation and tolerance.

Introduction

The demand for human *in vitro* fertilization (IVF) steadily increases each year, but success rates as measured by live birth(s) have remained only ~30-35% for decades (cdc.gov/art). Although several oocytes are recovered after controlled ovarian hyperstimulation and successfully fertilized in an IVF cycle, embryos can arrest during culture or fail to implant when transferred back to the uterus. One reason why IVF fails is because embryos with unbalanced whole chromosome(s) are transferred instead of euploid ones [247]. It is difficult to ascertain whether *in vitro* culture or hyperstimulation increased the aneuploidy frequency of embryos in comparison to *in vivo* conceptions. However, studies estimate a similar efficiency from natural human pregnancies (~30-35%) with up to 70% of spontaneous miscarriages diagnosed as chromosomally abnormal [13-16].

Although maternal age is highly correlated with the incidence of meiotic aneuploidies [248] [249], estimates of aneuploidy in IVF embryos from young, fertile couples via high-resolution techniques are also high. Recent studies using comprehensive chromosome screening of all blastomeres in cleavage-stage human embryos have established that aneuploidy in embryos ranges from 50 to 80% and that mitotic errors occur at an equal or greater frequency than meiotic errors [26, 30, 31, 46, 108, 109]. Mitotic nondisjunction, lagging chromosomes during anaphase, and/or breakage–fusion–bridge cycles may not only lead to aneuploidy, but can also give rise to a mosaic embryo with different chromosomal copy number amongst cells [26]. Because of mosaicism, traditional morphological assessment of embryo quality and preimplantation genetic screening can underestimate the degree of chromosomal errors affecting the whole embryo as discussed at length above.

Supernumerary embryos from fertility clinics as well as those dedicated for clinical trials have been used at length to study aneuploidy. Despite this, federal law, bioethical, and cost limitations often prevent further studies of genetic mechanisms in human embryos and thus alternative animal models are utilized. The mouse embryo has provided an excellent tool for developing methodologies however there are many differences between human and mouse reproduction that limit translational studies. Mouse embryos have less aneuploidy (~1-4%) [18-20], are polyovulatory, have an estrus cycle, and the sperm does not provide a centrosome for setting up the first mitotic cell divisions [155]. To gain further insight on the processes that drive human embryonic aneuploidy, the more closely-related rhesus monkey may be more fitting. Previous studies with rhesus macaque embryos using DNA-FISH probes to human chromosomes 13, 16, 18, X, and Y indicated that the level of aneuploidy in rhesus macaque embryos is more comparable to human than mouse [23-25]. Given that only a few chromosomes were analyzed by low-resolution techniques, however, the actual percentage of rhesus macaque embryos carrying whole or sub-chromosomal aberrations remains unknown. Frequent observation of abnormal nuclear structures in blastomeres from rhesus macaque embryos as compared to other mammalian species [27] suggests that the incidence of chromosomal abnormalities in non-human primates is similar to humans. With this supporting evidence, the hypothesis of this part of the study is that rhesus macaque embryos have a similar frequency of aneuploidy as human embryos. In this chapter, whole genome amplification and single-cell DNA-Sequencing (DNA-Seq) of blastomeres and polar bodies was used to establish the frequency of all whole and sub-chromosomal errors in forty-two rhesus macaque cleavage-stage embryos.

Methods

Rhesus Macaque Embryos

Controlled ovarian stimulations were performed on adult female rhesus macaques of average maternal age (9.2 ± 2.3 years old) as previously described [250]. Briefly, 30 IU of recombinant human follicular stimulating hormone (donated from Organon, Roseland, NJ) was intramuscularly injected twice daily in cycling females at the start of menses for six consecutive days. On days 7 and 8 of the controlled ovarian stimulation protocol, 30 IU of both recombinant human follicular stimulating hormone (donated from Organon) and recombinant human luteinizing hormone (donated from Al Partlow) were co-injected twice each day. When estradiol levels reached greater than 200 pg/ml, the following day females were intramuscularly injected with 0.1 ml/kg of Antide, a gonadotropin-releasing hormone antagonist (donated from the Salk Institute, La Jolla, CA), to prevent an endogenous luteinizing hormone surge. Approximately 36 hours prior to follicle aspiration, a single dose (1,100 IU) of human chorionic gonadotropin (EMD Serono Ovidrel®, Rockland, MA) was intramuscularly injected to initiate oocyte maturation. Laparoscopic follicular aspirations were aseptically conducted on anesthetized animals using suction to obtain cumulus-oocyte complexes collected in Tyrode's albumin lactate pyruvate HEPES media with 0.3% bovine serum albumin (Sigma-Aldrich, St. Louis, MO) and 1% Heparin sodium salt solution. Controlled ovarian stimulation were isolated from follicular aspirates and denuded by gentle micropipeting in HEPES-buffered Tyrode's albumin lactate pyruvate media containing 0.3% bovine serum albumin and 3% hyaluronidase (Sigma-Aldrich, St. Louis, MO). MI and MII oocytes as well as germinal vesicle oocytes were incubated in Tyrode's albumin lactate pyruvate plus 0.3% bovine serum albumin media at 37°C with

5% CO_2 for 4-6 hours. To minimize variability between sperm donors, fresh semen was collected from only 1 of 4 adult male rhesus monkeys of average paternal age (9.4 ± 1.5 years old) the same day as oocyte retrieval for conventional IVF. Mature MII oocytes were fertilized with sperm diluted to 20 x 10^6/ml in 100 µL drops of Tyrode's albumin lactate pyruvate complete media (0.3% bovine serum albumin and 0.006% sodium pyruvate) as previously described [251, 252]. Following IVF at 37°C with 5% CO_2 for 14-16 hours, excess sperm was removed from the fertilized oocytes to visually assessed for two pronuclei and/or two polar bodies. Confirmed zygotes were transferred to custom Eeva™ 12-well polystyrene petri dishes (Progyny, Inc., San Francisco, CA; formerly Auxogyn, Inc.) and cultured in 100 µL of one-step commercial media supplemented with 10% serum protein (LifeGlobal, Guildford, CT) under mineral oil (Sage™, Trumbull, CT) at 37°C with 6% CO_2, 5% O_2 and 89% N_2. Media was changed every two days by transferring the embryos to a new imaging dish until collected for analysis. All animal procedures were performed under the direction and assistance of the veterinary staff and animal technicians in the Division of Comparative Medicine at Oregon National Primate Research Center (ONPRC). The collection and preparation of oocytes and sperm was performed according to the approved Institutional Animal Care and Use Committee Assisted Reproductive Technologies Support Core protocol #0095 entitled, “Assisted Reproduction in Macaques.”

Time-Lapse Imaging

Rhesus macaque embryos were monitored with an Eeva™ darkfield 2.2.1 or bimodal (darkfield-brightfield) 2.3.5 time-lapse microscope system (Progyny, Inc., San Francisco, CA) as previously described [91]. The Eeva™ TLM systems were comprised of an inverted

microscope with light-emitting diode illumination, 10X Olympus objective, auto-focus, and 5-megapixel complementary metal-oxide semiconductor digital camera, all of which fit into a small tri-gas incubator (Panasonic Healthcare, Japan). Embryos were imaged every 5 min. with a 0.6 second exposure time for one day in the case of 2-cell embryos, 1-2 days for 4-cell embryos, and 1-3 days for the 5- to 16-cell stage.

Embryo Disassembly

The zona pellucida was removed from each embryo by a ~30 sec. exposure to warm Acidified Tyrode's Solution (EMD Millipore, Temecula, CA) and washed with Ca^{2+} and Mg^{2+}-free phosphate buffered saline (PBS). Cleavage-stage embryos were disaggregated into single blastomeres and polar bodies if present with Quinn's advantage Ca^{2+} and Mg^{2+}-free medium with HEPES plus 10% human albumin (Sage™, Trumbull, CT) with or without brief exposure to warm 0.05% trypsin-EDTA (Thermo Fisher Scientific, Waltham, MA) as necessary. Each blastomere and polar body was washed three times with Ca^{2+} and Mg^{2+}-free PBS and collected individually in ~2 µL of Ca^{2+} and Mg^{2+}-free PBS for transfer to a sterile Ultraflux™ PCR tube (GeneMate, VWR, Radnor, PA). All of the above was performed under a stereomicroscope equipped with a digital camera (Leica Microsystems, Buffalo Grove, IL), which has movie-making capabilities, to document the collection of every sample. Once tubed, samples were flash frozen on dry ice and stored at -80°C. Only embryos for which the disassembly process occurred effectively with no apparent loss of material were carried forward for library preparation and sequencing.

Somatic Cells

Human B-lymphocytes (GM12878, Coriell Institute, Camden, NJ) were obtained and processed as previously described [253]. Female human skin fibroblasts from patients with Monosomy X or Trisomy 21 (GM10179 and AG05024, respectively, Coriell Institute, Camden, NJ) as well as karyotypically normal male and female rhesus macaque skin fibroblasts (AG08312 and AG08305, respectively, Coriell Institute, Camden, NJ) were grown to 70% confluency in Dulbecco's Modified Eagle's medium F12 (Gibco, Gaithersburg, MD) supplemented with 10% fetal bovine serum (Sigma-Aldrich, St. Louis, MO). Cells were incubated with warm 0.05% trypsin-EDTA for suspension and the trypsin inactivated with Dulbecco's Modified Eagle's medium F12 plus 10% fetal bovine serum. The cell suspension was serially diluted in Ca^{2+}/Mg^{2+}-free phosphate-buffered saline until single cells were detected in microdrops under the stereomicroscope. Individual cells were isolated in ~2 µL of Ca^{2+} and Mg^{2+}-free phosphate-buffered saline and transferred to the low-retention PCR tubes, quick frozen on dry ice, and stored at -80°C until DNA library preparation. Karyotyping of 50 metaphases for human and rhesus macaque primary fibroblasts was conducted by the OHSU Research Cytogenetics Laboratory.

Parental DNA

Whole blood was collected in K_2EDTA vacutainer collection tubes (BD Diagnostics, Franklin Lakes, NJ) from the male and female rhesus macaques used to produce embryos in this study by the Colony Genetics Resource Core within the Primate Genetics Program at ONPRC. Parental DNA was extracted using the Gentra® Puregene® blood kit (Qiagen, Germantown, MD) according to the manufacturer's protocol. Extracted DNA was stored at -80°C for the construction of sequencing libraries.

DNA Library Preparation

Single blastomere, polar body, and skin fibroblast samples underwent DNA extraction and whole genome amplification (WGA) using the PicoPlex single-cell WGA Kit (Rubicon Genomics, Ann Arbor, MI) according to the manufacturer's instructions with slight modifications. The three-step, one-tube protocol applies a proprietary amplification process with quasi-random primers to assure the production of highly reproducible sequencing libraries. DNA was released from samples with cell extraction enzyme at 75°C for 10 min. The DNA was subsequently pre-amplified with PicoPlex pre-amp enzyme and a primer mix via a 95°C hotstart for 2 min. and 12 cycles of gradient PCR. Pre-amplified DNA was further amplified with PicoPlex amplification enzyme and 48 uniquely-indexed Illumina sequencing adapters provided by the kit or custom adapters with indices designed by Andrew Adey's laboratory (Molecular & Medical Genetics, OHSU) as previously described [253]. Adapter PCR amplification consisted of a 95°C hotstart for four min., four cycles of 95°C for 20 sec., 63°C for 25 sec., and 72°C for 40 sec. and lastly, seven cycles of 95°C for 20 sec. and 72°C for 55 sec. Individual libraries were quantified with a Qubit HS DNA kit (Life Technologies, Eugene, OR) and validated for sequencing by PCR amplification of the adaptor sequences using the PCR Primer Cocktail (Illumina TruSeq® kit, San Diego, CA) and visualized by 2% agarose gel electrophoresis. Only libraries with DNA quantities greater than the no-template controls were included in sequencing. Quantitated and validated libraries were pooled for multiplexed-sequencing taking into account the expected and desired sequencing coverage. 50 ng of DNA was prepared from each blastomere or fibroblast, 25 ng from polar bodies, and 5 ng from samples with low to no detectable DNA after WGA and/or no DNA smear indicative of a positive library

following gel electrophoresis. Pooled libraries were purified with AMPure® XP beads (Beckman Coulter, Indianapolis, IN) according to the PicoPlex instructional manual. Purified pooled libraries were again quantified with a Qubit HS DNA kit and quality assessed by a 2200 TapeStation and/or a 2100 Bioanalyzer (both from Agilent, Santa Clara, CA). Parental DNA samples (1ug) were fragmented using the Diagenode Bioruptor Pico (Denville, NJ) for a 300-400 base pair size selection. The NEBNext® DNA Library Prep Master Mix Set and NEBNext Multiplex Oligos for Illumina (NEB, Ipswich, MA) were then used to generate whole-genome sequencing libraries for each sample following the manufacturer's protocol. The libraries were quantified with the Qubit High Sensitivity dsDNA Assay (Invitrogen) and size distribution assessed with a 2100 Bioanalyzer High Sensitivity DNA Analysis Kit (Agilent).

Multiplex DNA Sequencing

Pooled libraries of individual blastomeres, polar bodies, and single somatic cell libraries from skin fibroblasts and parental DNAs were sequenced on Illumina platforms according to the following scheme: rhesus macaque single fibroblast control samples (N=7) were first sequenced on an Illumina MiSeq (San Diego, CA) using the 150-base pair paired-end protocol and generated a total of ~28.4×10^6 reads (~1.67×10^6 reads/sample). An additional 22 single fibroblasts were sequenced on an Illumina NextSeq 500 (San Diego, CA) using a 75-cycle kit with a modified single-end workflow that incorporated 14 dark cycles at the start of the first read prior to the imaged cycles. This excluded the quasi-random priming sequences that are G-rich and lack a fluorophore for the two-color chemistry utilized by the NextSeq platform during cluster assignment. From these cells, a total of ~34.6×10^6 reads (~1.57×10^6 reads/sample) were generated.

Based on the similar number of reads obtained per sample between the two protocols, blastomere and polar body samples were sequenced with the Illumina MiSeq using the 150-base pair paired-end protocol and Illumina NextSeq using a customized 75-base pair single-end protocol. Average sequencing statistics are provided in **Table 1**. Parental DNA multiplexed libraries were sequenced at the Oregon State University Center for Genomic Research and Biocomputing on the HiSeq 3000 platform using the 150 paired-end protocol for a total of 2.84×10^9 reads (1.56×10^8 reads/sample).

All raw sample reads were de-multiplexed and sequencing quality assessed with FastQC as previously described [254]. Illumina adapters were removed from raw reads with the sequence grooming tool, Cutadapt [255], which trimmed 15 bases on the 5' end and five bases from the 3' end, resulting in reads of 120-base pair on average. Trimmed reads were aligned to the most recent rhesus macaque genome reference, RheMac8 [256], using the BWA-mem option of the Burrows-Wheeler Alignment Tool [257] with default alignment parameters. To avoid read pile-ups due to common repeats, all repeat sequences were "masked" (converted to an "N") in the RheMac8 reference genome using Repeat Masker [258]. Resulting bam files were filtered to remove alignments with quality scores below 30 (Q<30) as well as alignment duplicates that were likely the result of PCR artifacts with the Samtools suite of tools [259].

Copy Number Variant Calling

Variable Non-Overlapping Window CBS (VNOWC) Pipeline

Although PCR-based WGA is more effective for CNV analysis than isothermal amplification (non-PCR)-based techniques as previously shown [50], potential biases in read accumulation and dropout are expected to exist in individual samples from PicoPlex WGA. To model the background rate of accumulation and dropout expected in a single-cell normal sample, five paired-end and twenty single-end sequenced rhesus macaque 42XX fibroblast libraries were combined to form a paired-end and single-end reference, respectively. These reference samples were used to generate variable-sized windows with a constant number of expected reads per window (target was 4,000). The same windowing method was applied for reads from forty single human fibroblast samples. At this step, the windowing approach was applied to each sample to generate read count only plots. For CNV calling, the appropriate species reference was used to calculate observed-to-expected ratios of read counts in each window given the total number of mapped reads for the sample. R package DNAcopy (version 1.44.0, [260]) was used to perform circular binary segmentation (CBS) across each chromosome and identify putative copy number changes between windows. Since the initial window ratios assume that reads are spread evenly across a euploid genome, a recalibration step was necessary to correct the expected number of reads given putative changes in copy number. Samples with mostly empty windows were presumed to have a base copy number of one, while samples with reads in the majority of windows were assumed to have a base copy number of two. The copy number estimates provided by CBS are rounded to the nearest integer and plotted, along with the corrected ratios for each window. A bioinformatics pipeline for calling chromosomal copy number was developed to implement the above steps (available at https://github.com/nathanlazar/Oocyte_CN). Findings from this custom CNV pipeline were validated with a secondary approach via Gingko (http://qb.cshl.edu/ginkgo), an open-source web tool for evaluating single-cell CNVs. To determine the false discovery rate of the VNOWC pipeline, human trisomy 21 and monosomy X reads from 10-cell

karyotypically euploid fibroblasts were subsampled 100 times to levels typical of a single-cell sample (1M, 500K, 250K and 100K reads). These subsampled reads were mapped to 4 different sets of window sizes (made expecting 500, 1000, 2000, 4000 reads per window in controls) for a total of 1600 CNV runs per cell line. Counts and standard deviations for unexpected whole and segmental CNVs greater than 15MBs were reported.

CBS/HMM Intersect (CHI) Pipeline

A pipeline for GC bias correction, read normalization across both the genome and within each individual sample, and CNV calling was implemented as previously described [253]. Both the Hidden Markov Model (HMMcopy, version 3.3.0, Ha *et al.* 2012) and Circular Binary Segmentation (DNAcopy, version 1.44.0, [260]) packages were used to call CNVs based on parameters determined in Knouse *et al.* [261]. All calls from the HMM and CBS methods generated CNV profiles of variable sized windows that were intersected on a window-by-window basis.

Integration of VNOWC and CHI Pipelines

To optimize the accuracy of CNV calling, all samples were analyzed for whole chromosome losses and gains, broken chromosomes, and small CNVs (less than 15 MB in length) by both the VNOWC and CHI methods. Shared CNV calls between the two methods were retained and discordant CNV calls for aneuploid whole and broken chromosomes were further examined. Chaotic aneuploid samples confirmed by both methods and discordant small CNV calls were not additionally analyzed. During the further assessment, the individual VNOWC chromosome plot of the discordant CNV call was first examined to determine if the call represented the integer loss or gain for the majority of

estimated copy number points within the appropriate range of windows. Secondly, the smoothed, GC corrected individual chromosome HMM CNV plot from the CHI method was analyzed to determine if the majority of the Log2 transformed values were above 0.4 for a gain or below -0.35 for a loss. Thirdly, the smoothed, GC corrected individual chromosome CBS CNV plot from the CHI method was examined to determine if the majority of the Log2 transformed values were above 1.32 for a gain or below 0.6 for a loss. If two out of these three criteria were satisfied, the CNV call was retained or otherwise, a conservative assessment was made to categorize the chromosome in question as intact and euploid. This integration of a dual-pipeline bioinformatics strategy provided higher confidence calls than using each method alone. Approximate DNA breakpoint locations were identified in rhesus macaque chromosome ideograms adapted from http://www.biologia.uniba.it/macaque/, http://www.biologia.uniba.it/primates/2-OWM/MMU/MMU, and [262].

SNP Parentage Analysis

The whole genome reads from each parent and embryonic sample were processed using a pipeline following the best practice recommendations of the Broad Institute's Genome Analysis Toolkit [GATK; [263, 264]], but adapted for macaque. Briefly, paired-end reads were trimmed using Trimmomatic adaptive quality trimming [265] and aligned to the Mmul_8.0.1 reference genome using BWA-MEM [266]. BAM post-processing included local re-alignment around indels using GATK [264], and marking of duplicate reads using Picard tools (http://broadinstitute.github.io/picard). GATK's HaplotypeCaller was used to produce gVCF files for each parent and embryonic sample, followed by joint genotype calling using GenotypeGVCFs. Parent and embryonic

samples were each joint genotyped as a separate set. SNPs located within repetitive regions that were identified using RepeatMasker [267] available from: http://www.repeatmasker.org) were removed. The sequence data was managed and analyzed using DISCVR-Seq (Bimber, B., 2015; available from: https://github.com/bbimber/discvr-seq/wiki), a LabKey Server-based system [268]. Due to the low coverage sequencing of the embryonic samples, many of the parental SNPs were observed in only one read per sample. To restrict the set of SNPs to only those of high confidence, it was required that there be at least two reads that matched either the reference or alternate allele in each embryonic sample. Furthermore, SNPs were only selected for which the two parents contained opposite homozygous genotypes, meaning all reads matched one allele in one parent and the alternative allele in the other parent. While these restrictions reduced the number of SNPs per sample, it was more reliable and informative for determining parentage in the chromosomes of each blastomere and polar body. The ratio of maternal to paternal SNPs was used to assess parental inheritance and overall ploidy for visualization by heat map via Morpheus (Broad Institute, Cambridge, MA) and histogram (Matlab R2016a). Significance of SNP parental ratios was examined by cumulative binomial test with Bonferroni correction.

Results

Experimental design for detection of aneuploidy and ploidy errors in cleavage embryos

To determine the aneuploidy frequency in disassembled rhesus macaque cleavage-stage embryos, an experimental approach was developed utilizing single-cell DNA-Seq and time-lapse monitoring (TLM) to non-invasively assess preimplantation development (**Figure 3**). Oocytes were collected over the course of 13 different IVF cycles from 13 females that underwent controlled ovarian hyperstimulation. Mature metaphase (MII) oocytes were fertilized with sperm via conventional IVF and presumed zygotes with two polar bodies and/or two pronuclei were assessed by TLM to note division and morphological parameters indicative of embryo chromosomal status. After ~24-96 hours, each cleavage-stage embryo was disassembled into blastomeres and polar bodies if still present. Samples from 43 whole embryos were individually isolated for PCR-based whole genome amplification and DNA-Seq. Mapped reads were assessed by chromosomal copy number variation (CNV) analysis for aneuploidy detection and single nucleotide polymorphism (SNP) assessment to determine the parental origin of chromosomes.

Chromosomal copy number calling in single embryonic cells

Samples that were successfully amplified were pooled for multiplex sequencing where up to 300 samples were sequenced in one run. Across all successfully sequenced libraries, the average number of filtered and uniquely mapped sequencing reads obtained from

individual polar bodies and blastomeres was 0.6 and 1.2 million, respectively. To determine chromosomal copy number, a bioinformatics pipeline was developed to compare read counts in contiguous windows across the genome between embryonic cells and a known rhesus macaque female euploid (42,XX) fibroblast control (**Figure 4A**) using a combination of Variable Non-Overlapping Windows and Circular Binary Segmentation (CBS) called VNOWC. Before applying this approach to embryos, the pipeline was trained and tested on a rhesus macaque male euploid (42,XY) cell line (**Figure 4A**) as well as human fibroblasts carrying known aneuploidies (trisomy 21 or monosomy X) (**Figure 4B**) to calculate the window coordinates. The number of uniquely mapped reads from rhesus macaque and human fibroblast samples were 0.9 and 1.1 million, respectively. The VNOWC bioinformatics pipeline was able to successfully detect both chromosome losses and gains in all rhesus macaque and human fibroblast samples, including single cells (**Figure 4C**). The false discovery rate for the VNOWC pipeline was simulated for 3200 runs using reads from human monosomy X and trisomy 21 cells, where reads from trisomy 21 cells on average revealed several unexpected CNV calls for whole and segmental aneuploidies. In contrast, the monosomy X simulation had no unexpected CNVs when windows were sizes to contain 2000 and 4000 reads (**Figure 4D & E**). A previous study has also reported high false discovery rates when assessing CNVs with CBS but improved calling confidence when intersected with a Hidden Markov Model (HMM) [261]. Therefore, to validate the chromosome profiles for each sample and provide higher confidence CNV calling, a second bioinformatics pipeline was employed that utilized the intersection of copy number calls in variable sized windows by both CBS and HMM called the CBS/HMM Intersect (CHI) method. Overall, most CNV calls were shared between both pipelines (N=105/151; 69.5%) however discordant CNV calls detected between the VNOWC (N=33/151; 21.9%) and CHI methods (N=13/151; 8.6%) were mostly due to differences in sub-chromosomal variation (**Figure 4F**). Discordant calls were further analyzed based on

recently described criteria [253], and conservatively estimated that 58.1% (N=25/43) of the chromosomes in question were affected by aneuploidy.

Rhesus macaque cleavage-stage embryos are often aneuploid and mosaic due to mitotic errors

Using the dual-pipeline bioinformatics strategy, the chromosomal status of 423 individual samples from 43 rhesus macaque cleavage-stage embryos were evaluated. Of these embryos, 42 contained amplifiable DNA as determined by high mitochondrial (mtDNA) read counts and were fully sequenced up to the 14-cell stage for CNV calling (**Figure 5A**). This included a surprisingly large proportion (N=38/206) of what were later confirmed to be polar bodies by SNP analysis (described below) and assisted in the determination of meiotic versus mitotic errors (**Table 2**). Each blastomere or polar body was classified as euploid or aneuploid and the type of aneuploidy further characterized in embryos by the following criteria: (1) Meiotic errors were primarily identified by the presence of an aneuploid polar body. In the absence of polar bodies or presence of only one euploid polar body, aneuploidy was considered meiotic if the same chromosome was lost or gained in all sister blastomeres. (2) Mitotic errors were defined as different and/or reciprocal chromosomal losses and gains between blastomeres with euploid polar bodies if present. (3) Chaotic aneuploidy was determined as greater than five whole or segmental chromosomes affected in at least one blastomere where chromosome distribution amongst cells appeared unconstrained and random as previously described [1]. Based on the above criteria, 28.6% (N=12/42) of the embryos were comprised of only euploid blastomeres with no chromosomes affected, whereas 71.4% (N=30/42) of the embryos contained one or more aneuploid blastomeres (**Figure 5A & B**). Further analysis of the

aneuploid embryos revealed that 47.6% (N=20/42) consisted of either completely aneuploid blastomeres, whereas 23.8% (N=10/42) exhibited euploid-aneuploid mosaicism. The inheritance of meiotic errors (30%, N=9/30) and the occurrence of solely mitotic errors (30%, N=9/30) was confidently called in embryos, with the remaining 40% (N=12/30) either incurring both types of errors or unknown due to the complexity of chromosomal mosaicism. The incidence of chaotic aneuploidy in one or more blastomeres of embryos was 33.3% (N=14/42). Interestingly, this appeared to be mostly confined to embryos fertilized by a particular sperm donor (N=11/14) regardless of which female was used for IVF, suggesting paternal contribution to this type of chromosomal abnormality. Additionally, the gender ratio was equal with 21 of 42 embryos having a Y sex chromosome (**Figure 5A**). Representative examples of genome-wide chromosomal CNV plots from embryos with euploid, mosaic, aneuploid, and/or chaotic aneuploid blastomeres are shown in **Figure 5C**.

Reciprocal sub-chromosomal deletions and duplications are indicative of chromosome breakage

Besides whole and sub-chromosomal abnormalities, 10% (N=3/30) of the aneuploid embryos also contained blastomeres with chromosomes that underwent an unbalanced break, for which the reciprocal chromosome segments were found within a sister blastomere (**Figure 6A**). These regions were examined further and determined that the breakpoints often localized near heterochromatic regions of existing centromeres, inactivated ancient centromeres, or in the case of chromosome 10, the nucleolus organizer region [262]. Note that this region of chromosome 10 is adjacent to the centromere and corresponds to the fission breakpoint between the chromosomal region

homologous to human 10p and chromosomes 12 and 22 in the common primate ancestor [269]. The frequency of whole, segmental, and small sub-chromosomal (<15Mb) CNVs was then assessed for each chromosome (**Figure 6B**). Excluding chaotic aneuploid samples, chromosomes 1 and 2 were the most highly susceptible to segmental aneuploidy, while chromosome 19 experienced the greatest incidence of whole chromosomal instability. However, whole chromosome 19 losses and gains change to large segmental CNVs when the windows were reduced from 4000 to 2000 read counts. This inconsistency is likely due to high GC content in this chromosome, combined with low coverage sequencing as previously reported for human chromosome 19 [261]. In contrast, chromosome 20 [corresponding to chromosome 16 in humans) [270, 271]], was the least frequently affected by aneuploidy. Of note, blastomeres with large segmental CNVs were predominantly located at the terminal ends of chromosomes (N=33/37), indicating that chromosomal breakage-fusion-bridge (BFB) cycles likely occur in rhesus macaque embryos as described for human embryos [26].

SNP analysis confirms polar body identity and equivalent parental contribution to aneuploidy

It is generally accepted that polar bodies degenerate within 24 hours of extrusion from the oocyte or zygote [272], but unexpectedly a large proportion of polar bodies originally thought to be cellular fragments were identified in several embryos beyond the 2- to 4-cell stage (**Figure 7A**). To validate their identity, DNA was isolated from each of the parents and sequenced for comparison of maternal versus paternal SNPs in all embryonic samples. Although this approach prevented highly confident genotyping of individual SNPs, combining the data across the chromosome for numerous SNPs provided greater

assurance in SNP calling than each SNP alone. As shown in **Figure 7A**, the proportion of maternal SNPs was significantly different ($p<2.35x10^{-4}$, binomial test) from the expected 50%, with greater than 79% on average of SNPs in presumptive polar bodies identified as maternal in origin. While both polar bodies were obtained from only ~21% (N=9/42) of the embryos and primarily at the early cleavage stages, ~74% (N=28/38) of those isolated were euploid. This supports the finding that mitotic errors are either equally or more prevalent than meiotic errors in embryos from rhesus macaque females of average maternal age.

After confirming the identity of polar bodies, SNP genotyping was used to assess the parental origins of all chromosomes in each blastomere (**Figure 7B**) using an approach similar to that described for human embryos [273]. While the majority of embryos with euploid chromosomes (75%; N=9/12) were equally biparental in origin, the SNP analysis showed that two of the embryos contained blastomeres with chromosomes that were entirely from the mother (embryos 8 and 25). SNP genotyping also revealed at least one case of a paternally contributed meiotic error (embryo 15; chromosome 1 monosomy). Unexpectedly, although all zygotes in this study were confirmed to have either 2 polar bodies and/or 2 pronuclei, a significant proportion of embryos had abnormal ploidies. The proportion of embryos that were biparental (N=20/38), maternal-only (gynogenetic; N=5/38), paternal-only (androgenetic; N=1/38), polyploid (N=9/38), had a mix of biparental and uniparental or triploid cells (mixoploid; N=3/38) is shown by histogram in **Figure 7C** and via heat maps (**Figure 8**). Further analysis confirmed the uniparental inheritance of gynogenetic and androgenetic embryos and suggested that polyploid embryos were triploid with two copies of maternal chromosomes and one copy of each paternal chromosome (**Figure 7D**).

Multipolar divisions often lead to chromosome loss and chaotic aneuploidy

A number of the embryos sequenced in this study displayed multipolar divisions at the 1- or 2-cell stage of preimplantation development as detected by TLM analysis (N=13/42). In addition to the sequenced embryos reported here, for all dividing embryos cultured in our lab up until March 2017, 23.2% (N=42/181) underwent a multipolar division at the 1- or 2-cell stage. Moreover, some of the zygotes that underwent a multipolar division were noticeably speckled in appearance reminiscent of multiple MTOCs in mouse zygotes that undergo acentrosomal spindle assembly [155] and aster-like structures in human MI and MII oocytes [274] (**Figure 9**). When higher order mitotic divisions were evaluated in all embryos, only one of the 14 sequenced embryos with multipolar divisions was euploid, while the remaining embryos exhibited varying degrees of chromosomal abnormalities, with chaotic aneuploidy being the most prevalent in 57% (N=8/14) of the cases (**Figure 10A**). Notably, chaotic aneuploidy was observed in almost every blastomere in each of these eight embryos following multipolar divisions as demonstrated by the example in **Figure 10B**. Additionally, more than half of the embryos (N=6/10) with at least one empty blastomere (**Figure 5A**) had undergone multipolar divisions at the 1- or 2-cell stage. SNP analysis of parental ratios confirmed that multipolar divisions most often result in chaotic aneuploidy (**Figure 10C**) and all chaotic multipolar embryos originated from the same sperm donor, suggesting paternal contribution to this type of chromosomal abnormality (**Figure 11**). Also using SNP analysis for whole embryo ploidy determination, 71.4% of embryos that had a multipolar division were either mixoploid (N=1), gynogenetic (N=4), or triploid (N=5) where embryos were digynic with one paternal set of chromosomes.

In another notable multipolar embryo (**Figure 10D**), loss of one copy of chromosomes 4, 8, and 16 was detected in three blastomeres and the reciprocal three copies of these chromosomes were identified in two other blastomeres from the same embryo (**Figure 10E** & **F**). Based on the 3:1 chromosomal ratios, this indicates that chromosome lagging or mitotic nondisjunction occurred early in development and likely during the tripolar division observed at the zygote stage, which was propagated by subsequent bipolar divisions. However, the blastomeres with the chromosomal 4, 8, and 16 gains also exhibited only a single copy of chromosome 19 and uniparental disomy or complete loss of chromosome 15 (blastomere 5, 9, and 10, respectively). Missing chromosomes 15 and 19 were detected in additional cells (blastomere 3, 7, and 8) isolated from this embryo that appeared unusual in shape and size upon disassembly (**Figure 10E** & **F**). By employing SNP parentage analysis, the losses of chromosome 15 and 19 in these blastomeres were confirmed to be a nondisjunction event. This is based on findings of only paternal chromosomes 15 and 19 in blastomeres 3, 7, and 8, and the corresponding maternal chromosomes in blastomeres 5, 9, and 10 as well as biparental contribution of these chromosomes in blastomeres 1, 2, and 4 (**Figure 10G**), all of which is depicted in the embryo schematic shown in **Figure 10H**. Since multipolar divisions frequently result in asymmetrical segregation of chromosomes in other cell types [275] and the observed correlation of empty blastomeres and higher order divisions, these findings suggest that multipolar divisions further propagate chromosomal instability in embryos.

Discussion

It is now well established that human IVF embryos have a high incidence of aneuploidy which often leads to implantation failure and early embryo loss during pregnancy. While difficult to ascertain, aneuploidy is also thought to be largely responsible for spontaneous miscarriages following natural conceptions [13-16] and may explain cases of idiopathic infertility in the human population [276]. This generally does not occur in mouse embryos, which require chemical induction to achieve aneuploidy at a frequency similar to humans [20]. Unlike mice, both women and female rhesus macaques are monovular species, typically ovulating only one mature oocyte-containing follicle per month, and undergo similar menstrual cycles [277]. Moreover, human and rhesus macaque embryos share other key characteristics distinct from the mouse, including the developmental stage at which the major wave of EGA occurs and the typical percentage of embryos that will successfully reach the blastocyst stage [123, 278-280]. An examination of pregnancy success in the rhesus macaque time-mated breeding colony at the Oregon National Primate Research Center during a similar timeframe as this study (November-May; 2013-2017) revealed that, of the confirmed ovulation and mating cases, only 26.5% (N=72/272) resulted in a live birth to suggest a similar correlation between *in vitro* and *in vivo* conceptions as humans.

In this chapter, single-cell whole-genome sequencing was used to examine all blastomeres and polar bodies of 42 cleavage stage embryos. This assessment was carried out with an in-house built CNV pipeline called VNOWC. Although CNV calls were very accurate, there were evident false positives present in samples with sparser sequencing. To gather an estimate of the frequency of false positive calls, reads from the human trisomy 21 and monosomy X 10-cell pool fibroblast samples were simulated

through 1600 runs each for varying window sizes and number of mapped reads (**Figure 4D & E**). As expected, with increasing window sizing, the number of false positives for whole and segmental aneuploidies decreased but only for the monosomy X samples. The trisomy 21 samples had more false positive CNV calls that fluctuated with increased window sizes. To explain these results for the trisomy 21 sample, it is possible that real whole and segmental aneuploidies were present in the 10-cell pool but went undetected due to mosaicism. It is well known that cultured cells will develop aneuploidies with passaging, so the rhesus macaque and human fibroblast cells used to develop the VNOWC pipeline were karyotyped. Both the human monosomy X and trisomy 21 fibroblasts were stable with less than 6% of cells having additional aneuploidies, specifically chromosome losses which were likely the result of slide preparation artifacts. Since karyotyping results did not help explain the higher than expected false positives of trisomy 21 fibroblasts, all CNV calls from the VNOWC pipeline were cross referenced with the CHI CNV pipeline to confidently call CNVs in embryonic samples.

Overall, CNV analysis of 42 cleavage-stage rhesus macaque embryos demonstrated that macaques and humans also have high embryonic aneuploidy frequencies in common (73% vs. 50-80%, respectively). To note, in this study, whole chromosome aneuploidies were not observed for rhesus macaque chromosome 20 in non-chaotic, aneuploid blastomeres (**Figure 6B**). The low aneuploidy rate seen for chromosome 20 may explain why a greater number of euploid embryos were reported in previous rhesus macaque cytogenetic DNA-FISH studies that included probes for human chromosome 16 (rhesus macaque chromosome 20) [23-25]. In addition to whole aneuploidies, segmental aneuploidies were also frequent (**Figure 6B**) and represented large segmental losses, duplications, and amplifications in blastomeres at the terminal ends of chromosomes, a finding that is supported by terminal imbalances and extensive post-meiotic chromosomal

rearrangements known as breakage-fusion-bridge cycles in human embryos [26]. Embryos were also assessed for ploidy errors with SNP genotyping to determine chromosome parentage. Surprisingly, ploidy errors were common in this study, as ~47% of embryos were not entirely biparental. A major disadvantage with the study design was that very few sperm donors provided the paternal half of the genome for embryos. Only 5 males were used for the 13 IVF cycles reported in the CNV analysis part of the study. For the SNP analysis, to determine the ploidy of 38 embryos, only 3 males were used. Since the centrosome from the sperm sets up the first cell divisions of the cleaving embryo, the repeated utilization of only 3 males skews the results to errors that are more likely to be derived from defects created by the sperm.

Even still, there are very few studies that examine the frequency of ploidy errors in conjunction with aneuploidy detection in embryos. In the fertility clinic, embryos with ploidy errors are often avoided by performing intracytoplasmic sperm injection to ensure that only one sperm fertilizes an MII oocyte. Embryologist also confirm biparental contribution to human zygotes by detecting the presence of two polar bodies and two pronuclei. In this study, rhesus macaque zygotes were also required to have two polar bodies however the presence of two pronuclei was not detected in every embryo as some zygotes underwent syngamy before they were checked in the morning following conventional IVF. Nonetheless, abnormal ploidy was detected in rhesus macaque embryos that satisfied the same criteria used in human fertility clinics. This extent of ploidy errors in conjunction with CNV errors has been reported in bovine using in-vitro matured oocytes [21]. Studies examining ploidy and CNV status for the same embryo have not been conducted extensively in human embryos to determine how frequently this happens. With this in mind, the ploidy status of zygotes produced by conventional IVF should be interpreted with a degree of caution as the presence of 2 polar bodies and/or two pronuclei was

insufficient for discerning ploidy in some cases. On that premise, the methods presented here for examining ploidy and CNVs in the same embryo provides a new approach to broaden PGS platforms through sequencing by incorporating SNP genotyping when the parental DNA is available. Along with the prevalence of uniparental disomy in human embryo studies [26], a better understanding of ploidy errors within the embryo may help explain why seemingly normal euploid embryos fail to implant [281].

Multipolar divisions were also observed in this study at the zygote or 2-cell stage and happened more frequently than in human embryos, at least for the few studies that have reported this event [77, 282]. Interestingly, several embryos that underwent a multipolar division in this study did not have extensive fragmentation (discussed in chapter 2) and often appeared to have normal morphology and even blastomere size (**Figure 10B**). This finding would indicate that static morphological assessment of embryos cannot detect multipolar divisions and that TLM is required to distinguish normal, non-fragmented cleavage-stage embryos from those that likely have errors resulting from a multipolar division. The most prevalent type of chromosomal abnormality observed in multipolar embryos was chaotic aneuploidy and all of these embryos shared a common sperm donor. Because the centrosome for the first mitotic division(s) is paternally inherited in most mammalian species except rodents [283, 284], this indicates that aberrant or supernumerary centrosomes from the sperm likely contributed to multipolar divisions. Curiously, one multipolar embryo was mixoploid, containing a mix of biparental and androgenetic blastomeres. Although the zygote of this embryo had 2 polar bodies, it is possible that three pronuclei were present but went undetected. A scenario for how this mixoploid embryo was generated could be that two sperm fertilized the oocyte resulting in 2 male pronuclei and 1 female pronucleus. As a result of the two centrosomes deposited,

the zygote underwent a multipolar division after syngamy of one male and one female pronucleus where the second male pronucleus was partitioned into its own blastomere.

Upon observing tripolar divisions at the zygote stage, it was anticipated that most these embryos would be triploid resulting from polyspermy. However, this was not the case. Of the multipolar embryos that were polyploid, a 60-75% ratio of maternal SNPs to paternal SNPs was always observed indicating these embryos were digynic triploids with one paternal set of chromosomes. Other findings that merit discussion are that gynogenetic and biparental embryos also had multipolar divisions, indicating that sperm centrosome duplications or defects are not necessary for multipolar division to occur. Gynogenetic and triploid embryos also often exhibit supernumerary centriole pairs and multipolar spindles [167, 285]. In some zygotes, what appeared to be distinct puncta for MTOCs were detected in some gynogenetic and triploid embryos that underwent a multipolar division (**Figure 9**). These puncta were consistent with MTOCs seen during multipolar spindle formation in another study where mouse embryos use this process for the first cell divisions [155]. Since the centrosome-depositing sperm is also responsible for oocyte activation via calcium oscillations during fertilization [150, 151], it seems likely that premature oocyte activation and/or defective centrosome inheritance from the father may also contribute to the multipolar divisions observed in gynogenetic and digynic triploid embryos.

Overall, the findings presented here not only confirm that the rhesus macaque embryo is similar to the human in terms of a high aneuploidy frequency but also demonstrates the utility of single cell sequencing and time-lapse imaging for studying causes and consequences of aneuploidy and ploidy errors at this stage.

Paired-end 150bp Blastomeres (N=29)								
Raw reads	**Read length**	**% GC**	**Reads post trimming**	**Trimmed & deduplicated**	**mapped**	**pass Q30**	**Unique mapping positions**	
4,579,692.00	35-150	44.59	3,567,220.07	3,552,733.10	3,517,620.10	3,237,942.00	2,427,136.21	avg.
2,537,386.22	35-150	0.87	1,591,431.34	1,582,714.13	1,559,103.89	1,406,019.91	1,180,587.32	std. dev.
Single-end 75bp Blastomeres (N=139)								
Raw reads	**Read length**	**% GC**	**Reads post trimming**	**Trimmed & deduplicated**	**mapped**	**pass Q30**	**Unique mapping positions**	
2530976.755	55.96	41.58	2,461,793.04	1,800,188.60	1,419,676.28	1,196,124.78	1,044,505.79	avg.
1536725.046	1.00	0.75	1,479,438.55	1,039,125.40	1,147,964.39	965,430.40	846,093.14	std. dev.
Paired-end 150bp Polar Bodies (N=4)								
Raw reads	**Read length**	**% GC**	**Reads post trimming**	**Trimmed & deduplicated**	**mapped**	**pass Q30**	**Unique mapping positions**	
2,856,618.50	150.00	44.75	2,303,146.00	2,294,064.00	2,264,921.00	2,127,426.75	1,908,039.25	avg.
2,187,016.89	0.00	0.96	1,608,668.77	1,598,895.84	1,596,803.36	1,510,886.02	1,431,205.95	std. dev.
Single-end 75bp Polar Bodies (N=34)								
Raw reads	**Read length**	**% GC**	**Reads post trimming**	**Trimmed & deduplicated**	**mapped**	**pass Q30**	**Unique mapping positions**	
936,714.79	56.70	41.39	910,916.12	814,811.52	499,811.48	440,753.18	408,524.55	avg.
799,727.74	0.73	0.66	786,779.52	641,007.08	666,038.51	562,754.21	507,440.18	std. dev.

Table 1. *Average sequencing statistics for blastomeres and polar bodies*

Summary of Copy Number States for Sequenced Cleavage-Stage Embryos														
IVF Experiment	Maternal ID	Paternal ID	sequenced	Failed Amp	Euploid	Aneuploid	Chaotic Aneuploid	Euploid-Aneuploid Mosaicism	Embs. w/ Euploid PB(s)	Embs. w/ Aneuploid PB(s)	Embs. w/ Euploid & Aneuploid PB	Embs. PB(s) not detected	Meiotic Origin of Aneuploid Blastomeres	Mitotic Origin of Aneuploid Blastomeres
Experiment 1	29597	24519	1	0	0	0	0	1	0	0	0	1	0	0
Experiment 2	23959	24583	2	0	0	0	1	1	1	1	0	0	1	1
Experiment 3	26129	28281	1	0	0	0	1	0	0	0	0	1	0	0
Experiment 4	28797	24583	5	0	2	0	0	3	4	0	0	1	0	3
Experiment 5	22644	26028	2	0	0	1	0	1	1	0	0	1	0	1
Experiment 6	25710	24583	6	1	0	2	0	3	2	0	0	3	1	1
Experiment 7	25194	26028	4	0	0	1	3	0	0	1	0	3	1	0
Experiment 8	25490	26028	4	0	0	0	4	0	0	2	0	2	2	0
Experiment 9	29328	26848	1	0	1	0	0	0	1	0	0	0	0	0
Experiment 10	25636	26848	2	0	2	0	0	0	2	0	0	0	0	0
Experiment 11	24903	24583	7	0	4	1	1	1	6	1	0	0	1	2
Experiment 12	29251	26848	4	0	3	1	0	0	3	0	1	0	0	1
Experiment 13	25567	26028	4	0	0	0	4	0	0	3	0	1	3	0
		total(s)	43	1	12	6	14	10	20	8	1	13	9	9

Table 2. *Summary of copy number states for sequenced cleavage-stage embryos*

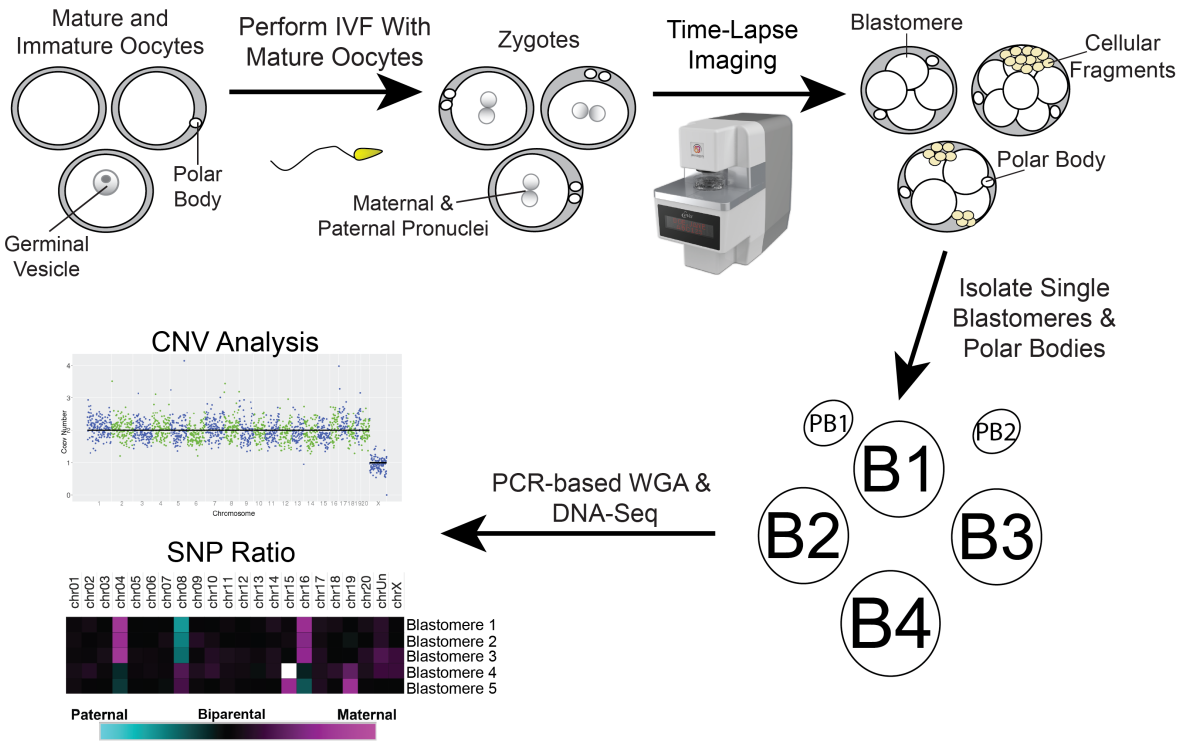

Figure 3. *Approach for assessing CNVs and chromosome parentage in embryos.* Mature and immature oocytes were obtained from reproductive-age female rhesus macaques undergoing controlled ovarian stimulation. MII oocytes displaying one polar body were fertilized by conventional IVF with sperm from reproductive-age males. Early mitotic divisions of presumptive zygotes identified by two pronuclei and/or two polar bodies were monitored by time-lapse imaging. Cleavage-stage embryos were disassembled into individual blastomeres and polar bodies. Single cells underwent PCR-based whole genome amplification (WGA) and mapped reads were analyzed by DNA-sequencing for copy number variation (CNV) and single nucleotide polymorphism (SNP) assessment.

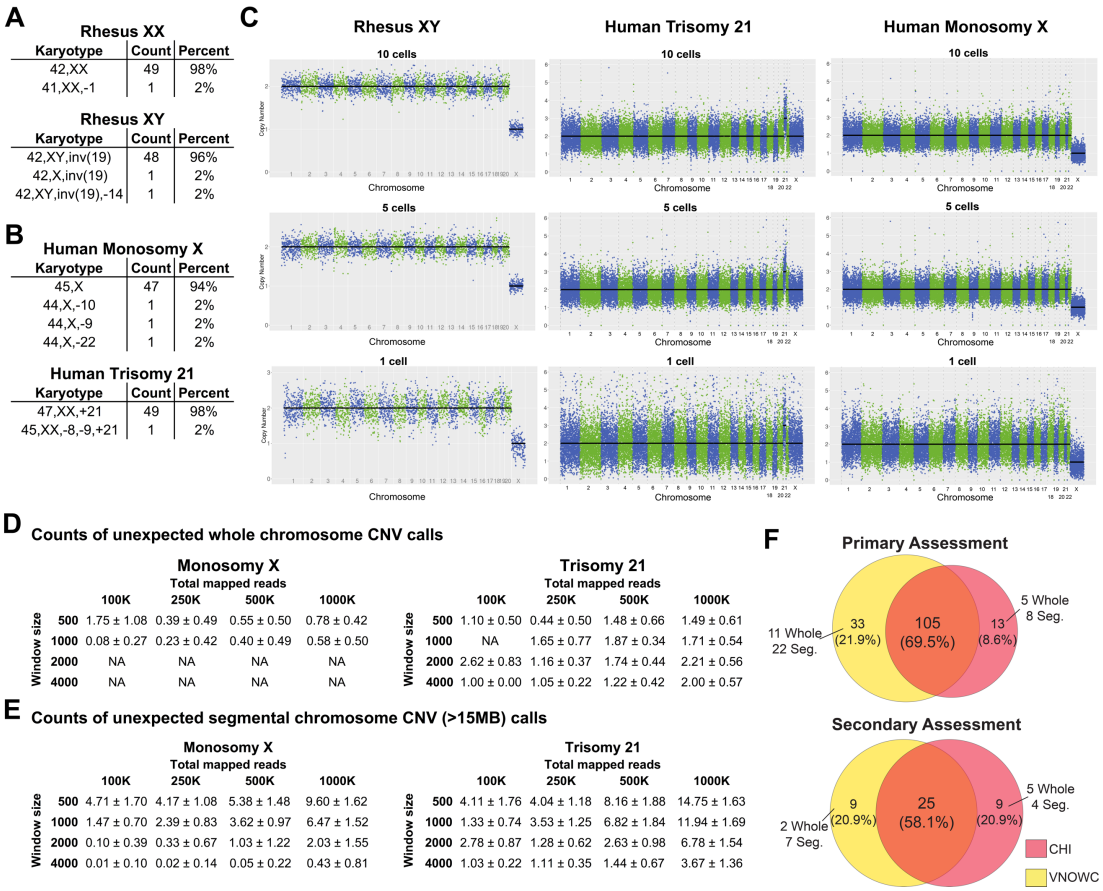

Figure 4. *Single cell CNV pipeline development.*

Karyotyping results of 50 metaphase spreads for (**A**) rhesus macaque XX passage 3 fibroblasts, rhesus macaque XY passage 3 fibroblasts, (**B**) human monosomy X passage 6 fibroblasts, and human trisomy 21 passage 9 fibroblasts. (**C**) Chromosome CNV plots from 10-, 5-, and 1-cell rhesus macaque male fibroblasts (42,XY) and human female fibroblasts with known trisomy 21 (47,XX) or monosomy X (45,X). Simulated (**D**) whole and (**E**) segmental chromosome false discovery counts for 10-cell trisomy 21 (47,XX) or monosomy X (45,X) samples where mapped reads were sub-sampled down to 100K, 250K, 500K, and 1000K across 500, 1000, 2000, and 4000 reads per window. (**F**) Venn diagrams depicting the numbers and percentages of overlap (orange) versus discordant

CNV calls between VNOWC (yellow) and CHI (pink) CNV pipelines following primary and secondary assessment of whole and segmental (seg.) aneuploidies.

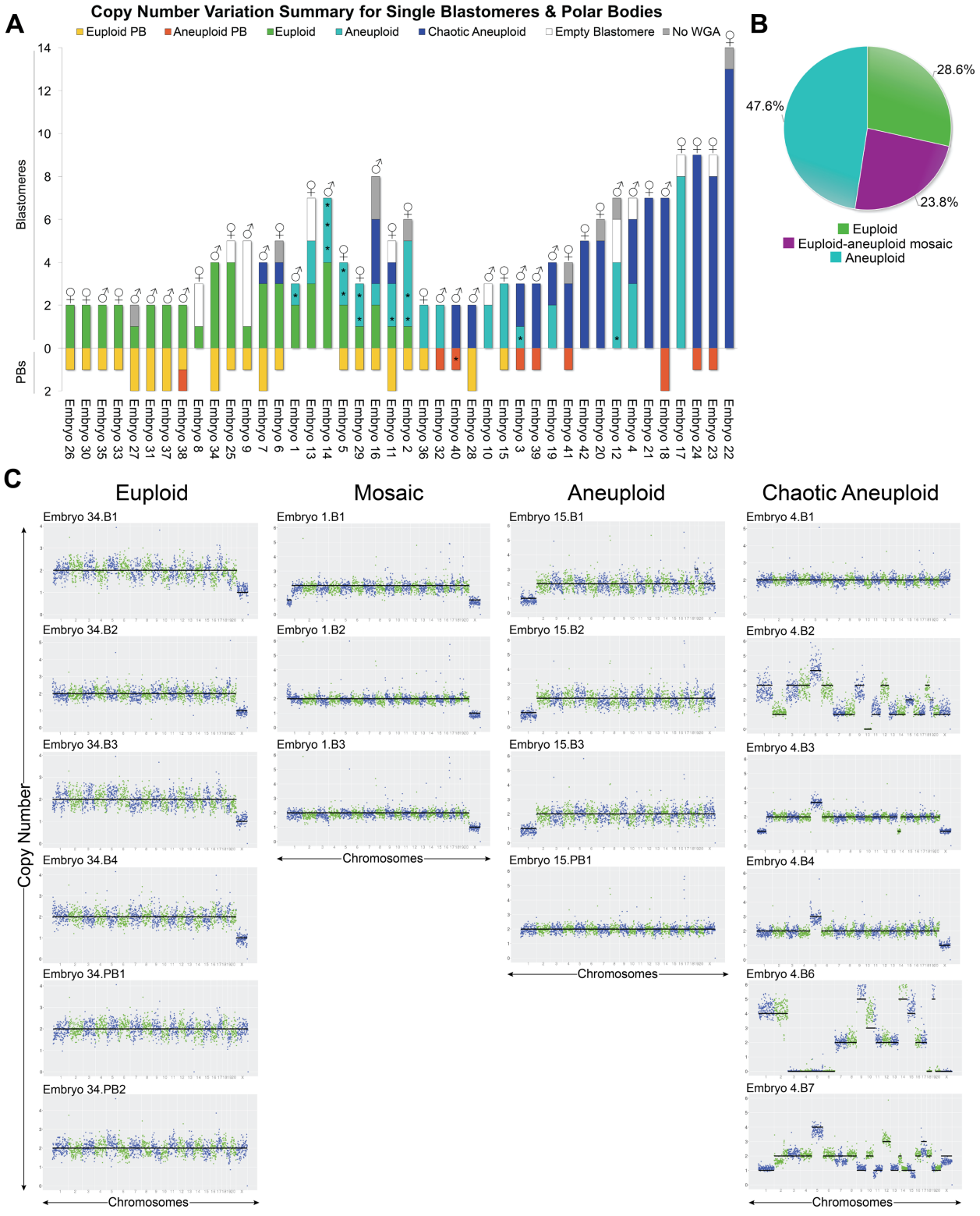
A
Copy Number Variation Summary for Single Blastomeres & Polar Bodies
Euploid PB
Aneuploid PB
Euploid
Aneuploid
Chaotic Aneuploid
Empty Blastomere
No WGA
Blastomeres
PBs
Embryo 26
Embryo 30
Embryo 35
Embryo 33
Embryo 27
Embryo 31
Embryo 37
Embryo 38
Embryo 8
Embryo 34
Embryo 25
Embryo 9
Embryo 7
Embryo 6
Embryo 1
Embryo 13
Embryo 14
Embryo 5
Embryo 29
Embryo 16
Embryo 11
Embryo 2
Embryo 36
Embryo 32
Embryo 40
Embryo 28
Embryo 10
Embryo 15
Embryo 3
Embryo 39
Embryo 19
Embryo 41
Embryo 42
Embryo 20
Embryo 12
Embryo 4
Embryo 21
Embryo 18
Embryo 17
Embryo 24
Embryo 23
Embryo 22
B
28.6%
47.6%
23.8%
Euploid
Euploid-aneuploid mosaic
Aneuploid
C
Euploid
Mosaic
Aneuploid
Chaotic Aneuploid
Copy Number
Embryo 34.B1
Embryo 34.B2
Embryo 34.B3
Embryo 34.B4
Embryo 34.PB1
Embryo 34.PB2
Embryo 1.B1
Embryo 1.B2
Embryo 1.B3
Embryo 15.B1
Embryo 15.B2
Embryo 15.B3
Embryo 15.PB1
Embryo 4.B1
Embryo 4.B2
Embryo 4.B3
Embryo 4.B4
Embryo 4.B6
Embryo 4.B7
Chromosomes

Figure 5. *Assessment of whole and sub-chromosomal aneuploidies in single blastomeres and polar bodies.*

(A) Summary of CNV in rhesus macaque embryos (N=42) from the 2- to 14-cell stage analyzed by single-cell DNA-Seq. Stacked bars represent euploid (yellow) and aneuploid (orange) polar bodies; euploid (green), aneuploid (light blue), and chaotic aneuploid (dark blue) blastomeres; no WGA (gray); and empty blastomeres (white) detectable by mtDNA read counts, but no genomic DNA. N= 231 samples. Blastomeres and polar bodies classified as aneuploid that only contained broken chromosomes are labeled with an asterisk (*). ♂: Y chromosome present ♀: Only X chromosome(s) present. (**B**) Overall percentage of 42 embryos with euploidy, aneuploidy, or mosaicism. (**C**) CNV plots from representative examples of embryos categorized as euploid, euploid-aneuploid mosaic, aneuploid, or chaotic aneuploid.

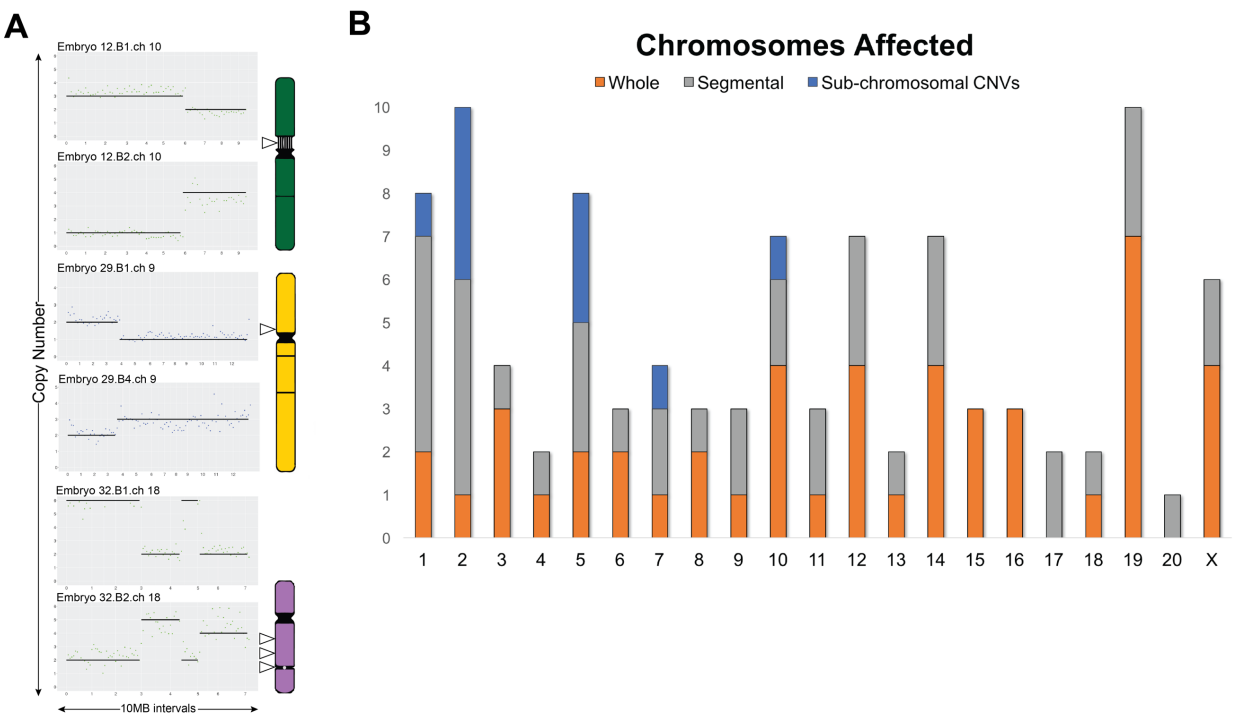

Figure 6. *Copy number variations per chromosome and reciprocal breaks.*

(**A**) The CNV plots of three embryos, in which broken chromosomes resulted in a reciprocal loss and gain of chromosome segments between two blastomeres (left). Rhesus macaque chromosome ideograms showing the approximate breakpoint locations (arrowheads; right) with horizontal lines representing conserved breakpoints between human and rhesus macaque syntenic regions and the vertical lines in chromosome 10 delineating the heterochromatic nucleolus organizer region adjacent to the centromere. The light gray circle in chromosome 18 designates the ancestral inactivated centromere location, which overlapped the reciprocal breakpoint in blastomeres 1 and 2. (**B**) Stacked bar chart representing whole (orange) or segmental (gray) chromosome CNVs observed in all non-chaotic aneuploid samples. The frequency of small sub-chromosomal CNVs (<15MB) is also shown for each chromosome (blue). B, blastomere; PB, polar body; ch, chromosome.

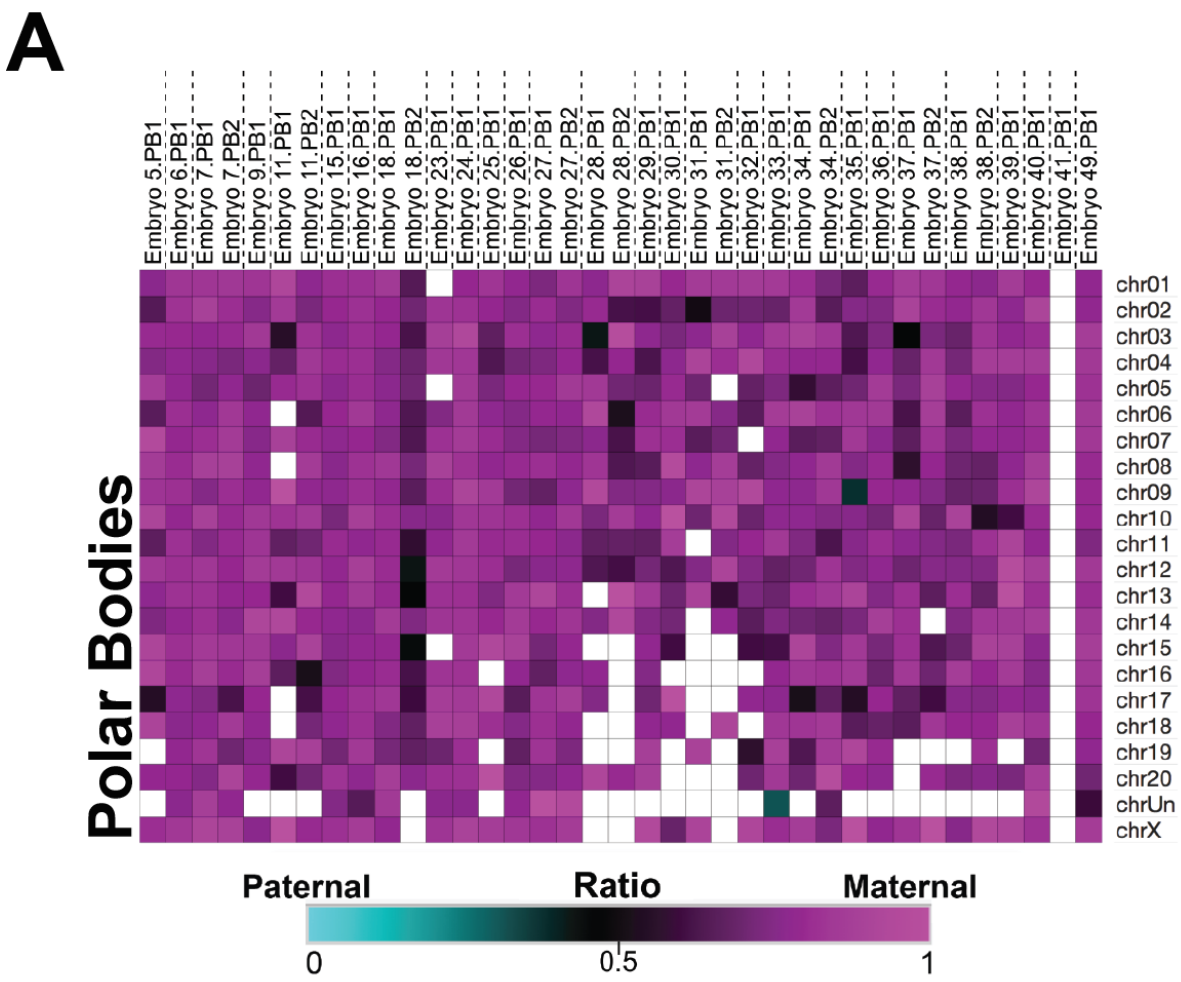

Figure 7. *SNP profiling confirms polar bodies and reveals the complexity in parental contribution to aneuploidy*.

(A-B) Heat maps of the SNP parentage ratios in all samples. Each embryo is separated by vertical dotted lines. Pink boxes indicate maternal, blue boxes paternal, and black boxes represent biparental inheritance. White boxes show that either the chromosome was not detected in a sample or it could not be called with high confidence. **(A)** The ratio of parental SNPs in presumptive polar bodies confirmed that they were predominantly maternal in origin.

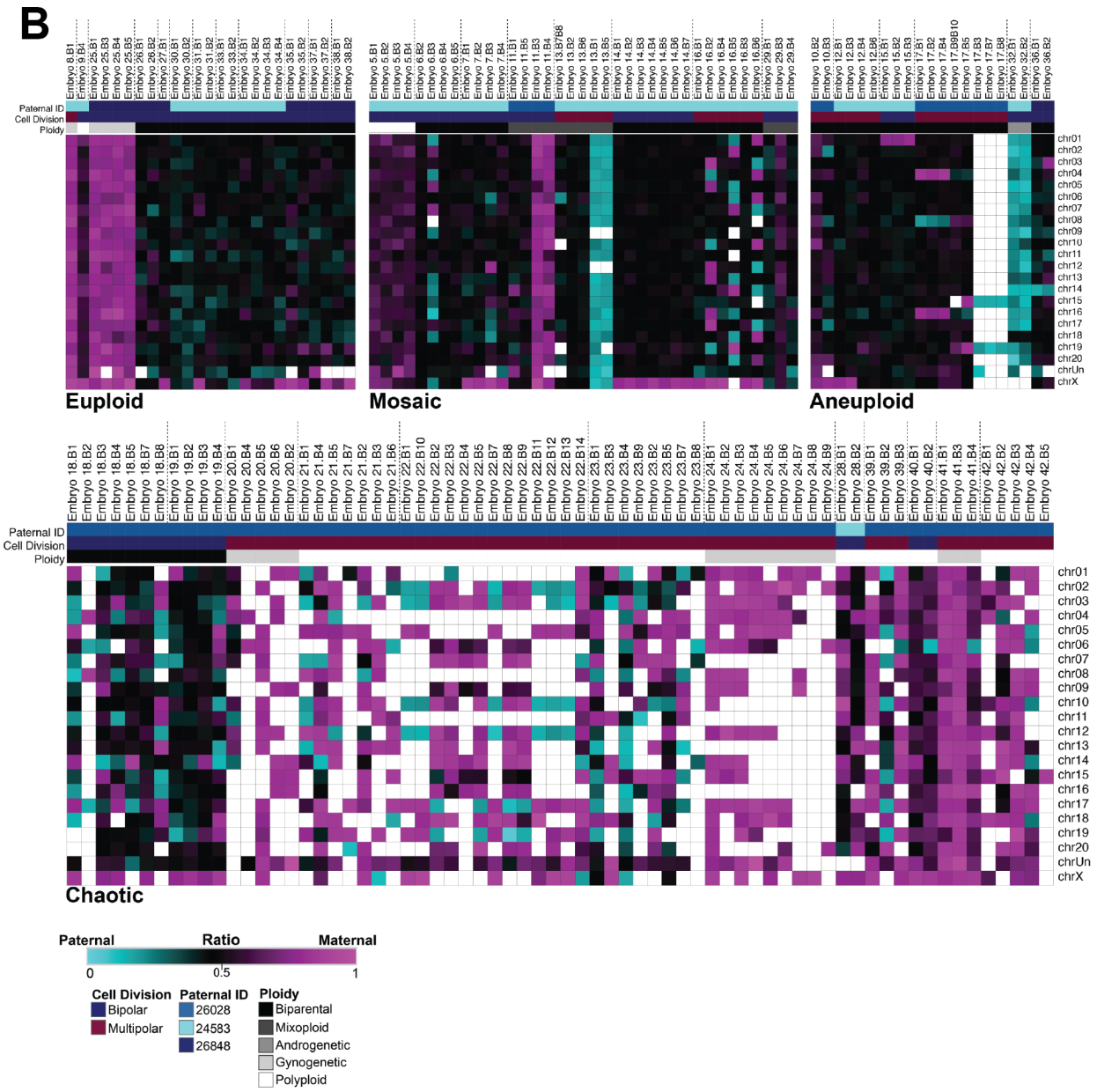

Figure 7. *SNP profiling confirms polar bodies and reveals the complexity in parental contribution to aneuploidy*.

(B) Maternal versus paternal SNP analysis of euploid, aneuploid, a mixture of euploid and aneuploid blastomeres (mosaic), or chaotic aneuploid embryos. Samples were further sorted based on the paternal donor, cell type, mitotic divisions, and copy number status, which uncovered at least one instance of a paternally contributed meiotic error in chromosome 1.

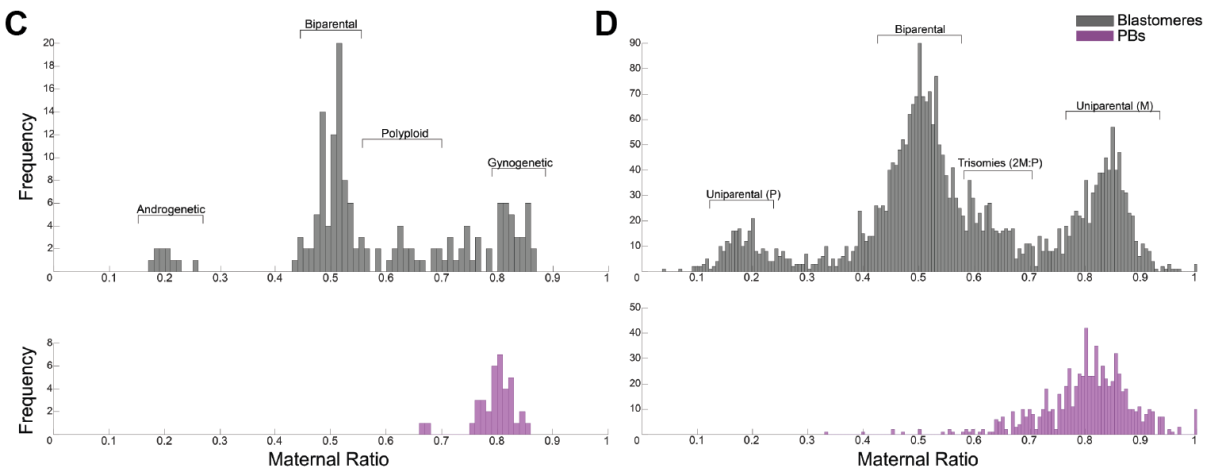

Figure 7. *SNP profiling confirms polar bodies and reveals the complexity in parental contribution to aneuploidy*.

(C-D) Histograms showing the distribution of SNP ratios across blastomeres (dark gray) and polar bodies (pink). **(C)** The frequency of SNPs ratios in each sample showed that the majority of rhesus macaque embryos were biparental, but a proportion of androgenetic, gynogenetic, polyploid, and mixoploid embryos were also observed. **(D)** SNPs ratios further stratified into individual maternal versus paternal chromosome number confirmed uniparental or biparental inheritance.

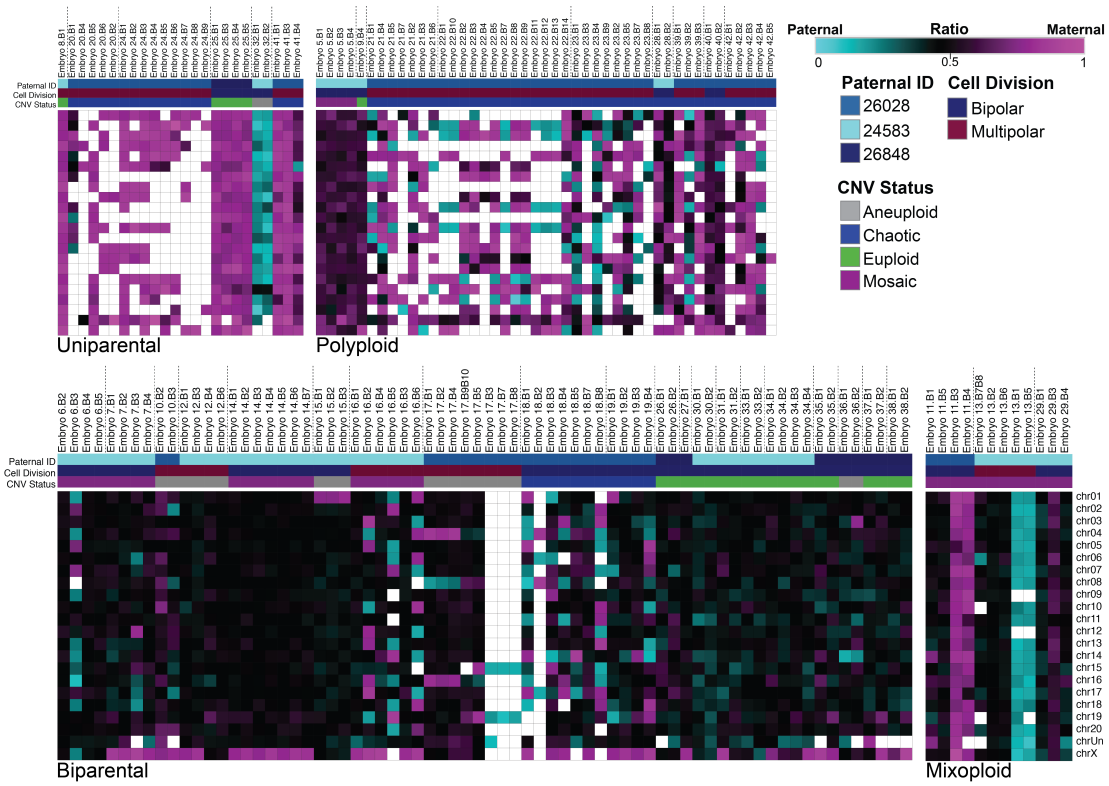

Figure 8. *Use of SNP genotyping to determine embryo ploidy and parental inheritance.* Heat maps of maternal versus paternal SNP ratios determined that embryos were uniparental (androgenetic or gynogenetic), polyploid shifted towards maternal SNPs, or biparental in origin. A small proportion of the biparental embryos were mixoploid and contained androgenetic, parthenogenetic, or polyploid blastomeres amongst euploid blastomeres.

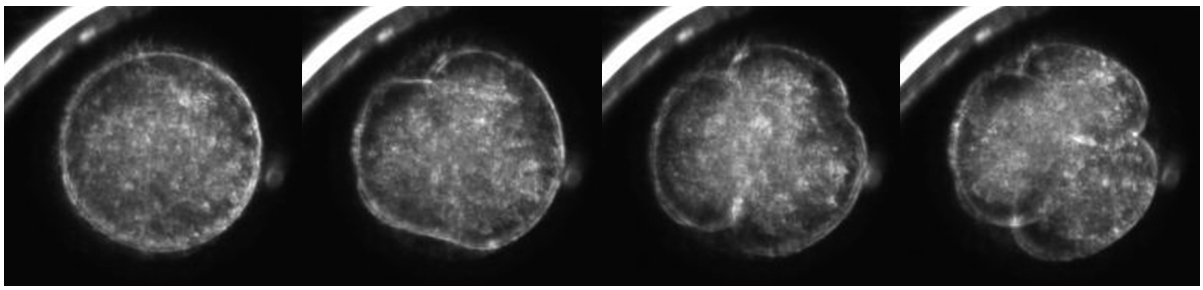

Figure 9. "*Speckled" embryo undergoing tripolar division.*

Several zygotes that underwent a multipolar division has dynamic "speckles" at the zygote and early cleavage stages. The "speckles" bear resemblance to MTOCs.

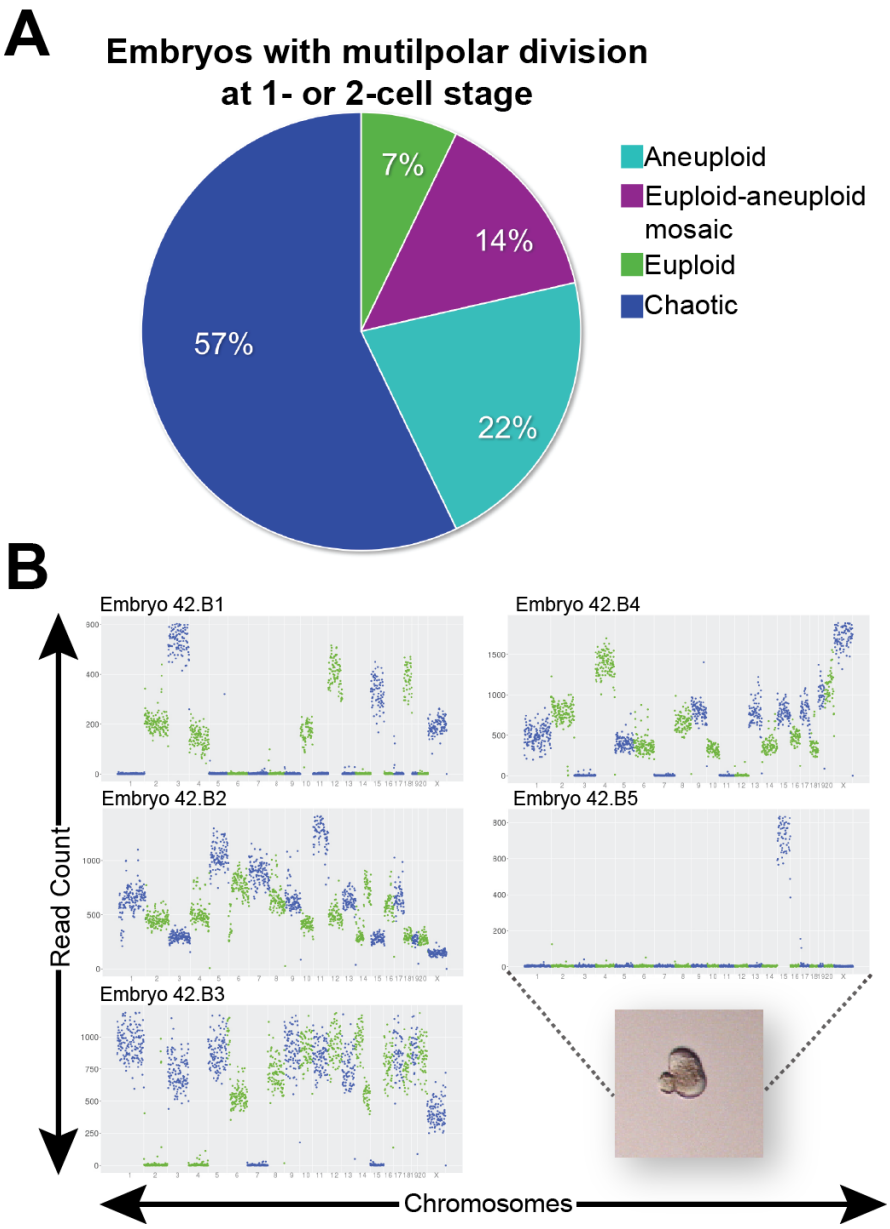

Figure 10. *Multipolar divisions in embryos often result in chromosome loss and chaotic aneuploidy.*

(A) Graphical representation of the overall ploidy in rhesus macaque embryos (N=14) with at least one multipolar division during early mitosis. **(B)** CNV plots of blastomeres from an embryo, which underwent a multipolar division at the zygote stage, showing chaotic aneuploidy in every cell. Inset is a stereomicroscope image of blastomere 5 with a protrusion reminiscent of a cellular fragment.

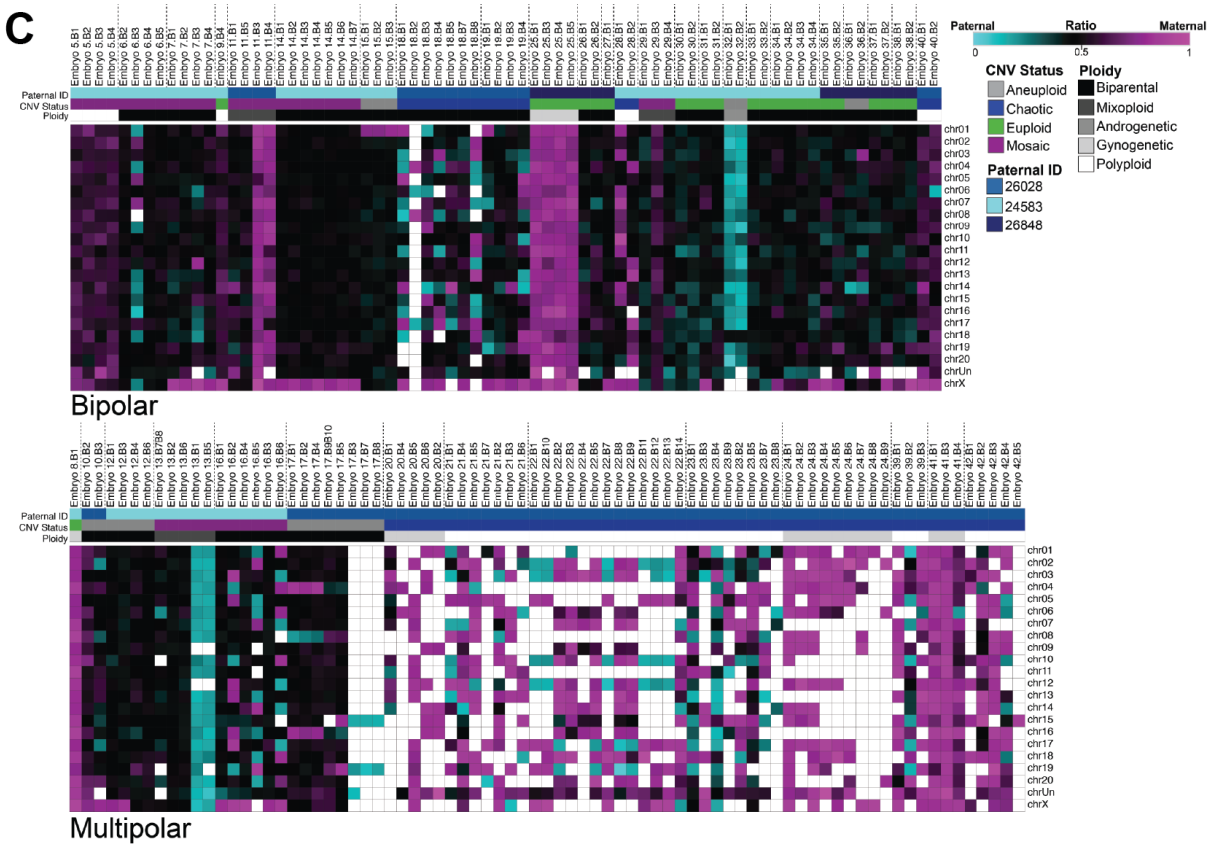

Figure 10. *Multipolar divisions in embryos often result in chromosome loss and chaotic aneuploidy.*

(C) Heat map of SNP parentage ratios in embryos that underwent bipolar or a multipolar cleavage during the first two cell divisions.

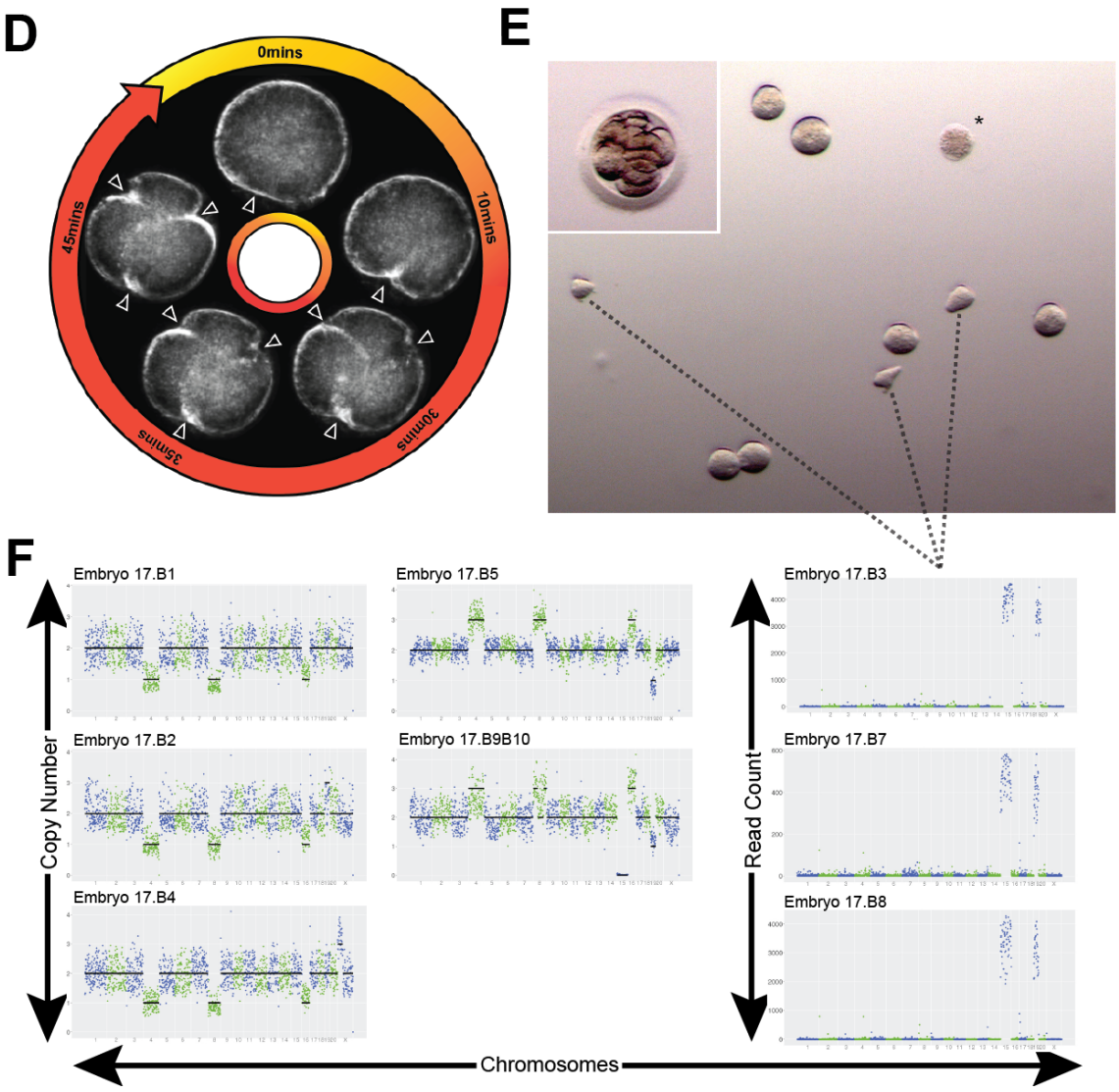

Figure 10. *Multipolar divisions in embryos often result in chromosome loss and chaotic aneuploidy.*

(D) Darkfield time-lapse images of an embryo at the zygote stage undergoing a tripolar division. Arrowheads point to three simultaneous cleavage furrows. **(E)** Stereomicroscope image of the same embryo still intact (inset) and then disassembled. Blastomere 6 lysed and is demarcated with an asterisk (*). **(F)** The CNV plots of all intact blastomeres from the embryo showing multiple reciprocal chromosome losses and gains. Dotted lines delineate irregularly shaped blastomeres that each contained only two chromosomes.

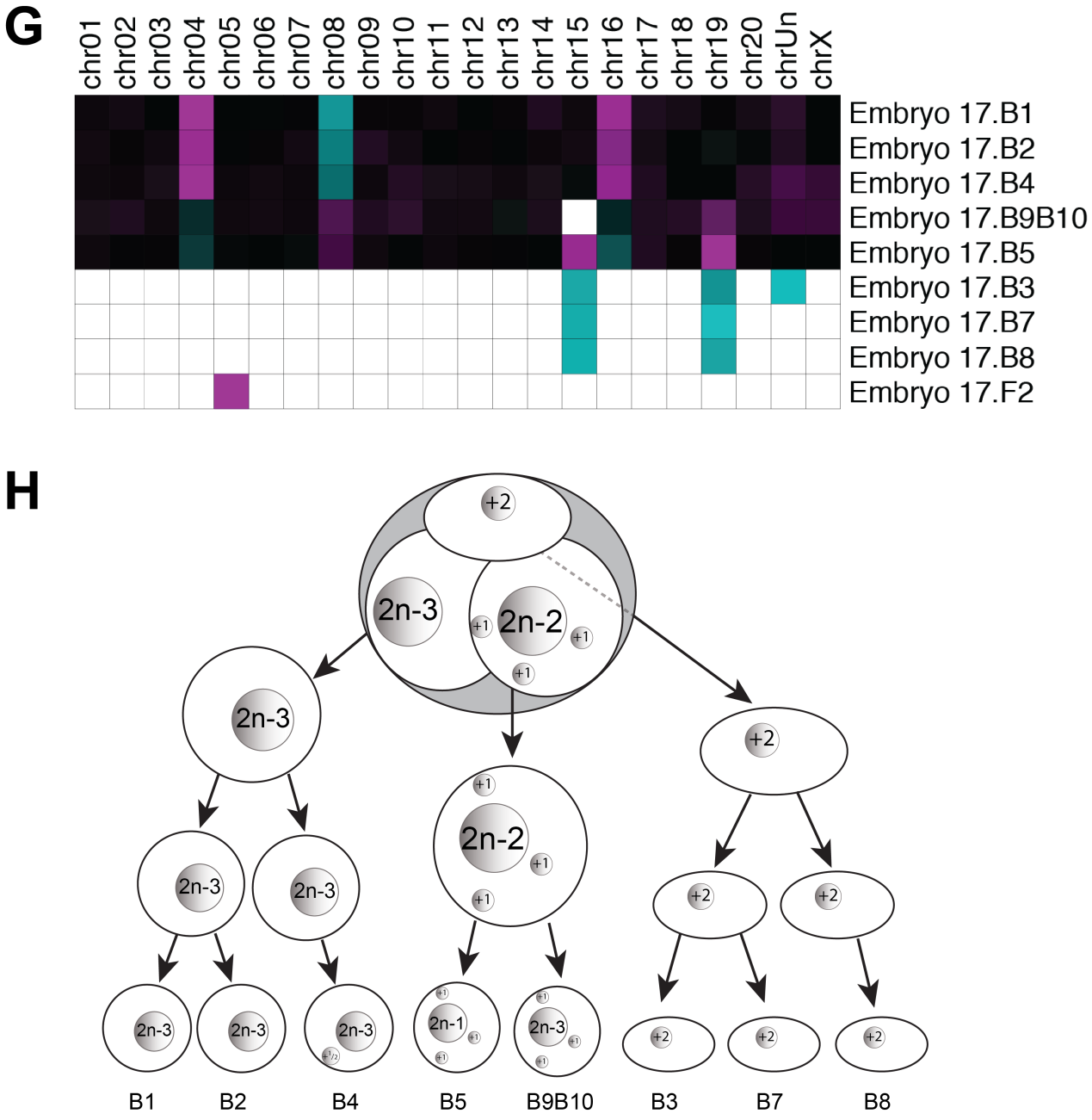

Figure 10. *Multipolar divisions in embryos often result in chromosome loss and chaotic aneuploidy.*

(G) Heat map of maternal versus paternal SNP ratios for the embryo demonstrates that the reciprocal loss and gain of these two chromosomes was due to either nondisjunction or anaphase lagging. **(H)** Schematic of the probable chromosome content of each cell from the embryo during early mitotic divisions based on imaging and CNV analysis.

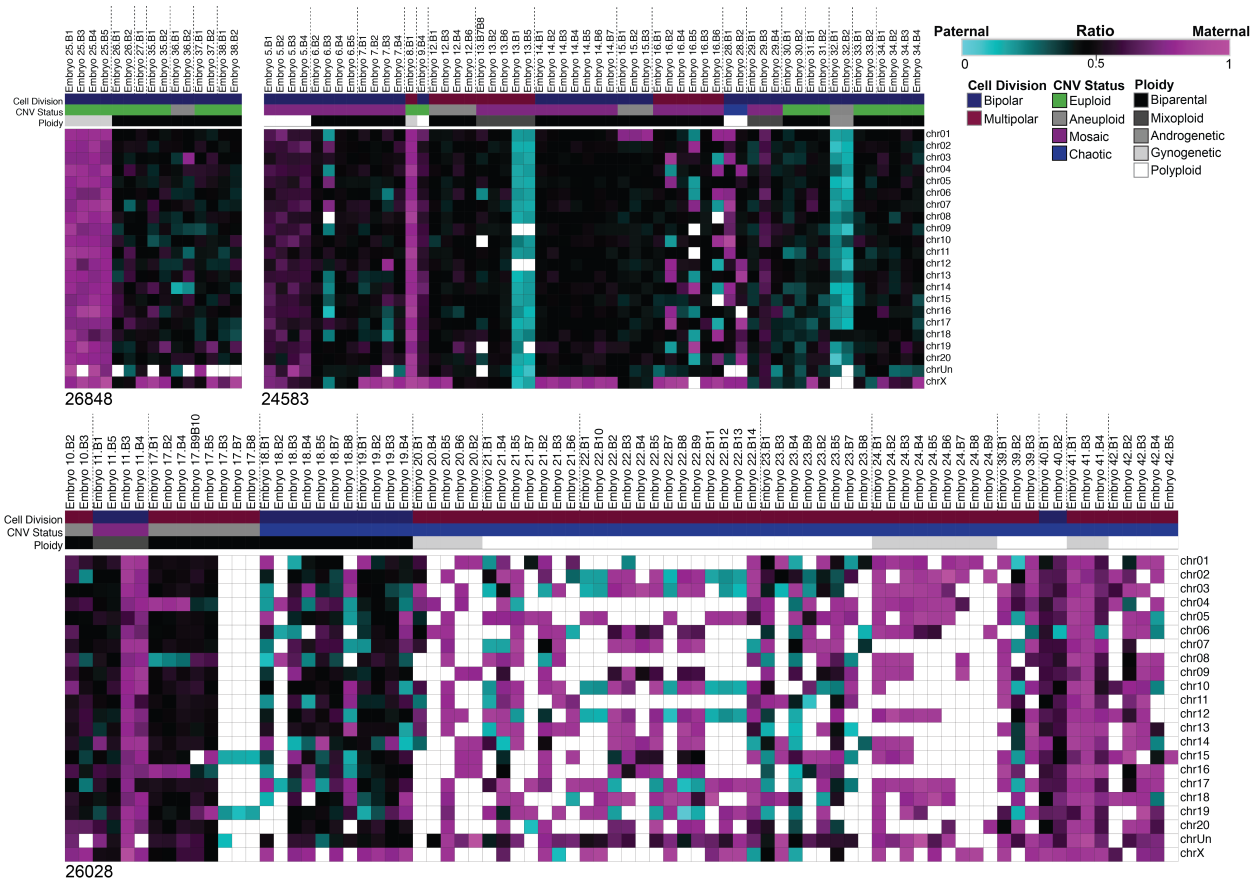

Figure 11. *SNP profiles based on paternal donor.*

Parental SNP analysis of embryos divided into different heat maps according to sperm donor ID.

Preface: Chapter 2

It is difficult to reconcile the degree of chromosomal instability detected in human and rhesus macaque embryos and the incredible success of in vitro fertilization. If 50-80% of human embryos have aneuploidy, it seems it would be much more difficult to become pregnant or select an embryo for transfer that is entirely euploid. Human and rhesus macaque embryos, among other species, have unusual cellular attributes and do not adhere to textbook descriptions of cell divisions. As discussed in chapter one, multipolar divisions and complex ploidy errors such as mixoploidy are observed, but in some cases, result in embryos that are mosaic with normal and abnormal cells. Sometimes cytokinesis during the first cell divisions does not behave as expected. Often, many cytoplasmic bodies will pinch off resulting in the generation of two daughter cells along with a dozen or so cellular fragments in the process. These unique cellular events will also often occur concurrently with chromosome segregation errors and ploidy states that are not biparental. To add, recent studies find that transferred human mosaic embryos implant and produce normal children. Such discoveries indicate that we do not fully grasp the consequences of aneuploidy in the embryo. That embryos with such a high frequency of chromosomal instability also undergo abnormal cellular dynamics may not be coincidental. In this chapter, cellular fragmentation and blastomere exclusion are examined to ask whether mechanisms exist for overcoming aneuploidy in the embryo. If the embryo does have the ability to tolerate aneuploidy, then approaches for screening embryos based on the detection of aneuploidy within a few cells merits reevaluation.

Chapter 2: Cellular fragmentation-mediated chromosome elimination and aneuploid blastomere exclusion.

Abstract

Human preimplantation embryos often sequester missegregated chromosomes into micronuclei during mitosis, while concurrently undergoing cellular fragmentation. In chapter two, to address the hypothesis that cellular fragmentation represents a response to missegregated chromosomes that are encapsulated into micronuclei, all cellular fragments from rhesus macaque preimplantation embryos underwent single-cell sequencing. Time-lapse monitoring and confocal microscopy of nuclear structures were also utilized concurrently with sequencing approaches to identify cellular events that would indicate a response to aneuploidy in the embryo. In ~20% of rhesus macaque embryos examined by sequencing, cellular fragments were found to contain whole or partial chromosomes. These chromosomes contained within cellular fragments were either maternal or paternal in origin. Not only were micronuclei observed in cellular fragments with confocal microscopy but detection of gamma-(serine 139 phosphorylated) H2A histone family, member X (γ-H2A.X) accumulation within these expelled micronuclei demonstrated that extensive DNA damage had occurred. In addition to the chromosomal and ploidy errors these embryos displayed, in some cases, cellular fragments and non-dividing blastomeres were prevented from incorporating at the blastocyst stage. In this chapter, the findings presented suggest embryos respond to segregation errors by eliminating micronuclei via cellular fragmentation and select against aneuploid blastomeres to overcome chromosome instability.

Introduction

Another determining factor for the capacity of an IVF embryo to successfully implant is the timing and degree of a dynamic process called cellular fragmentation, whereby cytoplasmic bodies pinch off of blastomeres during cytokinesis [286, 287]. The degree of cellular fragmentation is a morphological parameter for assessing embryo quality. Although once considered to be apoptotic bodies [197], studies have determined that cellular fragments are not the result of blastomere apoptosis and are distinct from cell death-induced DNA or chromosome fragments [288, 289]. Cellular fragmentation also occurs naturally following *in vivo* human conceptions [290, 291]. The appearance of cellular fragments in IVF embryos is highly associated with human embryonic aneuploidy and indicative of both meiotic and mitotic progression [97, 108] yet it is not associated with maternal age [292]. Clinical evidence shows that the degree of cellular fragmentation correlates negatively with implantation potential [199, 201, 293], and yet fragmented embryos can still implant and become healthy offspring [287]. The presence of cellular fragmentation has not been shown to be an indicator of developmental potential to the blastocyst stage [294] and, experimentally induced cellular fragments in the mouse do not appear to participate in compaction and are expelled during blastocyst hatching [295]. Since heavy fragmentation is strongly correlated with poor clinical outcomes, cellular fragments were once advised to be removed from the cleavage stage embryo through laser-assisted microsurgery based on improved blastocyst formation results in mouse [296]. However, improvement in human implantation was not observed following fragment removal [297] and damage to the embryo via lysed blastomeres was difficult to avoid [287] and thus this practice has since ceased.

Very little is known as to why and how embryos undergo cellular fragmentation. Cellular fragmentation is exhibited in human preimplantation embryos but is observed relatively infrequent in mouse embryos. Cellular fragmentation is also not seen in animal species with much larger oocytes such as the xenopus frog or zebrafish, and therefore is likely not simply a consequence of large cell size. Cell size reduction throughout the cleavage stages could potentially be a mechanism for cellular fragmentation [298], however given the correlation of poor embryo quality and aneuploidy with degree of fragmentation, this does not seem to be the case. The sizes of cellular fragments are similar to polar bodies. Additionally, the cellular fragments form during cytokinesis [299], a cellular event shared with polar body extrusion. Furthermore, cellular fragments appear at the zygote and earlier cleavage stages, where they most often occur following the division from one-cell to two-cells [300].

The underlying mechanisms for cellular fragmentation are understudied. One report suggests that there may be a paternal and maternal genetic component associated with cellular fragmentation as 2-cell embryos from mouse strain crosses lead to an increased incidence of cellular fragmentation [301]. In another mouse study, spindle removal from MII oocytes, which made experimental oocytes and blastomeres 'fragmentation prone', resulted in activation and cellular fragmentation during cytokinesis. The authors proposed that cellular fragmentation is a response to the loss of signal between the spindle complex and cortical microfilaments. However, in this study micromanipulation was performed in the presence of cytochalasin B, an inhibitor of cortical actin filament polymerization, and/or colcemid, a microtubule depolymerizer, and therefore results related to spindle removal alone are difficult to interpret [299]. Despite the lack of evidence in the study to support this hypothesis, the authors provide an interesting pathway to target for further research regarding the mechanism behind cellular fragmentation. Although cytochalasin B and

colcemid prevent cytokinesis in the oocyte and embryo at low concentrations, high concentrations of cytochalasin B or colcemid lead to multinucleation and nuclear expulsion of microcells in somatic cells. This suggests that cortical microfilaments at the cleavage furrow could be associated with cellular fragmentation [302-306].

Another avenue worth exploring for mechanism of cellular fragmentation are the cellular pathways that render asymmetrical cell division for polar body extrusion. There are several similarities between polar body extrusion and cellular fragmentation. First, both polar bodies and cellular fragments are similar in size and are often mistaken for each other. Second, both processes are involved with cytokinesis. Thirdly, chromosomes move to the cell cortex for elimination during meiosis for polar body extrusion [307, 308] and during mitosis when micronuclei are eliminated (discussed below). It would be interesting to examine components required for polar body asymmetrical division at cellular fragmentation sites along the blastomere plasma membrane during the zygote or 2-cell stage following karyokinesis. Targets to examine would be actin and myosin II for cortical polarity at cellular fragmentation sites [307] and microfilament for chromosome migration and elimination [309].

As stated above, extensive cytoplasmic fragmentation in human embryos is often seen in association with blastomere micro- and multi-nucleation, chromosomal instability, and copy number mosaicism between blastomeres [310-312]. Along with these abnormalities, our lab has previously demonstrated that cellular fragments can contain chromosomal material that are most likely missegregated chromosomes encapsulated in extruded micronuclei [108]. These micronuclei observed in human embryos are analogous to micronuclei observed in somatic cells [207, 216]. In cultured cells, chromosomes within micronuclei display an increased propensity to undergo double-stranded breaks and

structural rearrangements, which may be due to asynchrony in DNA replication timing between micronuclei and the primary nucleus [207]. Recently, Zhang *et al.* [313] showed that chromothripsis – the shattering, segmental loss, and rearrangement of a single chromosome – occurs in the micronucleus. It has been proposed that a similar phenomenon occurs in the micronuclei of human embryos [212, 213]. Interestingly, cellular fragments have been shown to fuse back with blastomeres [108, 314]. If a cellular fragment containing a micronucleus were to refuse with a blastomere after having undergone chromothripsis, this would likely be a detrimental event for the embryo. However, a recent report in mouse embryos suggests that embryonic micronuclei undergo perpetual unilateral inheritance instead [315].

In contrast to humans, mouse cleavage-stage embryos rarely exhibit micronuclei and cellular fragmentation even in sub-optimal culture conditions [108, 295, 315, 316]. Moreover, when micronuclei are induced experimentally, mouse embryos undergo cell lysis rather than cellular fragmentation [317]. Beginning at the morula (~16-cell) stage of preimplantation development and onward, however, ~10% of mouse embryos have been shown to contain one or more micronuclei, and a similar number are observed between *in vivo* and IVF-derived embryos [315]. This suggests that *in vitro* culture does not affect micronuclei abundance and may explain why mouse embryos exhibit a considerably lower incidence of aneuploidy at ~1-4%, depending on the strain [18-20]. Whether other mammalian species more closely related to humans such as non-human primates have similar micronuclei and fragmentation frequencies has not been investigated in detail and directly addressing this question may allow translation to human embryogenesis.

In addition to cellular fragmentation and micronucleation, human embryos are also often mosaic for euploid and aneuploid cells. Euploid-aneuploid mosaicism in embryos from the

cleavage to blastocyst stage has been described since the very earliest reports of preimplantation genetic screening [318]. However, while clinically classified as aneuploid, these euploid-aneuploid mosaic embryos can still result in the birth of healthy offspring upon transfer [20, 244, 245]. These studies call into question the accuracy of PGS, and more specifically trophectoderm biopsies for predicting which embryos will lead to normal pregnancy and healthy offspring [319]. Reports of healthy offspring from mosaic embryos indicate that corrective mechanisms exist to overcome chromosomal instability during preimplantation development either through a selective growth advantage for euploid cells or elimination of aneuploid cells. Unfortunately, the literature is lacking studies related to selection against aneuploid cells in embryos. Studies in cultured cells have demonstrated that aneuploid cells can undergo senescence, are targeted for clearance by the immune system, and an internal surveillance molecule called cyclic GMP–AMP synthase monitors micronuclei genome instability to trigger cell-intrinsic autoimmunity [320, 321]. As discussed above in chapter 1, excluded blastomeres may be a mechanism of correction by eliminating aneuploid cells. Although blastomere exclusion has been documented in the literature [225], little is known about these types of cells.

In this chapter, to address the hypothesis that cellular fragmentation represents a response to missegregated chromosomes that are encapsulated into micronuclei and that aneuploid blastomeres are eliminated from the embryo, the DNA content of each cellular fragment within the embryo was examined by DNA-Seq and SNP analysis for determining chromosome parentage. These cellular fragments were obtained from the 42 embryos described in chapter 1 in addition to the blastomere and polar body collected for CNV assessment. Additional embryos were cultured to the morula and blastocyst stage to procure and examine large excluded blastomeres that appeared to no longer divide or participate in embryo development. Finally, growing embryos from the cleavage to

blastocyst stage were fixed and immunostained for the nuclear envelope marker, Lamin B1 and DNA double stranded breaks to assess the presence of micronuclei, nuclear structure, and DNA damage within the nucleus and micronuclei. Results from this study determined that missegregated chromosomes are encapsulated within micronuclei and eliminated from the embryo through cellular fragmentation. In addition, non-dividing blastomeres are aneuploid and along with cellular fragments, are excluded from blastocysts prior to hatching. Both of these findings serve as potential mechanisms to surpass chromosomal instability during primate preimplantation development.

Methods

Rhesus Macaque Embryos

See page 35 in chapter 1 for detailed methods.

Time-Lapse Imaging

See page 36 in chapter 1 for detailed methods.

In addition to monitoring embryos throughout the cleavage stage prior to disassembly into individual cells and cellular fragments, several embryos were cultured up to 7 days to the blastocyst stage.

Embryo Disassembly

See page 37 in chapter 1 for detailed methods.

Upon disassembly, when possible, all cellular fragments were collected individually from each cleavage stage embryo. Since many large excluded blastomeres were contained within the blastocoel cavity of blastocysts, instead they were removed from the perivitelline space at the compact morula stage.

DNA Library Preparation

See page 39 in chapter 1 for detailed methods.

The pooling scheme for each round of sequencing was to target 2 million reads per sample based on the sequencing kit used. When pooling samples together for DNA sequencing, nuclear DNA in cellular fragments was assumed to be nonexistent if the concentration was less than non-template controls (<~3ng/ul). Only 5ng of these empty samples was added to the sequencing pool. The rationale for providing less DNA for sequencing empty cellular fragments was to allow for more sequencing coverage for samples that contained nuclear DNA. Cellular fragment samples with significant amounts of measureable DNA (>~10ng/ul) were added to sequencing pools at 25ng in order to detect the presence of potential CCFs. For excluded blastomeres, 50ng of the sample was added to each sequencing pool.

Multiplex DNA Sequencing

See page 40 in chapter 1 for detailed methods.

Using the custom designed indices described Vitak *et al*. [253], excluded blastomeres and cellular fragments were sequenced on the Illumina NextSeq again using our custom 75-base pair single-end protocol. Sequencing statistics are provided in **Table 3.**

Copy Number Variant Calling

See page 42 in chapter 1 for detailed methods.

In addition to employing the VNOWC and CHI CNV pipelines for examining excluded blastomeres, read count only plots were generated for each sample, particularly to find chromosomes in cellular fragments. Briefly, the mapped reads for each sample were binned with variable-sized windows of a constant number of expected reads per window (target was 4,000) but no circular binary segmentation or hidden markov model was used to assess copy number changes.

SNP Parentage Analysis

See page 44 in chapter 1 for detailed methods.

All SNPs in CCF regions of interest were retained, whereas chromosomes in blastomeres and polar bodies that had fewer than 10 SNPs were removed to further increase confidence in parental inheritance.

Immunofluorescence Confocal Imaging

Embryos were placed in warmed acidified Tyrode's solution for 30 seconds to remove the zona pellucida. Zona pellucida-free embryos were washed briefly in PBST, which consists of PBS (Invitrogen, Carlsbad, CA) with 0.1% BSA and 0.1% Tween-20 (Calbiochem, San Diego, CA). The embryos were then fixed in 4% paraformaldehyde in PBS (Alfa Aesar, Ward Hill, MA) for 20 minutes at room temperature. Once fixed, the embryos were washed

with gentle shaking three times for a total of 15 minutes in PBST to remove any residual fixative. Subsequently, embryos were permeabilized for antibody penetration in 1% Triton-X (Calbiochem, La Jolla, CA) for one hour at room temperature and then washed in PBST as described above. To block non-specific binding of the secondary antibody, embryos were transferred to a 7% donkey serum (Jackson ImmunoResearch Laboratories, Inc., West Grove, PA)/PBST solution overnight at 4°C and then washed in PBST as described above. For the visualization of LAMIN-B1 (ab16048, Abcam, Cambridge, MA) and γH2A.X (05-636, EMD Millipore, Temecula, CA), antibodies were diluted 1:1000 and 1:100, respectively, in PBST with 1% donkey serum and the embryos were sequentially stained overnight at 4°C. Between each antibody incubation, embryos were washed in PBST with gentle shaking four times for a total of 20 minutes to ensure removal of non-specific antibody binding. Primary antibodies were detected using the appropriate species reactivity with 488- or 647-conjugated donkey Alexa Fluor secondary antibodies (Thermo Fisher Sci., Rockford, IL) at a 1:250 dilution in 1% donkey serum in PBST at room temperature for 1 hour in the dark. Embryos were then washed in PBST to remove non-specific antibody binding as described above. For nuclear DNA detection, embryos were stained with 1 μg/ml DAPI for 15 minutes and then placed in a 30μl drop of Global media with 10% protein under mineral oil on a glass bottom petri dish (Mattek, Ashland, MA). Immunofluorescence was visualized using a Leica SP5 AOBS spectral confocal system. Z-stacks between 1 and 5 μM apart were sequentially imaged one fluorophore at a time to avoid spectral overlap between channels. Stacked images and individual channels for each color were combined for imaging files using the channel merger and Z-projection functions in FIJI [322].

Results

Experimental design for capturing chromosomes within cellular fragments and assessing the aneuploidy state of excluded blastomeres

Single-cell DNA-Seq and TLM was used to non-invasively assess preimplantation development as described in chapter 1. In addition to the 42 embryos assessed for CNVs, 92 zygotes underwent extended culture where 42 arrested and 50 reached the blastocyst stage. Since excluded blastomeres within the blastocoel cavity were inaccessible at the blastocyst stage, an additional 6 embryos were cultured to the day 6 compact morula stage where excluded blastomeres were recovered from the perivitelline space (**Figure 12**). The cellular fragments and excluded blastomeres sequenced were from embryos collected from 14 different IVF cycles. Cellular fragment collection occurred approximately 24-96 hours after IVF when cleavage-stage embryos were disassembled for blastomere and polar body collection. The cellular fragment and excluded blastomere samples were amplified by PCR-based whole genome amplification and sequenced as described in chapter 1. Mapped reads for excluded blastomeres were assessed by chromosomal CNV analysis for aneuploidy detection and read count pile up was used to determine if chromosomal material was present in cellular fragments. Both cellular fragments and excluded blastomeres were analyzed by SNP genotyping to determine the parental origin of chromosomes.

Micronucleation and cellular fragmentation frequency is conserved between human and rhesus macaque

One of the hallmarks of imminent aneuploidy in human embryos and other cell systems is the appearance of micronuclei containing anaphase-lagging chromosomes [108, 323, 324]. Another prevalent feature of cell divisions of cleavage stage embryos is cellular fragmentation, which our lab has previously hypothesized represents a response to the presence of missegregated chromosomes during meiosis and/or mitosis. Analogous to human embryos [286, 287], more than 50% of rhesus macaque cleavage-stage embryos exhibit some degree of cellular fragmentation. In lieu of embryo disassembly and single-cell sequencing, a subset of intact embryos between the zygote and blastocyst stage were fixed and subjected to multi-color confocal imaging to assess micronuclei formation and cellular fragment sequestration of nuclear DNA. Upon fixation and immunolabeling and staining with the nuclear envelope marker, LAMIN-B1 and DAPI for DNA, rhesus macaque preimplantation embryos were found to contain lagging chromosomes during mitosis (**Figure 13A**) and micronuclei as early as the zygote (**Figure 13B**) or 2-cell stage (**Figure 13C**). Micronuclei formation was found to often be concomitant with cellular fragmentation by the 2-cell stage (**Figure 13D**). Notably, some of these cellular fragments encapsulated nuclear DNA as indicated by positive DAPI staining. While micronuclei may not appear until the 6- to 9-cell stage or later in embryos that did not yet undergo fragmentation (**Figure 13E**), micronuclei are sometimes present in the ICM of blastocysts (**Figure 13F**). These findings demonstrate that embryonic micronucleation and cellular fragmentation is conserved between humans and rhesus macaques and that the emergence of micronuclei is tolerated throughout primate preimplantation development.

Cellular fragments can encapsulate whole or partial chromosomes lost from blastomeres

Although reciprocal losses and gains of chromosomes were occasionally observed between blastomeres in the 42 embryos described in chapter 1, this was not the case for the majority of embryos since most corresponding chromosome segments appeared to be missing from a given embryo. Based on previous findings of chromosomal material in cellular fragments and that fragmentation is highly associated with human embryonic aneuploidy [108], it was reasoned that the missing chromosome(s) had been sequestered into cellular fragments. To test this hypothesis, single cellular fragments were obtained from each of the 42 TLM cleavage-stage embryo described in chapter one. These single cellular fragments underwent the same whole genome amplification protocol as blastomeres and polar bodies. The VNOWC and CHI CNV pipelines are accurate for calling copy number differences in the context of a whole genome but not in the presence of single chromosomes. Therefore, read count only plots were used to assess the presence of chromosomes within cellular fragments. A number of fragmented embryos revealed chromosome-containing cellular fragments (CCFs), where several of them were complimentary to the chromosomes missing from blastomeres.

As shown in **Figure 14**, both copies of chromosome 9 and 12 lost from blastomeres of mosaic embryo 13 were located in a cellular fragment from the same embryo. Overall, the presence of entire or partial chromosomes in one or more cellular fragments was confirmed in ~20% (N=8/42) of embryos (**Figure 15A & B**). However, only ~7% (N=11/160) of cellular fragments examined contained chromosomal material (**Figure 15C**). These embryos with CCFs tended to be completely aneuploid however there were embryos that were mosaic or had euploid copy number profiles (**Figure 15D**). The

question of whether CCFs were actually polar bodies that had undergone cytokinesis was a point of concern and although the CCFs discovered were discrete, individual chromosomes instead of degraded DNA across the genome, this question merited further investigation. To address this, maternal versus paternal SNPs were analyzed as discussed in chapter 1. Parentage results determined that CCFs originated from the chromosomes of either the mother or the father (**Figure 16**). In addition, there did not appear to be a preferential sequestering of particular chromosomes into cellular fragments, as both small and large chromosomes were equally affected and partial chromosomes identified in fragments ranged in size from 6 to 85 megabases (**Figure 17)**.

Chromosome-containing cellular fragments are often found in embryos that undergo multipolar divisions and have abnormal ploidy

The presence of chromosomes within cellular fragments has been suggested but never examined to this extent. Although this is the first study that has sequenced cellular fragments from embryos, discovering that the majority of these embryos were aneuploid raised the question if other errors may be present. By assessing the overall ploidy of the 8 embryos with CCFs by SNP analysis (discussed in chapter 1) it was also determined that these embryos were either gynogenetic (N=3/8), androgenetic (N=1/8), polyploid (N=1/8), or mixoploid containing a mixture of biparental and either uniparental or polyploid blastomeres (N=2/8) (**Figure 18**). Only one embryo from which a CCF arose was entirely biparental (N=1/8) and this embryo experienced a multipolar division (**Figure 10D-F**). Although more numbers are needed to support this, these findings suggest that the type of chromosomal abnormality resulting in the production of CCFs reflect errors induced by abnormal ploidy. Another feature shared by the majority (N=6/8) of embryos with CCFs

was multipolar divisions at the 1- or 2-cell stage of preimplantation development as detected by TLM analysis (**Figure 18**). Defects in the sperm centrosome may have contributed to the multipolar divisions and/or ploidy errors seen in these embryos.

Chromosome-containing cellular fragments are susceptible to DNA breaks and damage

Based on observations of both whole and partial chromosomes within cellular fragments, the question was whether the presence of chromosomal segments was due to DNA fragility once the chromosome(s) was separated from the primary nucleus of a blastomere. To examine this, fragmented cleavage-stage rhesus macaque embryos were immunostained with LAMIN-B1 and gamma-H2A.X (γ-H2A.X), a marker of DNA damage and double-stranded breaks [325]. Analogous to human embryos [108], nuclear DNA positive for DAPI staining was detected in cellular fragments of rhesus embryos that also contained several micronuclei (**Figure 19**). These cellular fragments containing micronuclei appeared to lack or have a disrupted nuclear envelope as previously described for chromosome-containing micronuclei in cultured cells [216], which may cause susceptibility to chromosomal instability. When immunostained for γ-H2A.X, distinct puncta were detected in micronuclei within the blastomere from which they arose. Moreover, multiple γ-H2A.X foci were also identified in the DNA of cellular fragments (**Figure 20A**). One cellular fragment in particular contained an intact nuclear envelope and uniform γ-H2A.X immunostaining which is more likely indicative of DNA degradation rather than double-stranded breaks [326] (**Figure 20B**). By measuring the γ-H2A.X fluorescence intensity through single focal planes of the embryo, DNA damage was determined to be

markedly increased in CCFs compared to the blastomeric primary nuclei and micronuclei (**Figure 20C**). However, since these embryos were fixed at a static time point, it is unclear whether DNA degradation or double-stranded DNA breaks occurred before the cellular fragmentation event or after the micronuclei were sequestered into a cellular fragment.

Non-dividing aneuploid blastomeres and fragments are excluded during blastocyst formation

Since ~54% of the rhesus macaque embryos formed blastocysts (N=50/92) in this study and yet, only ~29% of the cleavage-stage embryos analyzed by DNA-Seq were comprised entirely of euploid blastomeres, it was reasoned that a proportion of the blastocysts were aneuploid to some extent, at least at the cleavage stage. Moreover, recent reports have found that euploid-aneuploid mosaic preimplantation embryos can result in healthy offspring [20, 244, 245]. By performing TLM analysis up to the blastocyst stage, five embryos displayed excluded fragments and/or large blastomeres that ceased dividing at the 2- to 4-cell stage and persisted up to the blastocyst stage. These cellular fragments and non-dividing blastomeres appeared to be confined to the perivitelline space or blastocoel cavity during the morula-to-blastocyst transition, respectively (**Figure 21A**). Two of these blastocysts with excluded blastomeres also underwent a 1- to 4-cell symmetrical cell division without cellular fragmentation at the 1- or 2- cell stage as mentioned above (**Figure 22**). Upon immunostaining a representative blastocyst with LAMIN-B1 and γH2A.X, a large bi-nucleated excluded blastomere was observed with extensive DNA damage as indicated by intense γH2A.X accumulation predominantly in the nuclei (**Figure 21B**). Numerous DAPI-positive nuclei were also detected in the zona

pellucida of the embryo that exhibited cellular fragment exclusion following hatching and DNA staining (**Figure 21C**). While these fragments could easily be collected from the empty zona pellucida, it was difficult to separate the excluded blastomeres from the rest of the embryo once the blastocoel cavity was formed. Therefore, three additional embryos were identified with blastomere exclusion at the early cleavage-stage by TLM and were disassembled prior to or during morula compaction. Once isolated, single-cell DNA-Seq was performed on the excluded blastomeres and these cells were determined to be aneuploid or highly chaotic with multiple losses and gains of chromosomes (**Figure 21D**). Because the TLM analysis demonstrated that these blastomeres never divided again, both blastomere and fragment exclusion might be mechanisms by which an embryo can select against aneuploid cells early on and overcome chromosomal instability.

Discussion

Besides aneuploidy, this study also shows that rhesus macaque cleavage-stage embryos exhibit micronuclei formation and cellular fragmentation at an equivalent frequency to human embryos [77, 108, 282, 286, 287], events that rarely occur in the mouse [108, 295, 315, 316]. Cellular fragmentation is often associated with aneuploidy and our lab has previously demonstrated with immunofluorescence that cellular fragments can contain chromosomal material [108]. By reconstructing the chromosomal content of each cell and cellular fragment within an embryo, this study is the first to determine that both whole and partial chromosomes lost from blastomeres are sequestered into cellular fragments. This ejected DNA is the result of missegregated chromosomes that were encapsulated within micronuclei and eliminated from the embryo through cellular fragmentation (**Figure 23B**). The finding of a shared nuclear envelope between a blastomere and fragment in **Figure 20B**_could indicate that defects affecting nuclear integrity might represent one of the mechanisms by which micronuclei are sequestered into fragments. As shown with immunostaining, these chromosomes undergo DNA damage within the micronucleus via double-stranded breaks. However, it is unknown if DNA damage occurs in the micronucleus prior to or after cellular fragmentation. It is also unknown if DNA-damage accumulation within the micronucleus plays a role in the fate of micronucleus ejection through cellular fragmentation. Findings of increased γH2A.X signal in CCFs as opposed to DNA damage within the primary nucleus and micronuclei within blastomeres could indicate that chromosomes experiencing instability are targeted for elimination. In this chapter, it was also demonstrated that cellular fragments and non-dividing, aneuploid blastomeres with extensive DNA-damage are excluded from blastocysts prior to hatching. The data presented here hint that extensively damaged DNA within micronuclei and the primary nucleus leads to CCFs and excluded blastomeres, respectively. However, in order

to support this hypothesis, live-cell time-lapse imaging that can track nuclear envelope dynamics and DNA damage with high precision is required.

Once separated from the primary nucleus, chromosomes within a micronucleus can undergo DNA damage and double-stranded breaks in cultured cells [207, 216]. More recent studies demonstrated that a process called chromothripsis, whereby chromosomes are “shattered” and rearranged in a single catastrophic event, also arises as a result of the DNA damage in micronuclei [313]. The occurrence of chromothripsis in embryos has been suggested [212, 213], but not yet confirmed due to the sequencing depth, genome coverage, and large read length size demands required to detect complex chromosomal rearrangements. Nevertheless, the segmental deletions produced from chromothripsis would likely be lethal for an embryo despite some reports of postulated chromothriptic-induced germline structural rearrangements causing severe congenital abnormalities in offspring [215]. Chromothripsis may have occurred in certain blastomeres if one or two chromosomes experienced segmental deletions following extensive double stranded breaks. For example, the CCF from embryo 21 shows that most of chromosome 3 was lost but two non-flanking segments were retained. This might be an example of chromothripsis but further approaches are needed to detect complex chromosomal rearrangements. Rearrangements are much more difficult to assess since the PCR-based whole genome amplification used in this study is limited for accurately calling structural variants. For this purpose, non-PCR-based multiple displacement amplification should be used to generate larger amplicons, but this technique has been shown to be inadequate for reliable CNV calling [50]. Assessing chromothripsis in CCFs and excluded blastomeres via high coverage paired-end sequencing to detect discordant read-pairs and splitting reads would indicate the presence of chromosomal rearrangements. However, artifacts of chimeric DNA from single-cell whole genome amplification generates many false positives

that are difficult to distinguish from real rearrangements. Thus, the development of additional bioinformatics approaches that can control for chimeric reads would also be required to evaluate chromothriptic events and should be explored in future studies.

Whether chromosome sequestration by cellular fragments and blastomere exclusion are attempts at embryonic rescue is difficult to ascertain, but there appeared to be an association between these two events and the prevalence of multipolar divisions and ploidy errors in this study. Using TLM to monitor human preimplantation development, it was shown that ~12% of human zygotes undergo multipolar divisions [282] and were less likely to form blastocysts and implant than zygotes that exhibit a bipolar 1st mitotic division [77]. Indeed, almost all of the rhesus macaque embryos with multipolar divisions arrested prior to reaching the blastocyst stage. Yet, two embryos did progress in development that underwent a 1- to 4-cell symmetrical cell division without cellular fragmentation at the 1- or 2- cell stage. These two embryos also exhibited exclusion of aneuploid blastomeres during the morula-to-blastocyst transition to suggest that multipolar divisions might provide a mechanism to overcome aneuploidy under certain circumstances (**Fig. 23C**).

Recently, it was shown that blastocysts with euploid-aneuploid mosaicism can still produce healthy offspring in both humans and mice and that mouse embryos without a sufficient number of normal blastomeres at the 8-cell stage are selectively eliminated during early post-implantation development [20, 244]. While it is not possible to perform whole-embryo CNV analysis on all blastomeres and CCFs from embryos that will be transferred, it is speculated that the euploid-aneuploid mosaic rhesus macaque embryos containing blastomeres with biparental origins would have likely implanted and continued in development. Given that embryonic micronuclei were detected in the ICM of certain blastocysts, however, the fate of mosaic embryos may also depend on which lineage the

aneuploid blastomeres are allocated to and whether there is lineage-specific selection against abnormal cells as shown for chemically-induced mouse embryos [20]. Based on data presented in this study, mosaic embryos may be able to overcome aneuploidy by eliminating aneuploid blastomeres and/or by eliminating highly damaged micronucleated chromosomes through cellular fragmentation. Altogether, this study demonstrates the complexity of how aneuploidy may be resolved through these mechanisms in primate embryos during preimplantation development. Future work is necessary to determine if the cellular events captured here are random and unique to the embryos described or represent a deliberate attempt at eliminating aberrant chromosomes and blastomeres.

Sample Name	Cell Type	Raw reads	Read length	% GC	Trimmed & deduplicated	mapped	pass Q30	Unique mapping positions
Embryo 13.F9	CCF	1,262,186	55.00	42.00	985,530	782,343	580,543	518,847
Embryo 17.F2	CCF	32,423	55.00	44.00	25,169	20,321	15,367	14,599
Embryo 20.F1	CCF	40,093	55.00	43.00	30,166	25,448	16,439	15,543
Embryo 20.F5	CCF	27,064	55.00	42.00	20,784	17,183	11,293	10,785
Embryo 20.F9	CCF	62,074	55.00	42.00	40,446	35,659	24,319	22,365
Embryo 21.F1	CCF	54,045	55.00	43.00	32,694	24,922	14,258	11,998
Embryo 21.F3	CCF	1,454,785	55.00	43.00	566,604	420,449	232,601	168,887
Embryo 24.F1	CCF	110,257	55.00	43.00	56,821	52,726	38,274	30,208
Embryo 29.F5	CCF	628,510	57.00	43.00	313,193	113,056	69,382	41,203
Embryo 32.F1	CCF	197,162	57.00	43.00	129,884	67,121	50,756	43,146
Embryo 8.F1	CCF	252,928	57.00	41.00	76,449	51,288	25,462	11,223
Embryo 43.B8	ExB	3,216,658	57.00	42.00	2,779,830	1,289,771	1,192,892	1,081,221
Embryo 44.B4	ExB	2,583,067	57.00	42.00	2,079,258	957,931	870,537	778,165
Embryo 45.B5	ExB	2,365,519	57.00	42.00	1,568,779	742,904	654,573	542,979
Embryo 45.B6	ExB	3,031,954	57.00	42.00	1,872,593	885,851	753,357	619,643
Embryo 46.B1	ExB	3,136,300	57.00	44.00	1,814,909	847,788	736,218	496,210
Embryo 46.B14	ExB	2,405,529	57.00	42.00	2,003,070	857,979	796,956	702,053
Embryo 46.B2	ExB	989,549	57.00	43.00	427,957	227,068	135,086	96,712
Embryo 46.B3	ExB	491,190	57.00	43.00	345,330	125,111	106,613	86,387
Embryo 47.B7	ExB	810,564	57.00	42.00	706,186	325,144	301,220	277,660
Embryo 47.B8	ExB	2,426,496	57.00	42.00	2,055,596	937,787	869,823	780,833

Table 3. *Sequencing statistics for chromosomes within cellular fragments (CCFs) and excluded blastomeres (ExB).*

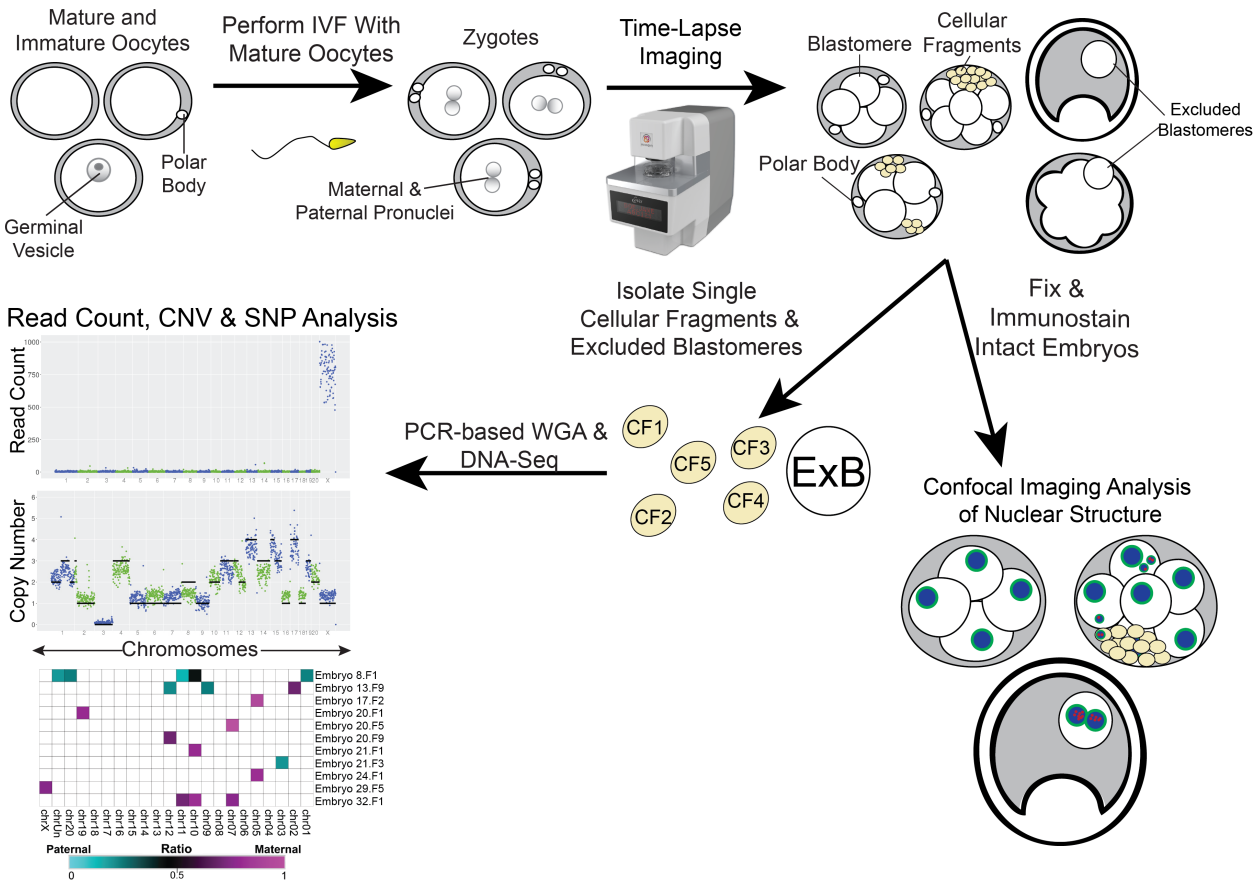

Figure 12. *Approach for finding chromosomes in cellular fragments and assessing large excluded blastomeres.*

As described in figure 3, MII oocytes underwent conventional IVF and zygotes were monitored by time-lapse imaging. Cleavage-stage embryos were disassembled into individual cellular fragments and excluded blastomeres were recovered from compact morulas. Single cellular fragments and excluded blastomeres underwent PCR-based whole genome amplification (WGA) and mapped reads were analyzed by DNA-Sequencing for read count pile up, copy number variation (CNV) and single nucleotide polymorphism (SNP) assessment. A subset of fragmented cleavage stage embryos and a blastocyst with an excluded blastomere were immunostained for to examine nuclear structures.

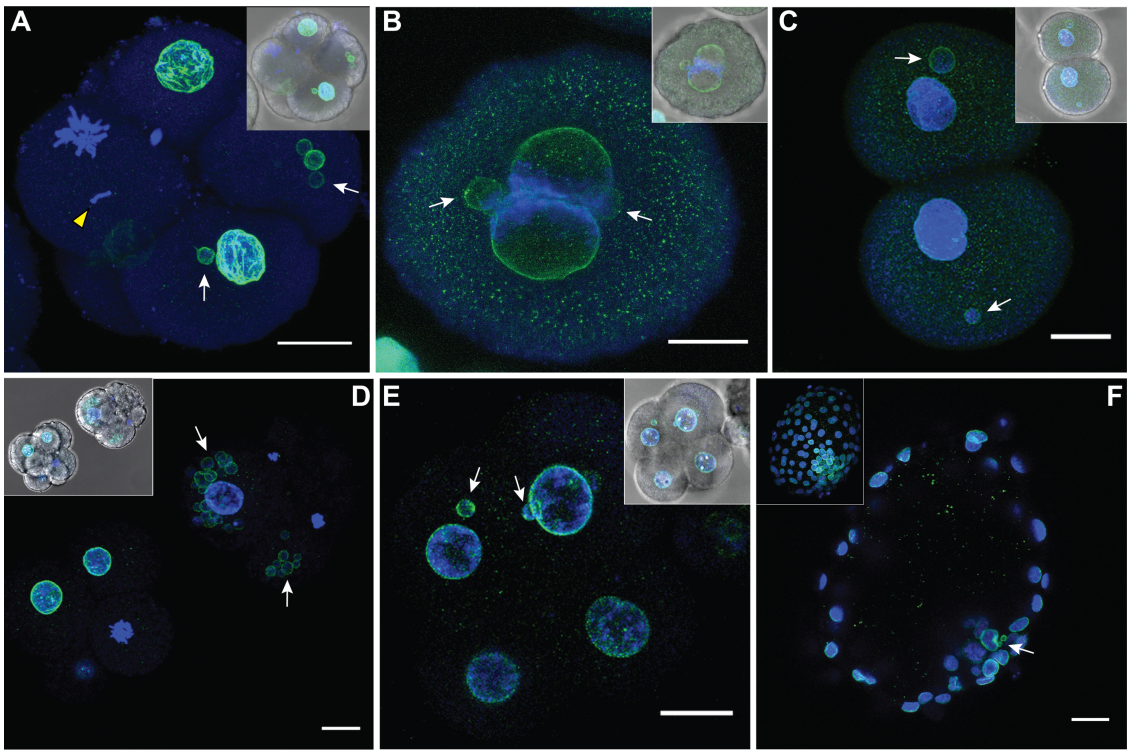

Figure 13. *Micronuclei in rhesus macaque embryos.*

Micronuclei were examined in rhesus macaque embryos at different stages of preimplantation development using the nuclear envelope marker, LAMIN-B1 (green), and DAPI (blue) for nuclear DNA. Images are representative of select stacks. Insets show a brightfield image for reference. Scale bars: 25 μm. **(A)** 5-cell embryo with a lagging chromosome (yellow arrowhead) in metaphase in one blastomere and micronuclei in two other blastomeres (white arrows). **(B)** Zygote undergoing syngamy with two micronuclei (white arrows). **(C)** 2-cell embryo with one micronucleus in each blastomere. **(D)** Comparison of a fragmented (white arrowheads) 2-cell embryo with multiple micronuclei (right) and a non-fragmented 7-cell embryo (left). **(E)** Single imaging plane of a Z-stacked 9-cell embryo exhibiting micronuclei in two blastomeres, but no visible cellular fragmentation. **(F)** Blastocyst with at least two micronuclei in the ICM; the inset shows the maximum intensity projection of the embryo.

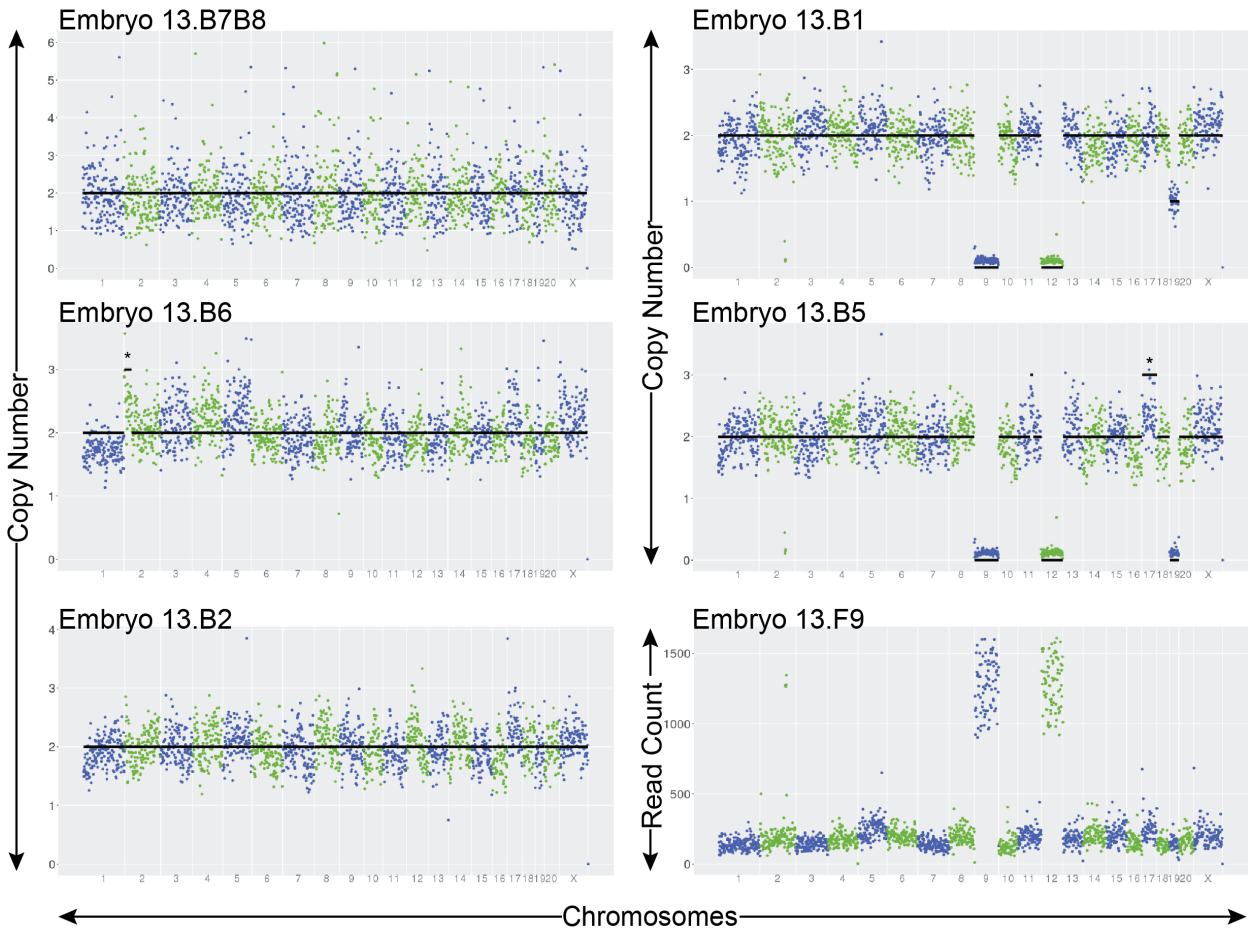

Figure 14. *Chromosomes are eliminated via cellular fragmentation.*

For mosaic embryo 13, CNV plots show a mix of euploid (left) and aneuploid (right) blastomeres where chromosome 9 and 12 are completely missing from blastomeres B1 and B5 along with losses in chromosome 19. A read count only plot reveals that the missing chromosomes 9 and 12 were detected in cellular fragment 9 (bottom right) of embryo 13. The asterisk (*) demarcates false positive CNVs detected only by the VNOWC pipeline, but categorized as euploid after cross examination with the CHI method.

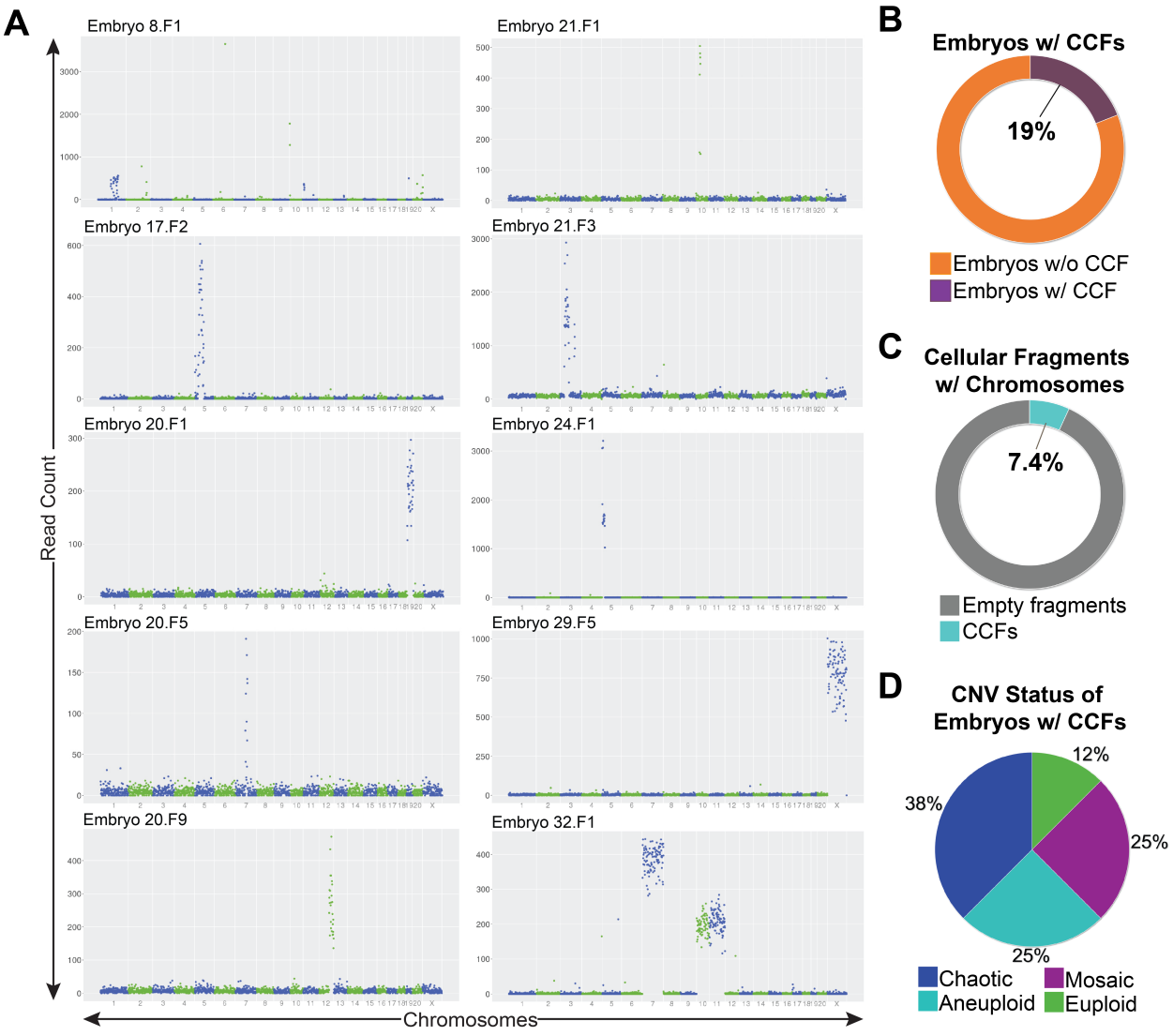

Figure 15. *The presence of chromosome-containing cellular fragments (CCFs) are mostly from aneuploid embryos.*

(A) Read count plots show individual, multiple, and/or partial chromosomes found in cellular fragments from different rhesus macaque embryos. (**B**) The percentage of embryos with CCFs (N=42 total embryos) and (**C**) the number of cellular fragments from all embryos (N=149) that contained chromosomal material. (**D**) The percentage of embryos with CCFs (N=8 embryos) that were chaotic (blue), aneuploid (turquoise), mosaic (magenta), and euploid (green).

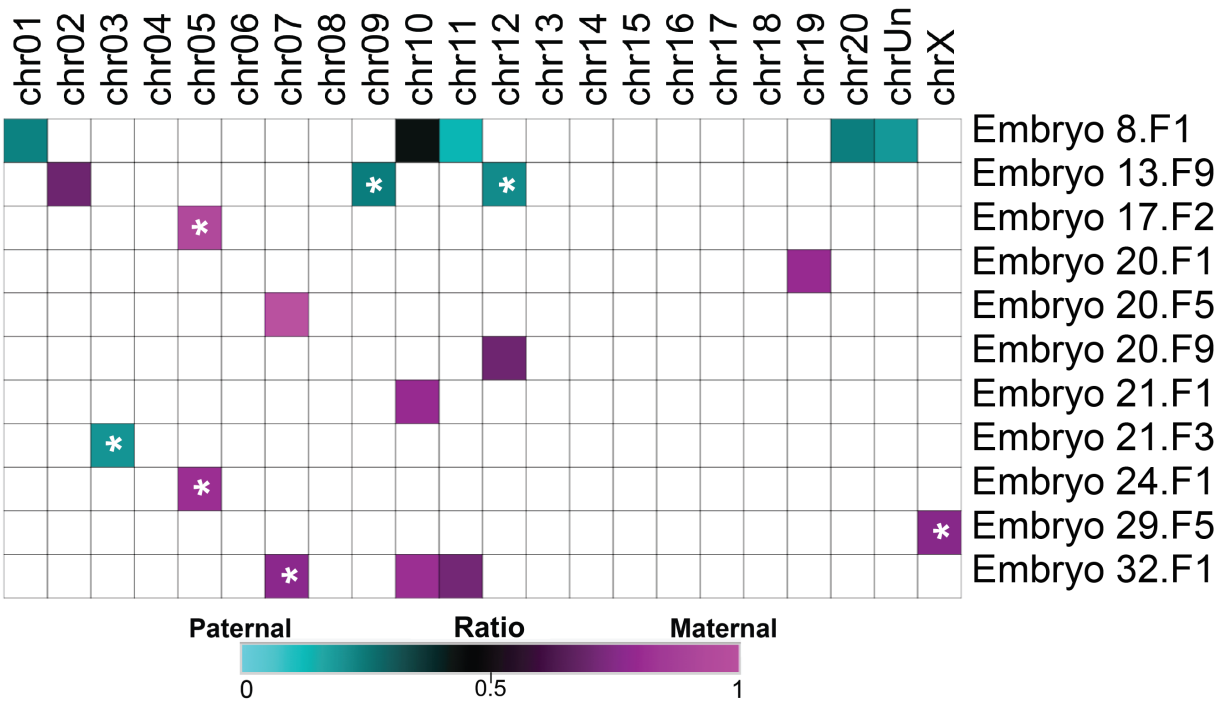

Figure 16. *Chromosome-containing cellular fragments (CCFs) are either maternal or paternal in origin.*

Heat map of maternal versus paternal SNP genotyping ratios showing that CCFs originate from either the mother or the father. White asterisk (*) demarcates significant p-values ($p<1.06X10^{-5}$) for cumulative binomial test with Bonferroni correction.

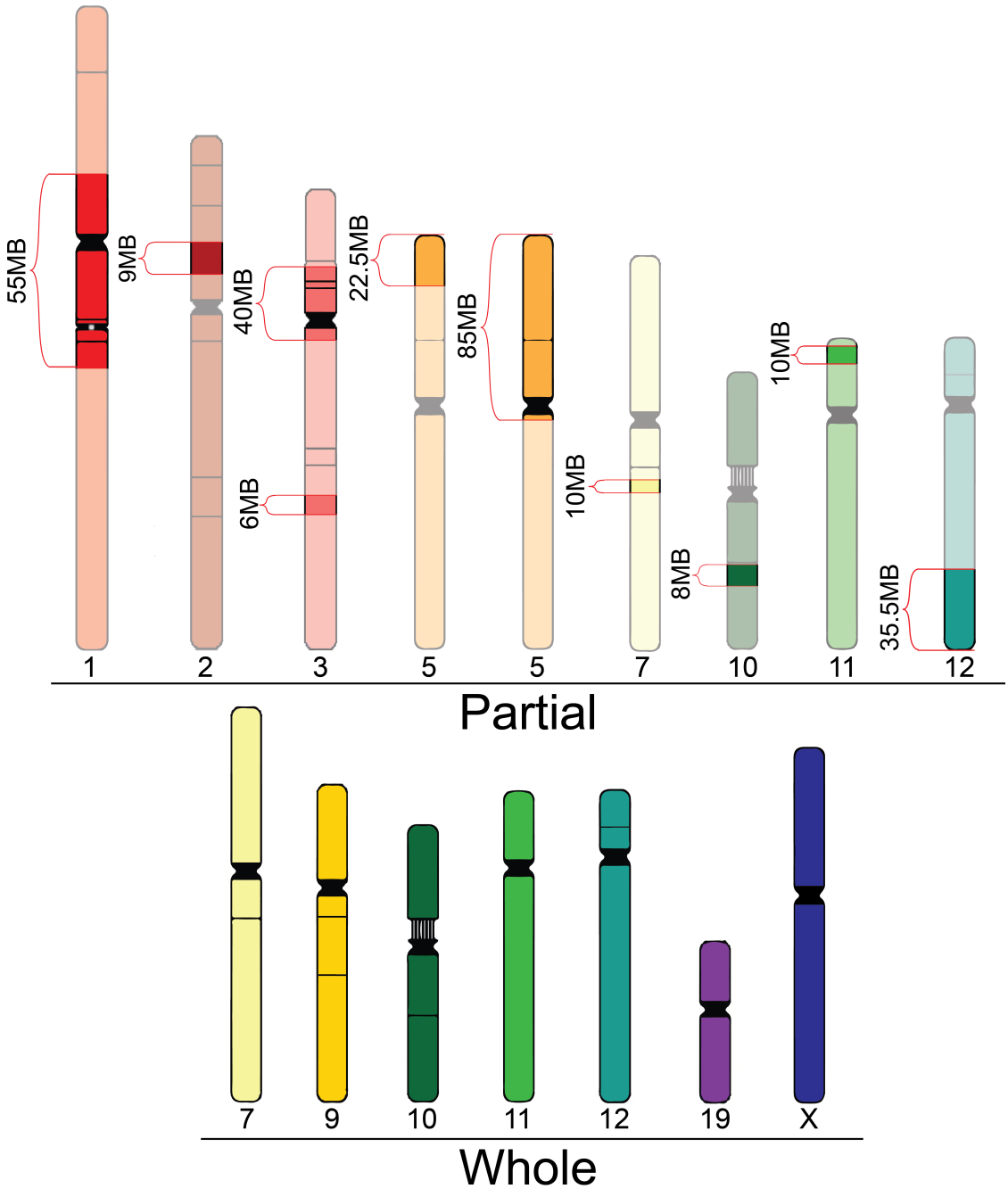

Figure 17. *Whole and partial chromosomes found in cellular fragments (CCFs) vary in size.*

Rhesus macaque ideograms representing the whole chromosomes (bottom) and chromosomal regions (top; highlighted) with approximate sizes identified in cellular fragments.

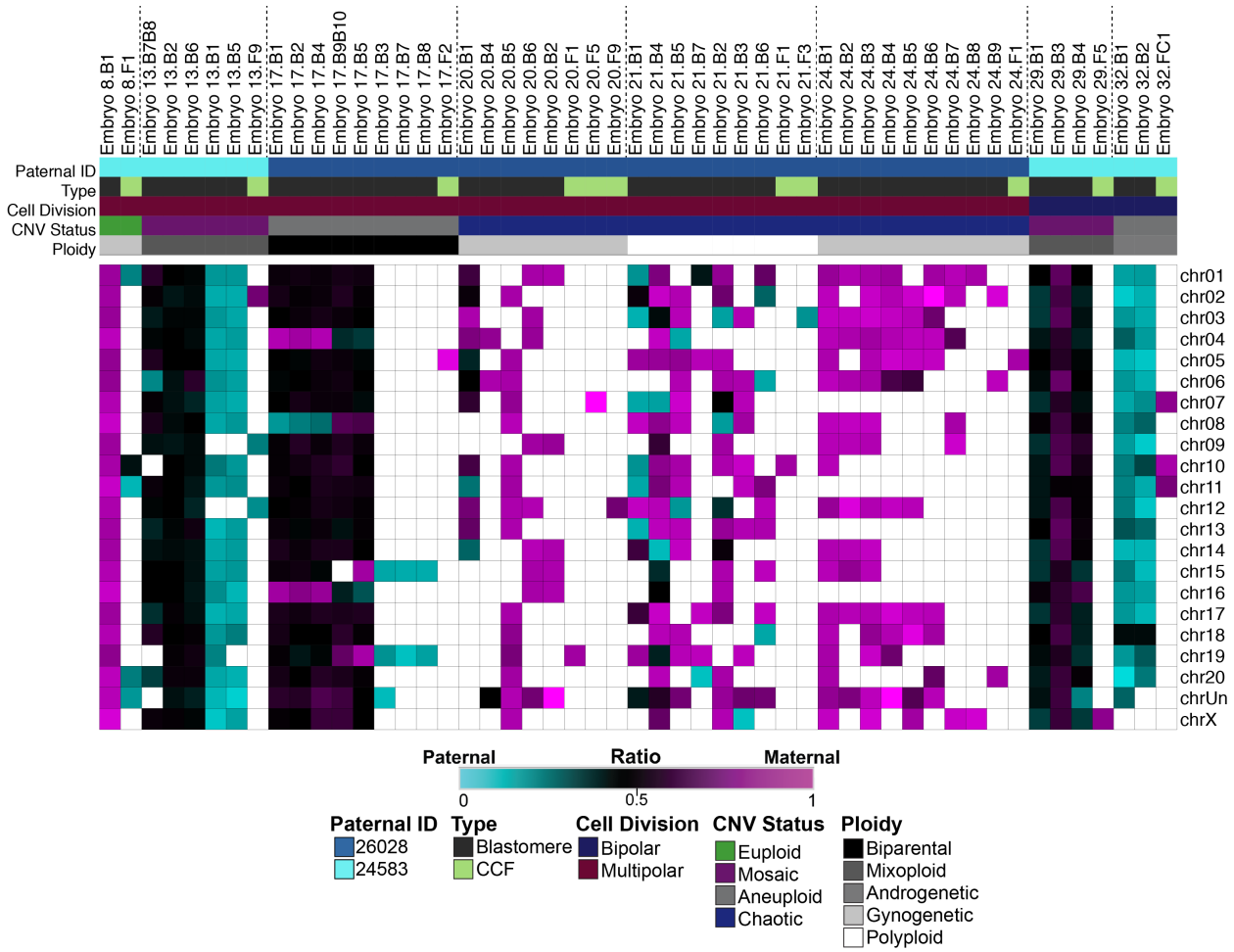

Figure 18. *Embryos with chromosomes found in cellular fragments (CCFs) often have abnormal ploidy and early multipolar divisions.*

Heat map of maternal versus paternal SNP genotyping ratios for embryos with CCFs.

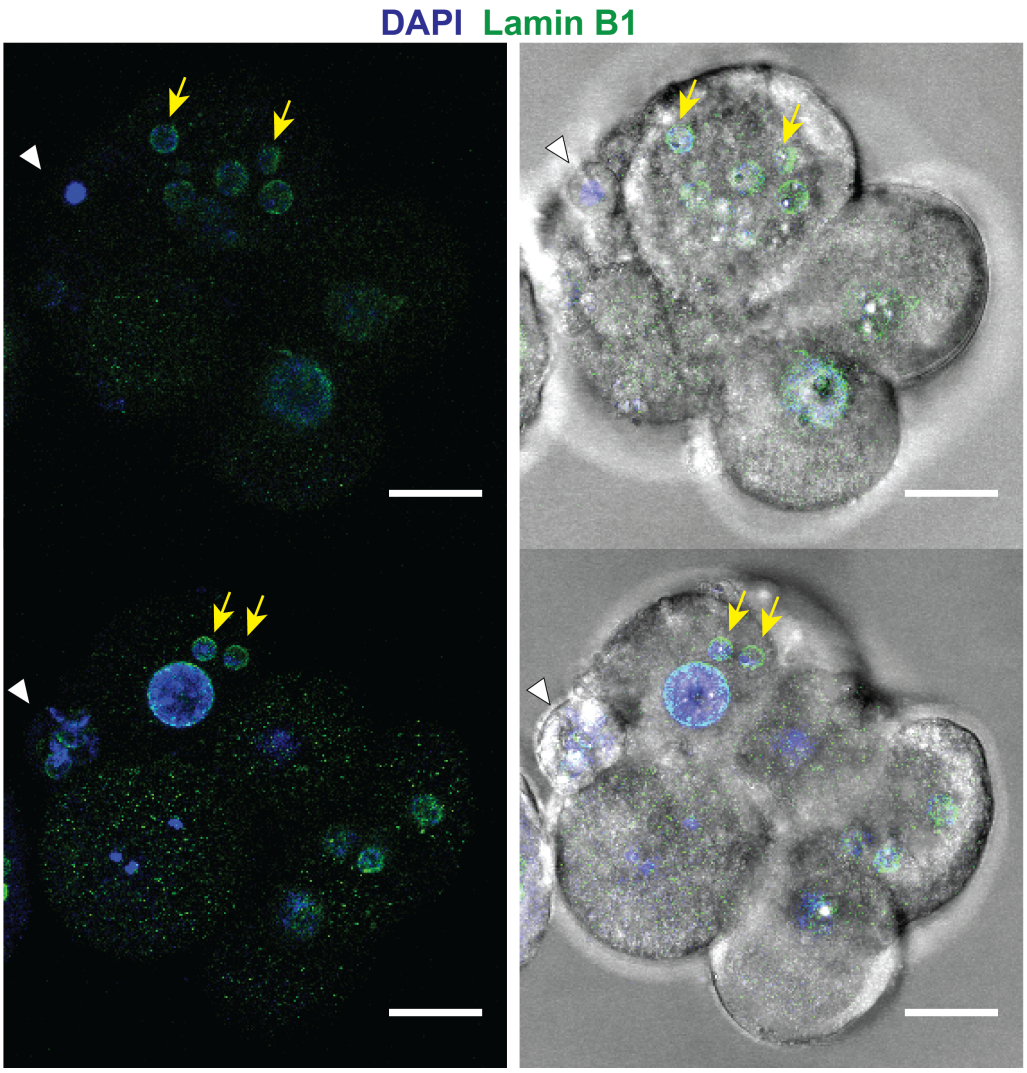

Figure 19. *DNA and micronuclei within cellular fragments detected in embryos by immunostaining.*

Eight-cell (top) and 7-cell (bottom) embryo with DNA and/or visible micronuclei within cellular fragments (white arrowheads). Note the similar in size of DNA signal in top embryo to the micronuclei in adjacent blastomere (yellow arrows). LAMIN-B1 (green) and DAPI (blue). Brightfield image (right panel) provided for reference. Only select stacks are shown. Scale bar: 25 μm.

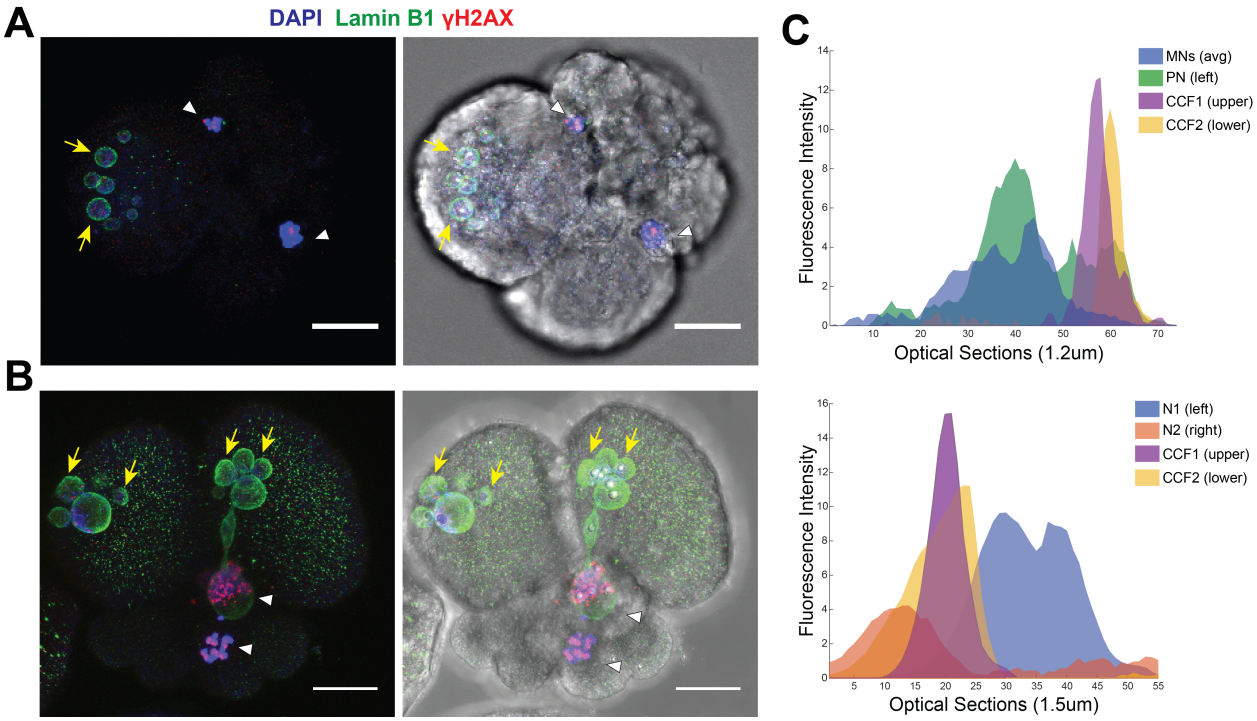

Figure 20. *Micronuclei containing damaged chromosomes are eliminated via cellular fragmentation.*

(A-B) 2-cell embryos with extensive cellular fragmentation and micronuclei also immunostained for the double-stranded DNA break marker, γH2A.X (red). (**B**) Note, the upper CCF1 has uniform γH2A.X as opposed to foci seen in lower CCF2. Only select stacks are shown. LAMIN-B1 (green) and DAPI (blue). Scale bar: 25μm. (**C**) Gamma-H2A.X fluorescence intensity measurements of nuclei (N or PN), micronuclei (MN), and chromosomes within cellular fragments (CCFs) for embryos to the left.

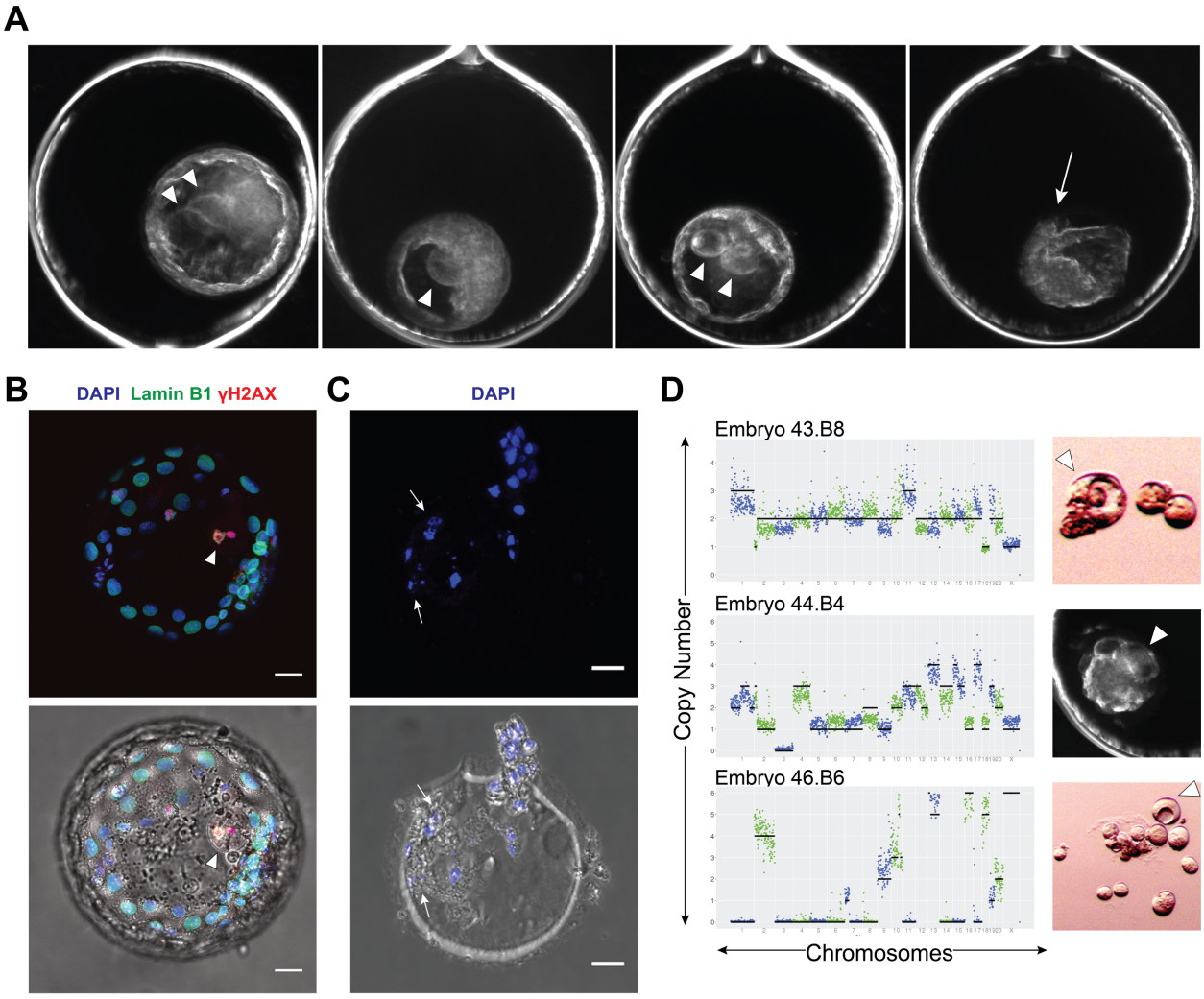

Figure 21. *Cellular fragments and aneuploid blastomeres are excluded upon blastocyst formation*.

(A) Darkfield time-lapse image frames from 4 rhesus macaque blastocysts exhibiting exclusion of either 1-2 non-dividing blastomeres confined to the blastocoel cavity (white arrowheads) or several cellular fragments into the perivitelline space of an embryo (white arrow). **(B)** One of the blastocysts with blastomere exclusion was immunostained with LAMIN-B1 (green) and γH2A.X (red) using DAPI (blue) for nuclear DNA. The large excluded blastomere appeared binucleated with strong γH2A.X signals (top; white

arrowhead), indicating that double-stranded DNA breaks had occurred. Brightfield image (below) provided for reference. **(C)** The zona pellucida from a blastocyst exhibiting cellular fragment exclusion left behind DNA material positive for DAPI staining upon hatching (white arrows). **(D)** Additional examples of large excluded blastomeres (white arrowheads in stereomicroscope images; right) collected during the morula-to-blastocyst transition were sequenced and the CNV plots (left) determined that each blastomere was aneuploid with numerous chromosome losses and gains. Scale bars: 25μm.

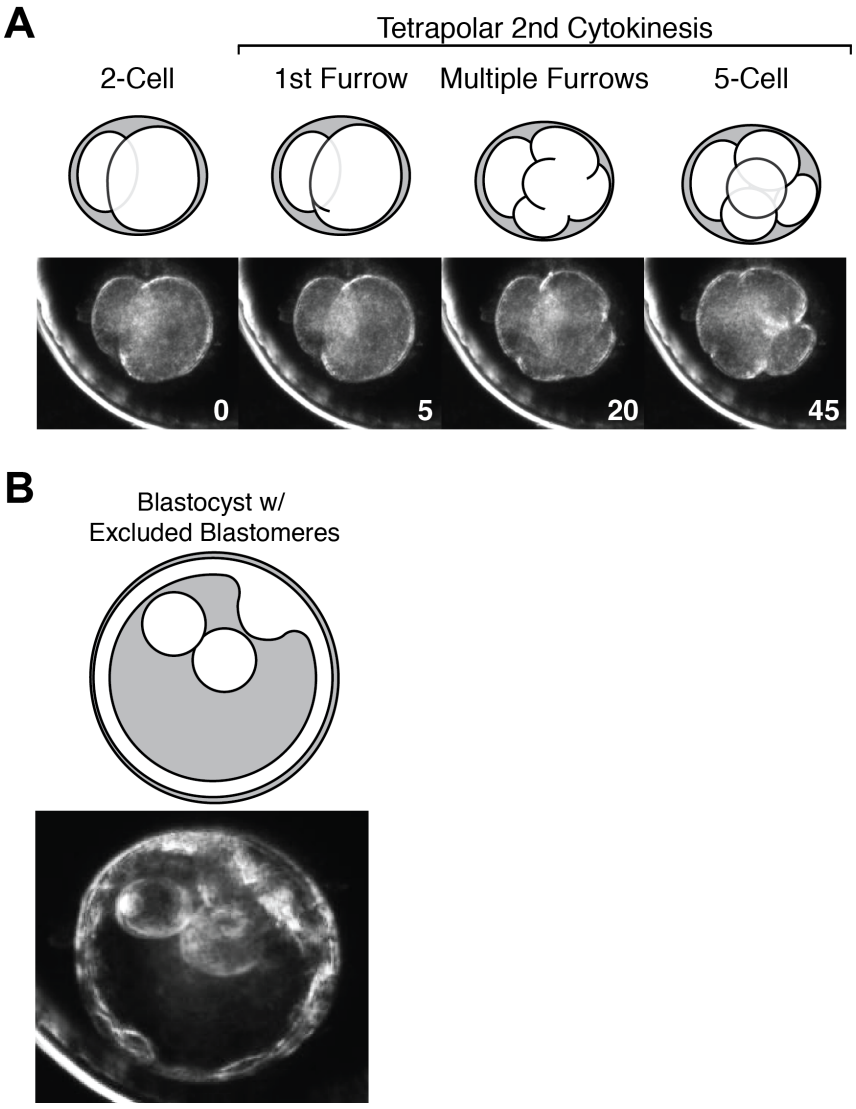

Figure 22. *Tetrapolar division at the 2-cell stage and blastomere exclusion.*

Schematic illustration and darkfield images of a rhesus macaque (**A**) 2-cell embryo undergoes a symmetrical tetrapolar second cytokinesis lasting approximately 40 minutes. The cell on the left never divides during this time. Numbers in bottom right corner of images represent the duration in minutes from the first, far-left image (t=0). (**B**) This embryo later had excluded blastomeres at the blastocyst stage. Rhesus macaque embryo imaged with the Auxogyn Eeva™ 2.2.1 darkfield time-lapse monitoring system.

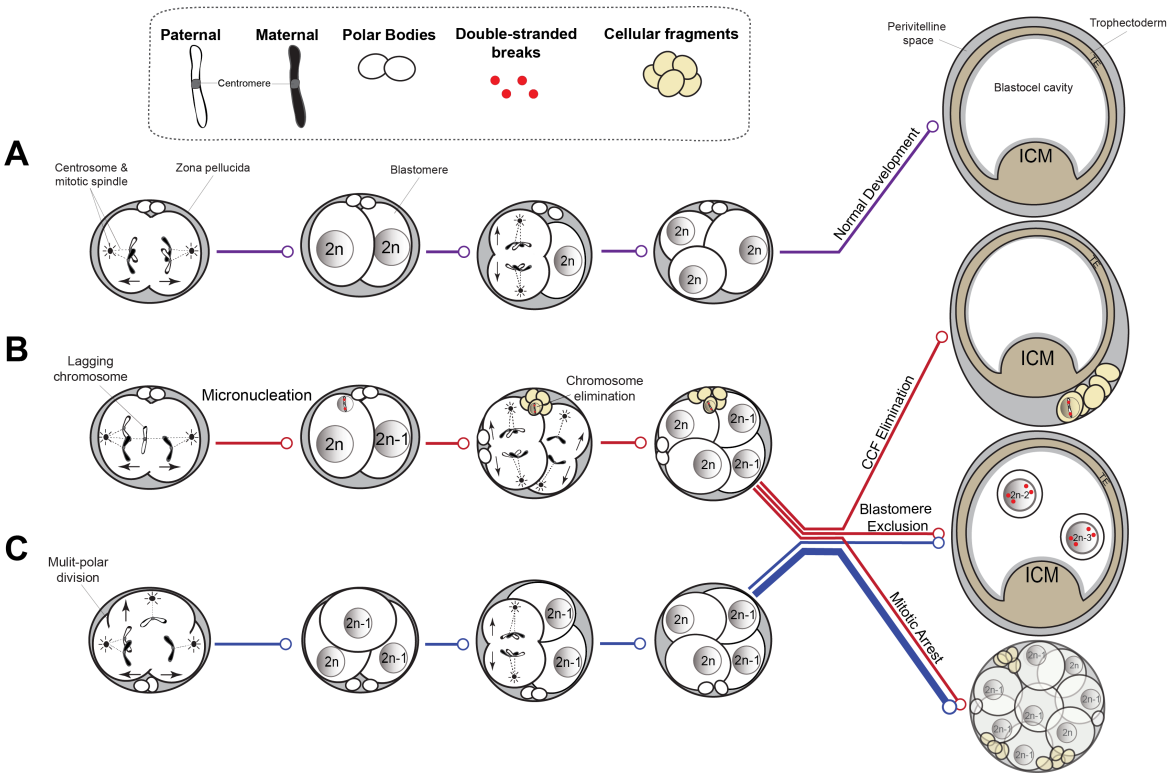

Figure 23. *Cellular fragments and aneuploid blastomeres are excluded upon blastocyst formation*.

(**A-C**) Simplified models depicting the effects of cellular fragmentation, blastomere exclusion, and multipolar divisions on early embryogenesis. (**A**) Normal embryo development, whereby a euploid zygote undergoes proper chromosome segregation with cell divisions devoid of cellular fragmentation and blastomere exclusion (purple lines). (**B**) Early embryogenesis of a euploid zygote that contains a lagging chromosome from merotelic attachments during the 1st mitotic division. The lagging chromosome becomes encapsulated in a micronucleus, where it undergoes DNA damage in the form of double-stranded breaks. Through the process of cellular fragmentation, the damaged chromosome is eliminated from the embryo and thus, the embryo is now mosaic, containing euploid and aneuploid blastomeres (red lines). (**C**) Abnormal cellular events, including a tripolar cleavage that occurs at the zygote stage, may also generate a mosaic

embryo (blue line). However, this is more likely to result in embryo arrest (thick blue line). (**B-C**) If the euploid-aneuploid mosaic embryo is able to progress in development to the blastocyst stage, the chromosome contained within a cellular fragment (CCF) may be sequestered to the perivitelline space. Severely aneuploid blastomeres fail to divide, undergo DNA damage, and become excluded from the embryo to the blastocoel cavity. Alternatively, aneuploid blastomeres may continue to divide until EGA or beyond, but the embryo will eventually arrest when aneuploidy is no longer tolerated and/or a critical number of euploid blastomeres is not achieved.

Preface: Chapter 3

Throughout chapters 1 and 2, comprehensive chromosomal screening of blastomeres and cellular fragments in cleavage stage embryos has demonstrated that rhesus macaque embryos are just as fraught with copy number and ploidy errors as human embryos. Although these studies provide insight into the complexity of chromosomal errors at this stage, this approach is not transferable to the clinical because embryos are destroyed in the process. However, the strength of these studies come from the associations made between embryo morphokinetics observed through TLM and CNV and ploidy outcomes determined with single-cell next generation sequencing. Not only does TLM technology have utility for improving culture environment during morphological assessment, but detection of abnormal nuclear structures and review of cell division parameters may assist in selecting embryos that are best for transfer. In this chapter, rhesus macaque embryos are assessed for nuclear morphologies and cell division parameters as previously described for human embryos to determine blastocyst development potential.

Chapter 3: Time-lapse imaging for rhesus macaque embryo quality assessment

Abstract

The use of time-lapse microscopic imaging has proven to be a powerful tool for the study of mitotic divisions and other cellular processes across diverse species and cell types. Although time-lapse monitoring (TLM) of human preimplantation development was first introduced to the IVF community several decades ago, it was not until relatively recently that TLM systems were commercialized for clinical embryology purposes. Traditionally, IVF embryos are evaluated by successful progression and morphology on a stereomicroscope at distinct time points prior to selection for transfer. Due to the high frequency of aneuploidy, embryos are often biopsied for trophectoderm cells at the blastocyst stage for preimplantation genetic screening of whole or segmental chromosomal abnormalities. However, embryo biopsy is invasive and can hinder subsequent development and there are additional concerns over chromosomal mosaicism and potential resolution with PGS. Moreover, embryos are typically outside of the incubator in sub-optimal culture conditions for extended periods of time during these procedures. With TLM systems, embryos remain in the stable microenvironment of an incubator and are simultaneously imaged for non-invasive embryo evaluation using a fraction of the light exposure as compared to a stereomicroscope. Each image is then compiled into a time-lapse movie, the information from which can be extrapolated to correlate morphological, spatial, and temporal parameters with embryo quality and ploidy status. However, the promise of TLM technology has not reached fruition like preimplantation screening has and this is largely due to insufficient evidence from randomized controlled trials that TLM is superior to conventional methods and the initial

cost of investment for clinically approved systems. Considering the promise of TLM technology but the lack of IVF improvements using this approach, more studies are needed to identify additional morphokinetic parameters that are predictive of embryo potential. An alternative animal model may be useful to develop this technology for detecting high quality embryos and potentially the presence of aneuploidy. In light of the compelling similarities between rhesus macaque and human embryos for aneuploidy including degree of cellular fragmentation, multipolar divisions, mosaicism, and multinucleation, we hypothesize that the rhesus macaque embryo will have similar morphokinetic parameters to human embryos and that embryo quality can be predicted by measuring the timing intervals for the first three cell divisions. In this chapter, TLM was used to assess embryo quality by measuring cell division timing interval in rhesus macaque embryos as well as documenting certain morphological features often associated with aneuploidy outcomes. The first three cell divisions of rhesus macaque embryos were predictive of blastocyst formation with 86% accuracy, sensitivity, and specificity and were significantly more similar to human than mouse for embryos that reach the blastocyst stage. Although the sample size of euploid embryos was not large enough to determine if the timing intervals of the first three mitotic divisions are predictive of copy number status, the continuous monitoring of embryos throughout development in a controlled environment aided in identifying events such as multipolar divisions and micronuclei formation which often resulted in embryo arrest.

Introduction

As discussed extensively throughout this dissertation, human preimplantation embryos endure a high incidence of aneuploidy following IVF. Recent reports have also indicated that a high percentage of human blastocysts capable of implanting upon uterine transfer are also aneuploid to some degree [30, 244, 319]. As a consequence, embryos that exceed the threshold for aneuploidy tolerance will either arrest prior to implantation or later result in spontaneous miscarriage if allowed to proceed in development. There are a multitude of ways by which aneuploidy can arise as a cell is undergoing mitosis, including defective microtubule attachment to the kinetochore region of the centromere, abnormal centrosome number, compromised spindle assembly checkpoints, and premature loss or prolonged persistence of chromosome cohesion [327]. Regardless of the mechanism(s), these defects will result in mitotic non-disjunction, chromosomal breakage, and/or chromosome lagging during anaphase if not resolved. All of these phenomena have also been identified in human IVF embryos and contribute to the high degree of mosaicism observed amongst cells during preimplantation development [109, 328].

Under current clinical IVF practice, human preimplantation embryos are traditionally scored for quality at the 1-cell stage and then again on day 2 and/or day 3 between 48 and 72 hours after fertilization at the 4- to 8-cell stage. Morphological features, including cell number, degree of cellular fragmentation, presence of multinuclei, and blastomeres symmetry in size are typically used to evaluate embryo developmental potential at the cleavage-stage [329, 330]. Although these snapshots in time greatly assist in the identification of the embryos that are likely to arrest, subtle and yet, informative developmental features might be missed from the several hours in between designated embryo assessments. To address some of the chromosomal aspects that conventional

embryo scoring may fail to detect, embryos are often biopsied for preimplantation genetic screening. However, embryo biopsy and additional screening measures require removal of the embryos from the physiological conditions that an incubator provides and increased exposure to light used to visualize embryos on a stereomicroscope. In addition, the biopsy of embryos is considered invasive and there is some evidence to suggest that it may hinder subsequent preimplantation development [331].

Considering the limitations of evaluating human embryos based on static time points and the risks associated with embryo biopsy for PGS, non-invasive time-lapse imaging techniques aid in the identification and/or selection of human embryos that are chromosomally normal [30, 92, 94, 95, 108, 332] and similarly benefits prognosis for other mammalian species [333-336]. With TLM, additional and non-subjective data are also made available to assist in the selection of the best embryo [337]. Besides timing between cleavage divisions, other mitotic events discussed in previous chapters such as multipolar divisions, cellular fragmentation dynamics, and micronucleation, may also indicate embryo quality and/or the presence of aneuploidy. Under certain circumstances, some of these same or additional imaging behaviors, including exclusion of cellular fragments and non-dividing blastomeres, might instead signal the capacity of an embryo to overcome chromosomal instability.

Previous findings in our lab determined that the majority of aneuploid human embryos can be non-invasively distinguished from chromosomally normal embryos by assessing the time intervals of the first three mitotic divisions in conjunction with cellular fragmentation [108]. Based on these results, we hypothesize that the correlation between early mitotic division timing is predictive of chromosomal status as well as embryonic arrest versus blastocyst development in rhesus macaque embryos. We hypothesize that rhesus

macaque embryos have similar cell division parameters compared to previous reports in human embryos. In this chapter, cell division parameters and additional morphological features such as micronucleation and multipolar divisions were evaluated to ascertain whether implementing TLM can enhance embryo assessment.

Methods

Rhesus Macaque Embryos

See page 35 in chapter 1 for detailed methods.

Time-Lapse Imaging

See page 36 in chapter 1 for detailed methods.

In addition to monitoring embryos throughout the cleavage stage prior to disassembly into individual cells and cellular fragments, several embryos were cultured up to 7 days to the blastocyst stage. Each image was time stamped with a frame number and all images compiled into an AVI movie using FIJI software version 2.0.0 (NIH, Bethesda, MD). The time intervals between the appearance of the 1st cleavage furrow to the end of the 1st cytokinesis, the beginning of the 2nd mitotic division, and the start of the 3rd mitotic division were manually recorded by three separate individuals and represented as an average. The duration of 1st cytokinesis was measured as $(t2 - t1)$ * ((frame interval in minutes)/60), the time between 2- to 3-cell was measured as $(t3 - t2)$ * ((frame interval in minutes)/60), and the time between 3- to 4-cell was measured as $(t4 - t3)$ * ((frame interval in minutes)/60) (**Figure 24**). Additionally, other features such as cellular fragmentation, asymmetrical/multipolar division, cellular fragment/blastomere exclusion, and nuclear defects were also examined and recorded for each embryo. For multipolar divisions, the time intervals were zero and reflected 3-4 simultaneous cleavage furrows.

The timing of the first three mitotic divisions in each embryo was plotted in 2- and 3-dimensional parameter plots using R Studio (R Foundation for Statistical Computing, Vienna, Austria) and Matlab R2016a (Mathworks, Natick, MA). Statistical tests included Mann-Whitney test for differences in medians and Levene's test for differences in variance per parameter between embryo groups. Principal component analysis, pruned decision tree, K-means clustering, and unsupervised hierarchical clustering were performed using R Studio.

Mouse Embryos

Reproductively mature (3-5 week) C57BL6 × DBA/2 (B6D2F1) female F1 mice were given intraperitoneal injections of 10 IU of Pregnant Mare's Serum Gonadotropin (PMSG) (Sigma-Aldrich, St. Louis, MO) followed by 10 IU of human Chorionic Gonadotropin (Sigma-Aldrich, St. Louis, MO) 48 hours later as previously described [317]. Female mice were paired with wild-type B6D2F1 male mice and allowed to mate overnight. Following successful mating, the females were sacrificed ~18 hours later and their oviducts removed to obtain cumulus-oocyte complexes. Cumulus cells were removed and zygotes with two pronuclei placed in a custom 25-well polystyrene petri dishes (Auxogyn, Inc., Menlo Park, CA) containing 100 µL of Quinn's Advantage™ Cleavage Medium with 10% serum protein substitute (SPS; Sage™, Trumbull, CT) or Global media supplemented with 10% serum protein at 37°C with 6% CO_2, 5% O_2 and 89% N_2 with no difference observed between medias. All animal procedures were performed under the IACUC protocol #16146 entitled, "Molecular Analysis of Embryogenesis and Gametogenesis," which was approved by the Stanford University Administrative Panel on Laboratory Animal Care.

Results

Detecting abnormal nuclear structures with brightfield TLM.

A key advantage of using time-lapse imaging for embryo assessment is the ability to detect abnormal nuclear morphologies that reveal ploidy errors and chromosome missegregation events. As numerous studies in the cancer field have demonstrated, micronuclei formation around lagging chromosomes is a visual hallmark for inferring chromosomal instability and DNA-damage [313]. Findings presented in chapter 2 demonstrated that micronuclei can be eliminated from blastomeres through cellular fragmentation and these embryos from which they were eliminated were affected by copy number and ploidy errors. With brightfield TLM, these micronuclei as well as other nuclear defects can be observed in rhesus macaque embryos. When abnormal nuclear morphologies are present in blastomeres, conclusions can be made depending on when the nuclear defects occur. If micronuclei are present in a zygote, the embryo is affected by a meiotic error originating from the oocyte or the chromosome missegregation occurred upon pronuclear assembly from the sperm nucleus. This error would be propagated to all daughter cells unless eliminated in subsequent mitoses. Aneuploidy at the 1-cell stage is much less likely to be tolerated in rhesus macaque embryos since there are no known viable aneuploidies. Nuclear defects such as micronucleation at the 2-cell stage (**Figure 25B**) would also have a poor prognosis as all cells would be affected by genomic instability but may be tolerated at later cleavage stages in euploid-aneuploid mosaic embryos (**Figure 25C**). The occurrence of binucleation in the early cleavage stages (**Figure 25D**) is also common and can be a sign of successful karyokinesis but absence of cytokinesis leading to a tetraploid cell. Likewise, a binucleated cell may be diploid where a haploid genome underwent

endoreduplication. Since EGA does not occur until approximately the 8-16 cell stage in rhesus macaque embryos, abnormal nuclear morphologies that denote incorrect chromosome number are permissible up to this point.

The first three mitotic divisions are highly predictive of rhesus macaque embryo fate

Based on the high incidence of multipolar divisions at the 1- to 2-cell stage reported in chapter 1 and previous reports that the timing intervals of the first three mitotic divisions are predictive of blastocyst formation and/or ploidy status in human embryos [72, 91, 108], this study aimed to determine if early mitotic timing was similarly prognostic for rhesus macaque preimplantation development. Therefore, 92 rhesus macaque zygotes were monitored by TLM, but allowed to progress up to blastocyst stage. While 42 of these embryos arrested during mitosis prior to day 7, the remaining embryos reached the blastocyst stage with a blastocyst formation rate of ~54% (N=50/92). Of the 92 embryos, ~18.5% (17/92) underwent a multipolar division and ~88% (N=15/17) of those arrested following the abnormal division. Notably, the two multipolar embryos that still formed blastocysts exhibited a unique 1- to 4-cell symmetrical multipolar division without cellular fragmentation at the 1- or 2- cell stage (**Figure 22**).

The timing intervals of the first three mitotic division were recorded for all embryos. The duration of the first cytokinesis lasted from first cleavage furrow of the zygote (t1) to the end of cytokinesis (t2). The parameter for the second cell division was the time between the start of the first cleavage furrow at the 2-cell stage (t3) and the end of the first cytokinesis (t2). The parameter for the third cell division was the time between the start of

the cleavage furrow at the 3-cell stage for the cell that did not divide at the 2-cell stage (t4) and the end of the second division (t3) (**Figure 24**). An examination of the average time intervals between the first three mitotic divisions in embryos that successfully reached the blastocyst stage was 35.15 ± 15.26 minutes, 9.33 ± 2.52 hours, and 1.97 ± 2.32 hours, respectively. In contrast, the arrested embryos exhibited longer mitotic timing intervals and/or large standard deviations with averages of 59.21 ± 50.49 minutes, 8.80 ± 10.82 hours, and 6.27 ± 5.84 hours. Taken together, statistically significant differences ($p \leq 7.1 \times 10^{-4}$; Levene's test) in the variances of all three divisions were observed in blastocysts versus arrested embryos, but the medians of only the 1st and 3rd mitotic divisions were significantly different ($p \leq 7.6 \times 10^{-4}$; Mann-Whitney test) between the two embryo groups (**Figure 26A**). When each embryo was graphed as a symbol in 2- and 3-dimensional (**Figure 26B & C**) parameter plots, the blastocysts tended to cluster more tightly in a similar region of mitotic timing than the arrested embryos. Using these data, a prediction tree for determining the likelihood of an embryo developing into a blastocyst was constructed based on early mitotic timing. As shown in **Figure 27**, if the time to the 2nd division was ~6 to ~15 hrs., and the duration of the 1st division was less than ~40 mins., or the time between the 2nd and 3rd division was less than 0.375 hrs., then the embryo had a high probability of progressing to the blastocyst stage with ~86% accuracy, sensitivity, and specificity. A similar type of analysis was performed to determine if the first three mitotic divisions with or without cellular fragmentation assessment could predict abnormal chromosome number in embryos, but no statistical differences between groups were found (data not shown). This may be due to a gap in mitotic timing measurements since most euploid embryos were collected at the 2-cell stage.

Early mitotic timing is more similar between human and rhesus macaque than mouse

To determine if rhesus macaque embryos can also be a suitable model for studying cell division parameters for human embryos that go on to reach the blastocyst stage, the first three mitotic timing intervals of all rhesus macaque blastocysts were compared to those previously obtained for human blastocysts [72]. While a wider variance was observed for the duration of the 1st mitotic division in rhesus macaque embryos, the time to both the 2nd and 3rd mitotic divisions was quite similar between rhesus macaque (N=50) and human (N=36) blastocysts (**Figure 28A**). This was in contrast to mouse blastocysts measured in this study (N=37), which exhibited a distinctly long 2nd division of ~20.0 $\pm$ 3.14 hours ($p<1x10^{-4}$), likely due to species-specific differences in the onset of embryonic genome activation [123, 278, 279]. When the blastocysts from each species were graphed as different symbols in 2- and 3-dimensional parameter plots (**Figure 28B**), there was overlap in the timing intervals between rhesus macaque and human blastocysts and their distinction from mouse blastocysts became more apparent. Principal component analysis and k-means clustering for further stratification identified nine outliers that differed in mitotic timing from all three species (**Figure 29A**). Taking these outliers into consideration, the data were re-categorized into three discrete clusters that primarily included rhesus macaque (N=44/49) and human blastocysts (N=33/36) in the first cluster, the outliers (N=9) in cluster 2, and most of the mouse blastocysts (N=32/37) in the third cluster. Similar results were observed by unsupervised hierarchical clustering, which demonstrated more overlap in the assembly of rhesus macaque and human blastocysts than that of mouse (**Figure 29B**). Thus, besides having a higher frequency of aneuploidy than mice [18, 19], rhesus macaque and human embryos also exhibit comparable timing between mitotic divisions during early preimplantation development.

Discussion

Preimplantation genetic screening of embryos to detect aneuploidy is implemented in most fertility clinics in the United States. Randomized control trials using PGS to evaluate the copy number status have varied for demonstrating improvements in IVF outcomes. Studies have ranged from worsened outcomes to no differences in earlier studies, [37, 338, 339] to modest improvements over IVF without preimplantation genetic screening in prospective randomized trails [51, 340-342], however the study design of these trials have been called into question [343]. Nonetheless, embryo biopsy for PGS requires a highly skilled embryologist to perform an invasive procedure that could be detrimental to subsequent development. Additionally, mild segmental and whole chromosome aneuploidies in human mosaic embryos seem to be tolerated since they can implant and result in live births of healthy offspring [245]. Without strong clinical evidence to support the benefit for adding PGS to an IVF cycle, increased cost and missed opportunity for mosaic embryos may be the unfortunate real outcomes of this treatment. With the unclear benefit of PGS, new research has been geared toward alternative, non-invasive means of assessing embryo quality.

Progression through the cell cycle can delay if there is abnormal chromosome number. Therefore, cleavages that are outside of the ideal time frames for normal cell division parameters may indicate that the embryo has reduced developmental potential due to aneuploid blastomeres. Using TLM, deviation from the ideal cell division parameters for the first cell divisions of high quality embryos can be measured. In addition, the detection of abnormal nuclear structures that are indicative of chromosomal instability can be seen with brightfield TLM at early stages. The first cytokinesis for a normal human zygote should be on day 2 in the realm ~24–27 hours after fertilization. The duration of the first

cytokinesis should last 14.3 ± 6.0 minutes for those zygotes that go on to reach the blastocyst [72] and 14.4 ± 4.2 minutes for human embryos that will likely be chromosomally normal at the 4-cell stage [108]. For the 2nd and 3rd mitotic divisions, the ideal times when the cleavage furrow should appear is 11.8 ± 0.71 hours and 0.96 ± 0.84 hours respectively for human embryos that are chromosomally normal at the 4-cell stage [108]. In this study, rhesus macaque embryos that reached the blastocyst stage had similar intervals for the first three mitotic divisions with 35.15 ± 15.26 minutes (mins.), 9.33 ± 2.52 hours (hrs.), and 1.97 ± 2.32 hrs., respectively, especially when compared to mouse for the second division.

Although the data analyzed here were not sufficient for assessing cell division parameters for predicting copy number status in rhesus macaque embryos, this study did confirm that rhesus macaque is more similar to human than mouse and thus would be a more suitable model for developing this technology. Implementing TLM to measure cell division parameters as well as detect abnormal nuclear structures like micronuclei or multipolar divisions may prove an effective alternative, non-invasive method to PGS. Even if TLM does not replace PGS for detecting aneuploid embryos, the continuous monitoring of embryos in a stable environment is an excellent reason to utilize this technology over traditional embryo morphology assessment at static time points. More TLM studies are needed that implement tools to systematically and autonomously collect these measurements so that subjective biases can be avoided when assessing embryos. With the numerous similarities shared between human and rhesus macaque embryos, further TLMs are merited in the rhesus macaque model.

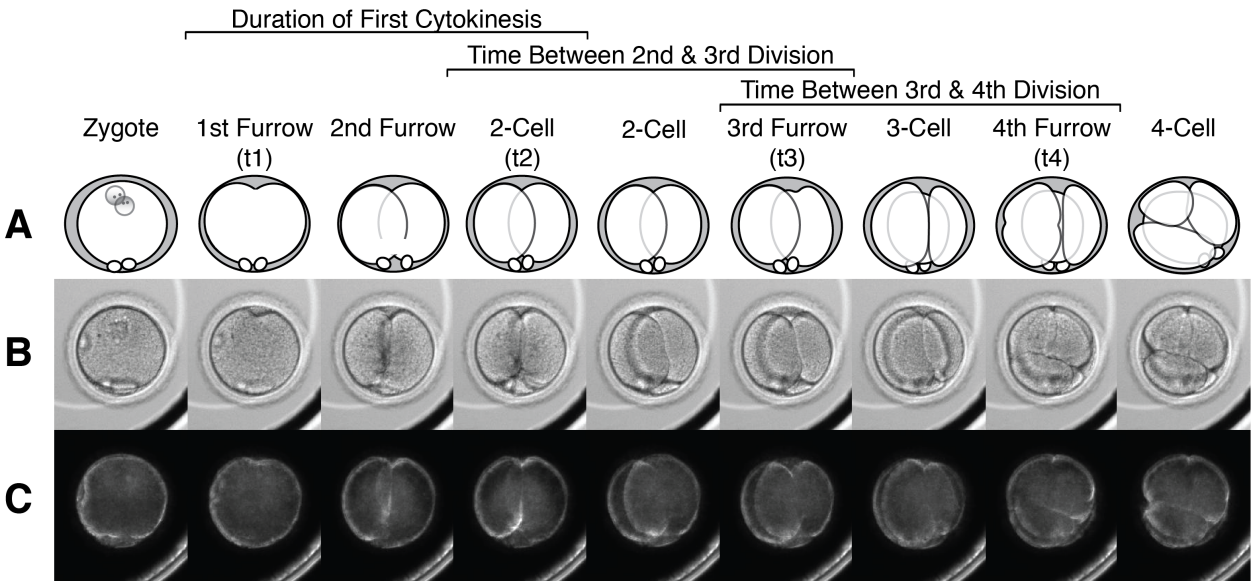

Figure 24. *Cell division parameters to the 4-cell stage.*

(A) Schematic illustration of a rhesus macaque embryo from zygote to 4-cell stage (below) imaged with the Auxogyn Eeva™ 2.3.5 bimodal time-lapse monitoring system. Large white circles are blastomeres and small while ovals are polar bodies. Intervals between morphokinetic time points (above) outline cell cycle parameters used to determine if dividing embryos are within timing windows for normal development. The zygote containing 2 pronuclei and 2 polar bodies, was imaged using **(B)** darkfield and **(C)** brightfield illumination for cleavages up to the 4-cell stage.

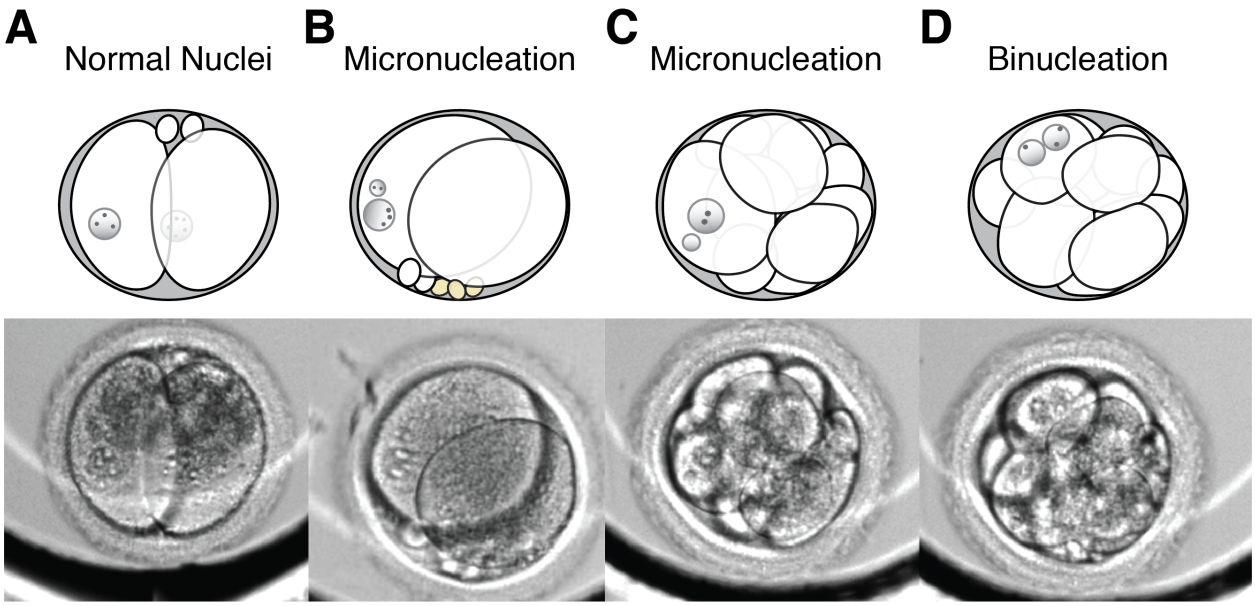

Figure 25. *Characteristic nuclear morphologies associated with chromosomal instability.* Rhesus macaque embryos at different stages of development with varying types of nuclear morphology ranging from (**A**) normal to micronucleation at the (**B**) 2-cell and (**C**) ~10-cell stage, or (**D**) binucleation. A cartoon of each embryo is shown above the brightfield image to aide in depicting the location of nuclear structures of interest. Cellular fragments are light-yellow ovals. Brightfield images were captured with the Auxogyn Eeva™ 2.3.5 bimodal time-lapse monitoring system.

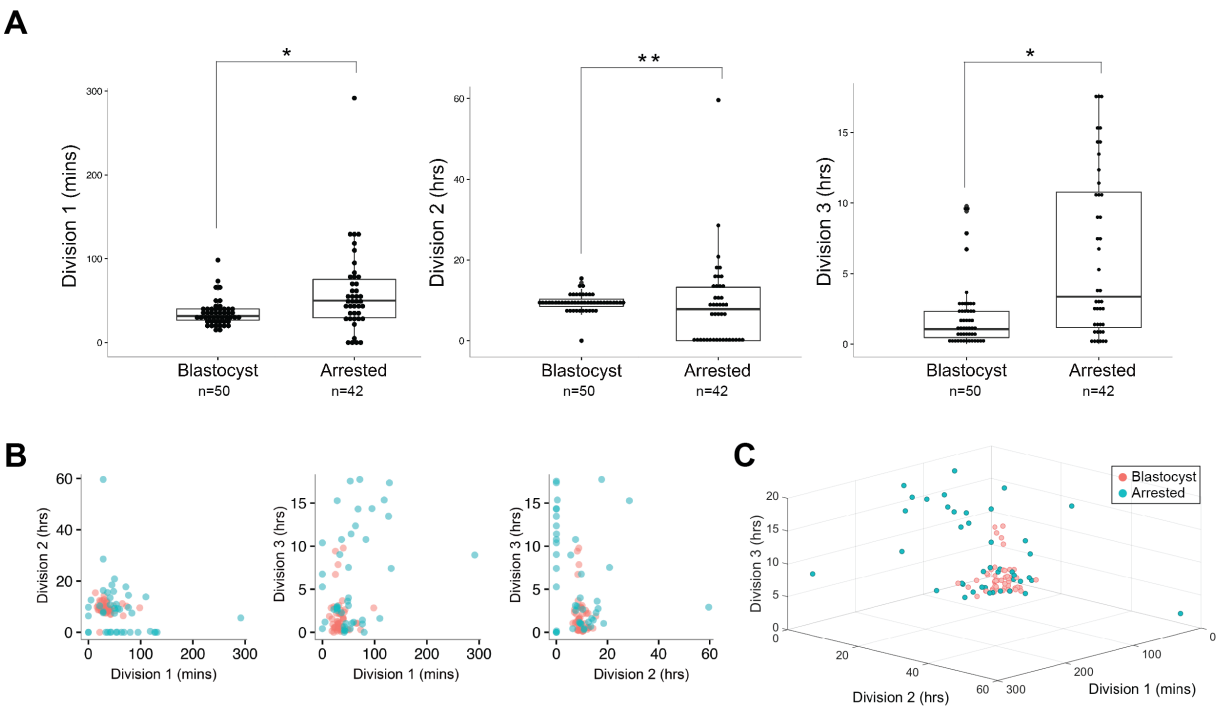

Figure 26. *Cell division parameters differ between embryos that reach blastocyst or arrest.* **(A)** Box and whisker plots showing the length of time for the duration of the 1st cytokinesis (Division 1) in minutes (mins.), time between the 1st and 2nd mitosis (Division 2) in hours (hrs.), and time between the 2nd and 3rd mitosis (Division 3) in hrs. between blastocysts and arrested embryos. *Both the median (Mann-Whitney test) and variance (Levene's test) between the two groups are significantly different ($p<0.001$); **only variance between the two embryo groups is statistically significant ($p< 0.0001$). **(B)** 2- and 3-dimensional scatter plots for Division 1, Division 2, and Division 3 in blastocysts (red) and arrested (blue) embryos.

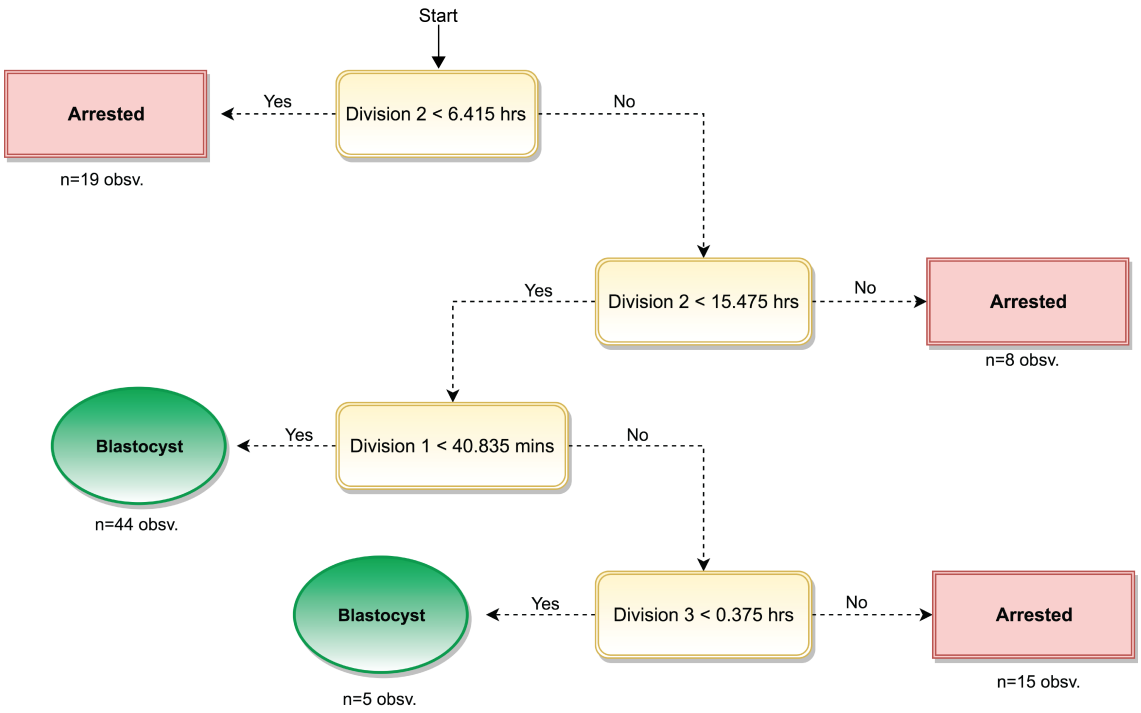

Figure 27. *The first three mitotic divisions predict rhesus macaque blastocyst formation.* Pruned decision tree for determining whether an embryo will likely reach the blastocyst stage or arrest prior to this based on the timing intervals of the first three cell divisions with a prediction accuracy, sensitivity, and specificity of ~86%.

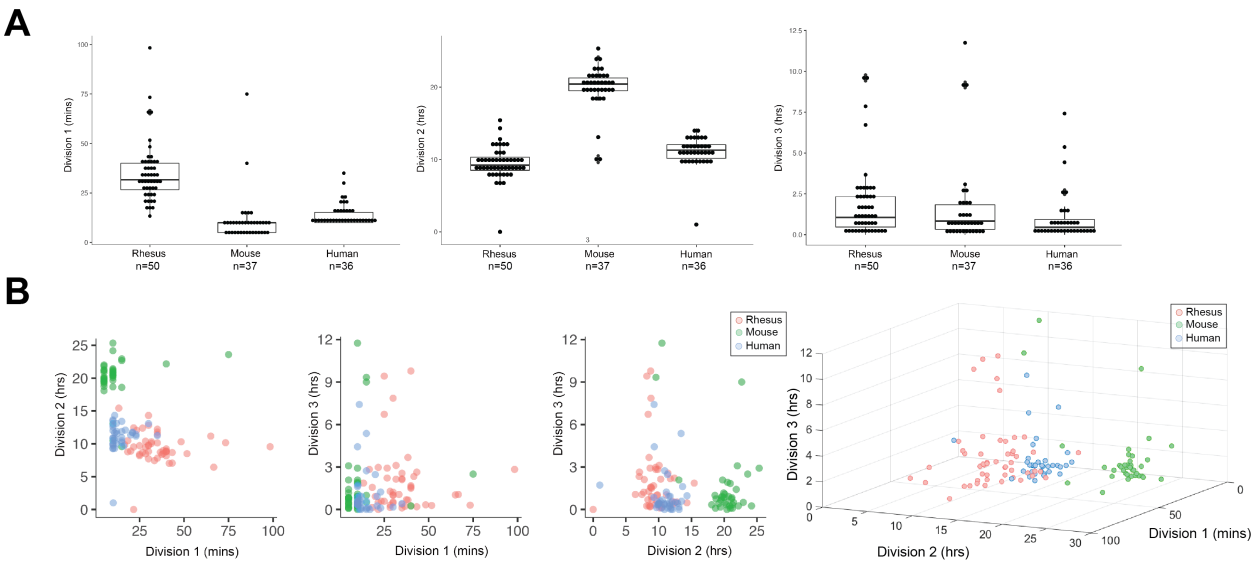

Figure 28. *Cell division parameters are more similar between rhesus macaque and human blastocysts than mouse.*

(A) Box and whisker plots of the time intervals for Division 1, Division 2, and Division 3 in rhesus macaque, mouse, and human blastocysts. **(B)** 2-D and 3-dimnesional scatter plots for Division 1, Division 2, and Division 3 in rhesus macaque (red), mouse (green) and human (blue) blastocysts.

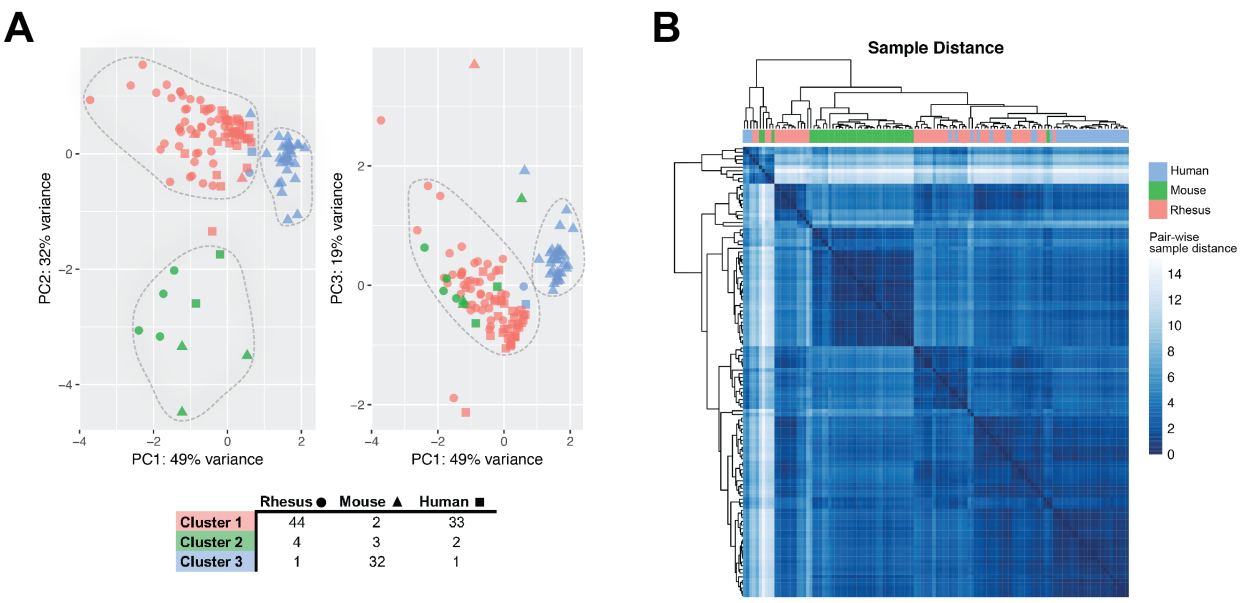

Figure 29. *Rhesus macaque and human blastocysts division parameters overlap based on principle component analysis and unsupervised hierarchical clustering.*

(A) Principle component analysis (PCA) plots of PCA1 versus PCA2 (left) and PCA1 versus PCA3 (right) based on median and scaled by median absolute deviation (MAD) with unsupervised K-mean clustering of similar groups; rhesus macaque = ●, mouse = ▲, human = ■. **(B)** Unsupervised hierarchical clustering of the first three mitotic divisions in rhesus macaque (red), mouse (green) and human (blue) blastocysts.

Conclusions

Significance to the Scientific Community

Infertility is relatively common in humans, impacting 10-15% of reproductive-age couples. The use of IVF has more than doubled in the past decade and is expected to continue to increase [11]. Despite considerable advances, IVF success rates still hover around ~30-35% for patients (when all age groups are combined) in the United States (cdc.gov/art), and this is primarily due to whole and sub-chromosomal abnormalities [3]. Although much of the increase in the number of IVF cycles performed each year can be explained by couples continuing to delay childbearing for a variety of reasons, aneuploidy is not only associated with female patients of an advanced maternal age. Remarkably, mothers of all ages can produce a high percentage of aneuploid embryos as shown in a previous study, wherein 83% and 70% of embryos from both young and fertile women exhibited whole-chromosomal imbalances and sub-chromosomal abnormalities, respectively [26]. In addition, the implementation of more advanced IVF techniques such as intracytoplasmic sperm injection, preimplantation genetic screening, and assisted hatching have not dramatically changed the percentage of live births [6-8, 344]. An approach that has significantly improved pregnancy and live birth rates is the transfer of frozen-thawed euploid blastocysts [30] and this is thought to be due to improved endometrial receptivity during a natural rather than stimulated cycle [345, 346]. Therefore, the development and implementation of strategies that directly target the embryo to ameliorate aneuploidy and improve IVF outcomes are still greatly needed. Such an improvement, however, may not be achievable since chromosomal instability is likely inherent to human pre-implantation development rather than an artifact of IVF.

Although the frequency of aneuploidy in human oocytes and pre-implantation embryos is fairly well defined across various ages thanks to the field of pre-implantation genetic screening, the etiology is far less understood. Until relatively recently, few human embryo studies have addressed aneuploidy arising from post-fertilization mitotic errors that lead to euploid-aneuploid mosaicism, and understandably so since such studies would require their destruction. To circumvent the creation and destruction of human embryos for research, studies often use supernumerary, immature, and/or suboptimal donated oocytes and embryos from IVF clinics. The effect of embryo quality can leave more questions than answers when interpreting results, especially when using morphology as a predictor of aneuploidy [120, 347]. Heterogeneity in the health status of patients, whether directly related to infertility or idiopathic, also poses a problem, especially when dealing with small samples sizes. To effectively investigate mechanisms that lead to aneuploidy generation, the ideal controlled experiments would require high-quality gametes and pre-implantation embryos from couples that are otherwise healthy and of average reproductive age. Such studies are exceedingly difficult for a number of reasons, including legislative regulations prohibiting the use of federal funding for human embryo research, along with bioethical views held by society and the scientific community [348], and potential medical risks that oocyte donors might encounter during ovarian stimulation [349].

For these reasons, among others not yet defined, human embryo research should be preceded and refined in a suitable animal model if available. As stated previously, most embryology research is carried out in the mouse, but this species has a considerably lower aneuploidy frequency than human embryos and the sperm does not contribute the centrosome to set up the first cell divisions. Bovine pre-implantation embryos have also been utilized for embryology research and a recent report showed that aneuploidy levels are just as frequent in the cow (74%) [21] as levels recorded in human and now in rhesus

macaques (this study). However, the bovine oocytes from the Destouni et al. study were collected directly from ovaries post-slaughter and underwent *in vitro* maturation, which is known to increase aneuploidy by itself [22]. Cleavage-stage bovine embryos are also opaque under basic light microscopes due to high lipid content, making it difficult to assess blastomere morphologies and nuclear structures without the aid of dyes, fluorescent markers, or stratifying organelles by centrifugation [350]. Although both murine and bovine embryos have their clear advantages for facilitating fast and cost-effective embryology research, the lower frequency of aneuploidy and cellular fragmentation in these models reduces their utility for discovering mechanisms that lead to aneuploidy generation in humans. Furthermore, mice produced for research are heavily inbred, and to a lesser extent, livestock also lack genetic diversity since certain strains are favored for meat and dairy production [351]. This lack of genetic diversity and breeding schemes to produce robust animals that reach sexual maturity at younger ages may select against defects in gametes or embryos that cause infertility and/or the early embryonic losses that we wish to study. Finally, the age of oocyte and sperm procured from these animals are several decades younger compared to the human equivalents. It is well established that with increased maternal age, abnormal segregation of chromosomes and altered patterns of recombination increase in the oocyte simply due to degradation of proteins necessary for meiosis and lack of appropriate maternal mRNA clearance [352-355]. Under these considerations, an animal model such as the macaque that takes 4-6 years to reach sexual maturity (as opposed to a few weeks in the mouse or 13-15 months in US cattle; http://www.partners-in-reproduction.com/) may provide oocytes that are more similar to their human counterparts and easily translatable. With this in mind, we aimed to determine whether rhesus macaque pre-implantation embryos would serve as a suitable replacement for the study of aneuploidy based on their numerous shared physiological traits and evolutionary proximity.

In this study, we indeed confirmed that the rhesus macaque embryo can act as a surrogate model since similar degrees of aneuploidy, cellular fragmentation, micronuclei formation, abnormal cell divisions, and ploidy errors were shared with human embryos. Not only were meiotic and mitotic errors distinguished by the detection of polar bodies and comparison to blastomere composition, but a range of aneuploidies were observed from trisomies and monosomies to chaotic aneuploidies as well as segmental aneuploidies resulting from mitotic breaks. We also demonstrated, for the first time, the relationship between micronuclei formation and cellular fragmentation in pre-implantation embryos by single-cell sequencing. Both of these cellular features are commonly seen in human embryos, but not in mouse, and less frequently (~15%) in the bovine model [356]. The elimination of micronuclei via fragmentation was observed in rhesus macaque embryos, indicating that the removal of missegregated chromosomes may occur instead of reincorporation into the primary nucleus. Immunofluorescence analysis of DNA damage primarily within the micronucleus confirmed that the DNA it contains is fragile and alludes to the possibility that early embryos undergo chromothripsis. Interestingly, the degree of DNA damage appeared to be intensified in micronuclei that were eliminated from the embryo through cellular fragmentation. With this finding, it is conceivable that damaged chromosomes are eradicated to avoid propagation of highly rearranged, unbalanced chromosomes. Furthermore, this study is one of the first of its kind to perform SNP analysis to determine chromosomal origins and overall ploidy using parental DNA and single-cell DNA sequencing of pre-implantation embryos. We determined that ploidy errors such as mixoploidy, gyno- and andro-genesis, and polyploidy, as well as multipolar divisions, were often observed in embryos with cellular fragments that contained missegregated chromosomes. The close association between ploidy and cell division errors points to

centrosomal defects playing a significant role in aneuploidy generation, but further studies are needed to resolve the critical players in this process.

The findings presented here offer the reproductive biology and IVF community new evidence for how an embryo might overcome chromosomal instability at an early stage to continue onward through development. Chromosome elimination through cellular fragmentation could be a means for trisomic rescue, or the more likely scenario, render an aneuploid blastomere deficient of genetic material required for genome activation and continued cell division. This is supported by the notion that aneuploid embryos are more likely to arrest at the stage of EGA onset. Indications of chromothripsis occurring in these eliminated chromosomes will also be of interest to the broader chromosome biology community, particularly cancer and tumorigenesis researchers. As a follow-up to a previous report from our lab [108], this study also examined the correlation between TLM of embryos and single-cell CNV assessment. Although the timing of the first three cell divisions was not indicative of chromosome copy number in rhesus macaque embryos due to the need of additional euploid embryos beyond the 2-cell stage, multipolar divisions at the 1- or 2-cell stage was linked with chaotic aneuploidy. Currently, only a few IVF clinics in the United States have adopted TLM because of the associated costs and rapidly growing practice of transferring vitrified blastocysts after PGS rather than the fresh transfer of cleavage-stage embryos. Furthermore, certain randomized control trials did not find that cell division parameters are predictive of blastocyst formation rate, CNV in trophectoderm biopsies, or live birth rate [357], which may be due to differences in study design and/or patient population. Future identification of optimal TLM morphokinetic parameters that accurately predict the developmental potential of an embryo for live birth should include detection of multipolar divisions and exclusion of arrested blastomeres.

Upon completion of the SNP analysis, we were surprised by the unexpectedly high number of rhesus macaque embryos that were uniparental or triploid and yet, morphologically indistinguishable from their biparental counterparts. This observation should raise concerns as to whether PGS screening for only chromosome copy number is sufficient or should include parental DNA assessment. Although the majority of human embryos are now generated from intracytoplasmic sperm injections of MII oocytes and therefore, unlikely to be polyploid, gynogenotes and androgenotes can still reach the blastocyst stage and deceptively appear to be euploid following PGS. This may mean some percentage of transferred human embryos have ploidy errors detected as normal chromosome complement, at least in the trophectoderm cells. Such a scenario is possible, since molar pregnancies do occur in IVF patients [358, 359] and it is well known that parthenotes provide “healthy”-looking blastocysts, a subjective feature that is often used to select embryos for transfer [360]. However, the incidence of ploidy errors at the blastocyst stage may be low enough that clinics will assume this risk rather than impose additional sequencing costs to obtain SNP panels for the parents. With the multiplexing strategy devised here, costs for CNV detection may be reduced, especially for high volume clinics or external clinical diagnostic centers. For this study, library prep and sequencing cost for six embryo samples and both parents amounted to ~$1,200. These numbers, of course, do not include personnel cost for preparing samples, running instruments, and downstream analyses, nor does it include price increases in industry and software costs. Nevertheless, by decreasing the costs of CNV testing with high capacity multiplexing, sequencing the parents seems a reasonable request considering the current price tag of PGS, which easily ranges from $2,000-5,000 at most clinics.

Future Directions

Since this dissertation concluded that the rhesus macaque pre-implantation embryo is a suitable animal model to study aneuploidy in human embryos, additional descriptive and future mechanistic studies are justified. One study currently underway involves injecting modified mRNAs for proteins with fluorescent tags into zygotes to visualize some of the events captured here in real-time by live-cell confocal imaging. One objective of these experiments is to observe micronuclei being eliminated through fragmentation. To achieve this, I confirmed that green fluorescent protein and mCherry are visible when attached to either Histone H2B or Lamin-B1 in live rhesus macaque and bovine embryos. Unlike plasmids, embryos respond to cytoplasmic microinjection of mRNAs at the zygote stage and initial observations show that the mRNA can persist until the blastocyst stage with similar fluorescent intensity amongst cells. Using a scanning confocal microscope with an environmental chamber under tri-gas conditions, injected embryos were imaged for up to 16 hours at 15-minute intervals with 10uM Z-stacks. The microinjection itself and phototoxicity from the 488 and 561 laser lines appear to delay cleavage and increases abnormal nuclear morphology compared to injected embryos that are not imaged by confocal microscopy. Thus, alternative microscopy approaches will be explored such as spinning disk confocal or multi-photon microscopy to reduce phototoxicity and improve embryo viability. Lightsheet microscopy may also be a potential alternative if a sample mounting technique that still facilitates normal pre-implantation development of live embryos can be devised. Additionally, SiR-Hoechst, a far-red cell permeable dye for DNA visualization [361], is being investigated as well and thus far, embryo development does not appear to be affected by short-term culture with this dye. By shifting the color spectrum further right to a larger wavelength with a brighter fluorophore, embryo phototoxicity might be reduced. However, preliminary experiments determined that SiR-DNA is only

detectable in the condensed chromatin of mitotic chromosomes, polar bodies, and sperm. Furthermore, an issue that is unique to pre-implantation embryos is the need for increased magnification, while also imaging multiple embryos that are ~100uM in diameter each. To accomplish this, XY stage movement for imaging multiple points of interest is likely required and an easily achievable task with a monolayer of attached cells. In contrast, large spherical pre-implantation embryos, exhibit considerable movement with each cleavage division and tend to move out of the imaging frame when the stage shifts. Therefore, we are also testing glass bottom microwell-containing petri dishes, both custom made and commercially available with viable biomaterials, for reducing embryo movement during motorized stage scanning.

Even though some cellular structures will still require fluorescent tags for visualization in embryos, certain abnormal nuclear features were actually visible in blastomeres using brightfield TLM. This detection capability will allow development of future studies to determine whether the presence of micro-, multi-, or bi-nucleation up to the 4-cell stage signals the occurrence of imminent aneuploidy in embryos at that or subsequent stages. While this type of study has not been conducted with rhesus macaque embryos, human embryo studies have shown that micronucleation at the 2-cell stage is similar between euploid and aneuploid blastocysts diagnosed by trophectoderm biopsy and PGS [347]. Thus, it remains to be determined if nuclear morphology alone, or in combination with cell division parameter measurements, are predictive of embryo developmental potential. Future work should identify additional parameters that could identify aneuploid blastocysts since most clinics will likely culture to this stage and there is some discrepancy between randomized control trials as to whether time-lapse imaging is beneficial to IVF patients.

Another important question remaining from this study is whether an event called chromothripsis occurs in embryonic micronuclei. Even though we were able to obtain individual micronuclei-containing cellular fragments, it will be an ambitious challenge to determine whether complex chromosomal rearrangements, which are characteristic of chromothripsis, occurred. While PCR-based WGA is significantly more effective for CNV analysis than isothermal amplification (non-PCR)-based techniques such as multiple displacement amplification (MDA) [50], the small size of DNA fragments produced by PCR-based approaches makes it difficult to accurately call structural variants. For this purpose, MDA should be used to generate larger amplicons, but this approach is again known to be inadequate for reliable CNV calling [50]. Nevertheless, we may attempt to assess chromothripsis in embryos via high coverage paired-end sequencing of CCFs and excluded blastomeres. Discordant read-pairs and splitting reads would indicate the presence of a chromosomal rearrangement, but artifacts of chimeric DNA from single-cell WGA can generate many false positives. Therefore, MDA of cellular fragments containing micronuclei and/or the development of additional bioinformatics approaches that can control for chimeric reads would be required to evaluate chromothriptic events confidently. Since micronuclei were only observed in 7.4% of cellular fragments here, pooling of cellular fragments into one sample should also be the target of future studies if polar bodies can be removed at the zygote stage.

This dissertation also revealed that centrosomal defects in sperm and/or competing MTOCs in oocytes might play a significant role in mitotic aneuploidy. Research is currently underway in the laboratory to visualize sperm centrosomes and microtubule dynamics following fertilization. Future research on the particular male in these studies, parent 26028, who generated most of the multipolar and chaotic embryos, may include intracytoplasmic injections of only the isolated centrosome-containing sperm tail to

determine if it can recapitulate multipolar divisions by itself. Through a collaboration with the laboratory of Dr. Ed Green at the University of California-Santa Cruz, sperm from male 26028 will also undergo genetic linkage mapping to identify areas of meiotic recombination. Along with a center-wide SNP profiling effort for all monkeys housed at ONPRC through the Primate Genetics Core, these data may allow us to determine if there are detrimental mutations in this or other individuals affecting the centrosomal network, MTOCs, or additional meiotic/mitotic apparatus structures.

Recent findings that mosaic embryos can still implant and create healthy offspring in humans and animal models [244, 245, 362], can be further tested with rhesus macaque embryos. Given current contention as to whether findings of mosaicism in transferred embryos are accurate calls or false positives [363], we must first determine if trophectoderm biopsies of 5-7 cells accurately reflect mosaicism in blastocysts at the single-cell level. To do this, trophectoderm biopsies should be dissociated into single cells for CNV calling and compared to entire blastocysts sequenced by similar methods using a high coverage/throughput sequencing platform. Potentially, mRNA could also be recovered from these single cells to couple qPCR validation of trophectoderm versus ICM markers to distinguish these two cell populations. Although these approaches would not be used for PGS since the first approach would increase sequencing costs by 5- to 7-fold and the second strategy would necessitate the destruction of embryos, this kind of study would be useful for determining the false positive rates of mosaicism in trophectoderm biopsies. As additional clinics consider transferring mosaic embryos for patients with a history of failed pregnancies, we should also thoroughly determine if aneuploidy calls are truly reflective of mosaicism in the ICM at the single-cell level rather than artifacts of low-input DNA CNV analyses. Previous groups have reported that copy number states are concordant between the trophectoderm and ICM via comparative genome hybridization

microarrays and DNA-FISH [46, 364], but other groups have contended that preferential allocation of aneuploid cells to the trophectoderm does exist [365]. Again, this has not yet been investigated at the single-cell level in blastocysts from any species and further research is required before making such a claim.

Overall, the rhesus macaque is a powerful model to ask and probe questions about aneuploidy in primate embryos. Future mechanistic studies are merited that explore pathways and environmental insults (such as diet and synthetic compound exposure) leading to aneuploidy in reproductively young and aged monkeys. Such studies will offer unexplored insight into these incredible phenomena. Ultimately, the hope is that the findings reported here will not only be of use to the clinical embryology field but will help reproductive and developmental biologists understand how early embryos overcome the complexity of and errors in meiosis and mitosis to produce healthy and otherwise ordinary offspring.

References

1. Delhanty, J.D., et al., *Multicolour FISH detects frequent chromosomal mosaicism and chaotic division in normal preimplantation embryos from fertile patients.* Hum Genet, 1997. **99**(6): p. 755-60.
2. Alper, M.M., et al., *To blastocyst or not to blastocyst? That is the question.* Human Reproduction, 2001. **16**(4): p. 617-9.
3. Munne, S., et al., *Chromosome abnormalities in human arrested preimplantation embryos: a multiple-probe FISH study.* American journal of human genetics, 1994. **55**(1): p. 150-9.
4. Baltaci, V., et al., *Relationship between embryo quality and aneuploidies.* Reprod Biomed Online, 2006. **12**(1): p. 77-82.
5. Fragouli, E., et al., *Morphological and cytogenetic assessment of cleavage and blastocyst stage embryos.* Mol Hum Reprod, 2014. **20**(2): p. 117-26.
6. Boulet, S.L., et al., *Trends in use of and reproductive outcomes associated with intracytoplasmic sperm injection.* JAMA : the journal of the American Medical Association, 2015. **313**(3): p. 255-63.
7. Kissin, D.M., et al., *Assisted hatching: trends and pregnancy outcomes, United States, 2000-2010.* Fertility and sterility, 2014. **102**(3): p. 795-801.
8. Harper, J.C. and S.B. Sengupta, *Preimplantation genetic diagnosis: state of the art 2011.* Human genetics, 2012. **131**(2): p. 175-86.
9. Franasiak, J.M., et al., *The nature of aneuploidy with increasing age of the female partner: a review of 15,169 consecutive trophectoderm biopsies evaluated with comprehensive chromosomal screening.* Fertil Steril, 2014. **101**(3): p. 656-663 e1.
10. Hassold, T. and D. Chiu, *Maternal age-specific rates of numerical chromosome abnormalities with special reference to trisomy.* Hum Genet, 1985. **70**(1): p. 11-7.

11. Mascarenhas, M.N., et al., *National, regional, and global trends in infertility prevalence since 1990: a systematic analysis of 277 health surveys.* PLoS Medicine, 2012. **9**(12): p. e1001356.

12. Delhanty, J.D., *Mechanisms of aneuploidy induction in human oogenesis and early embryogenesis.* Cytogenet Genome Res, 2005. **111**(3-4): p. 237-44.

13. Ogasawara, M., et al., *Embryonic karyotype of abortuses in relation to the number of previous miscarriages.* Fertil Steril, 2000. **73**(2): p. 300-4.

14. Zinaman, M.J., et al., *Estimates of human fertility and pregnancy loss.* Fertil Steril, 1996. **65**(3): p. 503-9.

15. Miller, J.F., et al., *Fetal loss after implantation. A prospective study.* Lancet, 1980. **2**(8194): p. 554-6.

16. Wilcox, A.J., C.R. Weinberg, and D.D. Baird, *Timing of sexual intercourse in relation to ovulation. Effects on the probability of conception, survival of the pregnancy, and sex of the baby.* N Engl J Med, 1995. **333**(23): p. 1517-21.

17. Dupont, C., et al., *Incidence of chromosomal mosaicism in morphologically normal nonhuman primate preimplantation embryos.* Fertility and sterility, 2010. **93**(8): p. 2545-50.

18. Lightfoot, D.A., et al., *The fate of mosaic aneuploid embryos during mouse development.* Dev Biol, 2006. **289**(2): p. 384-94.

19. Macaulay, I.C., et al., *G&T-seq: parallel sequencing of single-cell genomes and transcriptomes.* Nat Methods, 2015. **12**(6): p. 519-22.

20. Bolton, H., et al., *Mouse model of chromosome mosaicism reveals lineage-specific depletion of aneuploid cells and normal developmental potential.* Nat Commun, 2016. **7**: p. 11165.

21. Destouni, A., et al., *Zygotes segregate entire parental genomes in distinct blastomere lineages causing cleavage-stage chimerism and mixoploidy.* Genome Res, 2016. **26**(5): p. 567-78.

22. Treff, N.R., et al., *Next Generation Sequencing-Based Comprehensive Chromosome Screening in Mouse Polar Bodies, Oocytes, and Embryos.* Biol Reprod, 2016. **94**(4): p. 76.

23. Dupont, C., et al., *Incidence of chromosomal mosaicism in morphologically normal nonhuman primate preimplantation embryos.* Fertil Steril, 2010. **93**(8): p. 2545-50.

24. Dupont, C., et al., *Chromosomal instability in rhesus macaque preimplantation embryos.* Fertil Steril, 2009. **91**(4): p. 1230-7.

25. Dupont, C., et al., *Rhesus macaque embryos derived from MI oocytes maturing after retrieval display high rates of chromosomal anomalies.* Hum Reprod, 2009. **24**(4): p. 929-35.

26. Dhaese, I., et al., *Small intestinal motility in soluble guanylate cyclase alpha1 knockout mice: (Jejunal phenotyping of sGCalpha1 knockout mice).* Naunyn Schmiedebergs Arch Pharmacol, 2009. **379**(5): p. 473-87.

27. Chavez, S.L., et al., *Dynamic blastomere behaviour reflects human embryo ploidy by the four-cell stage.* Nature communications, 2012. **3**: p. 1251.

28. Johnson, D.S., et al., *Preclinical validation of a microarray method for full molecular karyotyping of blastomeres in a 24-h protocol.* Hum Reprod, 2010. **25**(4): p. 1066-75.

29. Chow, J.F., et al., *Array comparative genomic hybridization analyses of all blastomeres of a cohort of embryos from young IVF patients revealed significant contribution of mitotic errors to embryo mosaicism at the cleavage stage.* Reproductive biology and endocrinology : RB&E, 2014. **12**: p. 105.

30. Minasi, M.G., et al., *Correlation between aneuploidy, standard morphology evaluation and morphokinetic development in 1730 biopsied blastocysts: a consecutive case series study.* Hum Reprod, 2016. **31**(10): p. 2245-54.

31. Huang, J., et al., *Validation of multiple annealing and looping-based amplification cycle sequencing for 24-chromosome aneuploidy screening of cleavage-stage embryos.* Fertil Steril, 2014. **102**(6): p. 1685-91.

32. Franasiak, J.M., et al., *The nature of aneuploidy with increasing age of the female partner: a review of 15,169 consecutive trophectoderm biopsies evaluated with comprehensive chromosomal screening.* Fertility and sterility, 2014. **101**(3): p. 656-663 e1.

33. Baart, E.B., et al., *Preimplantation genetic screening reveals a high incidence of aneuploidy and mosaicism in embryos from young women undergoing IVF.* Human reproduction, 2006. **21**(1): p. 223-33.

34. Scott, R.T., Jr., et al., *Cleavage-stage biopsy significantly impairs human embryonic implantation potential while blastocyst biopsy does not: a randomized and paired clinical trial.* Fertility and sterility, 2013. **100**(3): p. 624-30.

35. Daphnis, D.D., et al., *Detailed FISH analysis of day 5 human embryos reveals the mechanisms leading to mosaic aneuploidy.* Hum Reprod, 2005. **20**(1): p. 129-37.

36. Kuo, H.C., C.M. Ogilvie, and A.H. Handyside, *Chromosomal mosaicism in cleavage-stage human embryos and the accuracy of single-cell genetic analysis.* J Assist Reprod Genet, 1998. **15**(5): p. 276-80.

37. Mastenbroek, S., et al., *In vitro fertilization with preimplantation genetic screening.* The New England journal of medicine, 2007. **357**(1): p. 9-17.

38. Gleicher, N., et al., *A single trophectoderm biopsy at blastocyst stage is mathematically unable to determine embryo ploidy accurately enough for clinical use.* Reprod Biol Endocrinol, 2017. **15**(1): p. 33.

39. McCoy, R.C., et al., *Common variants spanning PLK4 are associated with mitotic-origin aneuploidy in human embryos.* Science, 2015. **348**(6231): p. 235-8.

40. Handyside, A.H., et al., *Pregnancies from biopsied human preimplantation embryos sexed by Y-specific DNA amplification.* Nature, 1990. **344**(6268): p. 768-70.

41. Verlinsky, Y., et al., *Pregnancies following pre-conception diagnosis of common aneuploidies by fluorescent in-situ hybridization.* Hum Reprod, 1995. **10**(7): p. 1923-7.

42. Delhanty, J.D., et al., *Detection of aneuploidy and chromosomal mosaicism in human embryos during preimplantation sex determination by fluorescent in situ hybridisation, (FISH).* Hum Mol Genet, 1993. **2**(8): p. 1183-5.

43. Wells, D. and J.D. Delhanty, *Comprehensive chromosomal analysis of human preimplantation embryos using whole genome amplification and single cell comparative genomic hybridization.* Mol Hum Reprod, 2000. **6**(11): p. 1055-62.

44. Le Caignec, C., et al., *Single-cell chromosomal imbalances detection by array CGH.* Nucleic Acids Res, 2006. **34**(9): p. e68.

45. Wilton, L., *Preimplantation genetic diagnosis and chromosome analysis of blastomeres using comparative genomic hybridization.* Hum Reprod Update, 2005. **11**(1): p. 33-41.

46. Johnson, D.S., et al., *Comprehensive analysis of karyotypic mosaicism between trophectoderm and inner cell mass.* Mol Hum Reprod, 2010. **16**(12): p. 944-9.

47. Munne, S. and H.U. Weier, *Simultaneous enumeration of chromosomes 13, 18, 21, X, and Y in interphase cells for preimplantation genetic diagnosis of aneuploidy.* Cytogenetics and cell genetics, 1996. **75**(4): p. 263-70.

48. Scriven, P.N. and C.M. Ogilvie, *FISH for pre-implantation genetic diagnosis.* Methods Mol Biol, 2010. **659**: p. 269-82.

49. Chong, S.S., et al., *Single-cell DNA and FISH analysis for application to preimplantation genetic diagnosis.* Curr Protoc Hum Genet, 2010. **Chapter 9**: p. Unit9 10.

50. de Bourcy, C.F., et al., *A quantitative comparison of single-cell whole genome amplification methods.* PLoS One, 2014. **9**(8): p. e105585.

51. Harper, J.C. and S.B. Sengupta, *Preimplantation genetic diagnosis: state of the art 2011.* Hum Genet, 2012. **131**(2): p. 175-86.

52. Handyside, A.H., *24-chromosome copy number analysis: a comparison of available technologies.* Fertil Steril, 2013. **100**(3): p. 595-602.

53. Bi, W., et al., *Detection of >/=1Mb microdeletions and microduplications in a single cell using custom oligonucleotide arrays.* Prenat Diagn, 2012. **32**(1): p. 10-20.

54. Brezina, P.R., et al., *Single-gene testing combined with single nucleotide polymorphism microarray preimplantation genetic diagnosis for aneuploidy: a novel approach in optimizing pregnancy outcome.* Fertil Steril, 2011. **95**(5): p. 1786 e5-8.

55. Hou, Y., et al., *Genome analyses of single human oocytes.* Cell, 2013. **155**(7): p. 1492-506.

56. Fiorentino, F., et al., *Application of next-generation sequencing technology for comprehensive aneuploidy screening of blastocysts in clinical preimplantation genetic screening cycles.* Human Reproduction, 2014. **29**(12): p. 2802-13.

57. Wang, L., et al., *Detection of chromosomal aneuploidy in human preimplantation embryos by next-generation sequencing.* Biol Reprod, 2014. **90**(5): p. 95.

58. Vitak, S.A., et al., *Sequencing thousands of single-cell genomes with combinatorial indexing.* Nat Methods, 2017. **14**(3): p. 302-308.

59. Gisselsson, D., et al., *Telomere dysfunction triggers extensive DNA fragmentation and evolution of complex chromosome abnormalities in human malignant tumors.* Proc Natl Acad Sci U S A, 2001. **98**(22): p. 12683-8.

60. Talkowski, M.E., et al., *Next-generation sequencing strategies enable routine detection of balanced chromosome rearrangements for clinical diagnostics and genetic research.* Am J Hum Genet, 2011. **88**(4): p. 469-81.

61. Treff, N.R. and R.T. Scott, Jr., *Four-hour quantitative real-time polymerase chain reaction-based comprehensive chromosome screening and accumulating evidence of accuracy, safety, predictive value, and clinical efficacy.* Fertil Steril, 2013. **99**(4): p. 1049-53.

62. Vanneste, E., et al., *Aneuploidy and copy number variation in early human development.* Semin Reprod Med, 2012. **30**(4): p. 302-8.

63. Hochstenbach, R., et al., *Genome arrays for the detection of copy number variations in idiopathic mental retardation, idiopathic generalized epilepsy and neuropsychiatric disorders: lessons for diagnostic workflow and research.* Cytogenetic and genome research, 2011. **135**(3-4): p. 174-202.

64. Rienzi, L., et al., *No evidence of association between blastocyst aneuploidy and morphokinetic assessment in a selected population of poor-prognosis patients: a longitudinal cohort study.* Reproductive biomedicine online, 2015. **30**(1): p. 57-66.

65. Scott, R.T., Jr., et al., *Blastocyst biopsy with comprehensive chromosome screening and fresh embryo transfer significantly increases in vitro fertilization implantation and delivery rates: a randomized controlled trial.* Fertility and sterility, 2013. **100**(3): p. 697-703.

66. Werner, M.D., et al., *Clinically recognizable error rate after the transfer of comprehensive chromosomal screened euploid embryos is low.* Fertility and sterility, 2014. **102**(6): p. 1613-8.

67. Payne, D., et al., *Preliminary observations on polar body extrusion and pronuclear formation in human oocytes using time-lapse video cinematography.* Human reproduction, 1997. **12**(3): p. 532-41.

68. Hardarson, T., et al., *Internalization of cellular fragments in a human embryo: time-lapse recordings.* Reproductive biomedicine online, 2002. **5**(1): p. 36-8.

69. Mio, Y. and K. Maeda, *Time-lapse cinematography of dynamic changes occurring during in vitro development of human embryos.* Am J Obstet Gynecol, 2008. **199**(6): p. 660 e1-5.

70. Lemmen, J.G., I. Agerholm, and S. Ziebe, *Kinetic markers of human embryo quality using time-lapse recordings of IVF/ICSI-fertilized oocytes.* Reproductive biomedicine online, 2008. **17**(3): p. 385-91.

71. Nakahara, T., et al., *Evaluation of the safety of time-lapse observations for human embryos.* J Assist Reprod Genet, 2010. **27**(2-3): p. 93-6.

72. Wong, C.C., et al., *Non-invasive imaging of human embryos before embryonic genome activation predicts development to the blastocyst stage.* Nat Biotechnol, 2010. **28**(10): p. 1115-21.

73. Cruz, M., et al., *Timing of cell division in human cleavage-stage embryos is linked with blastocyst formation and quality.* Reproductive biomedicine online, 2012. **25**(4): p. 371-81.

74. Cruz, M., et al., *Embryo quality, blastocyst and ongoing pregnancy rates in oocyte donation patients whose embryos were monitored by time-lapse imaging.* Journal of assisted reproduction and genetics, 2011. **28**(7): p. 569-73.

75. Meseguer, M., et al., *The use of morphokinetics as a predictor of embryo implantation.* Human reproduction, 2011. **26**(10): p. 2658-71.

76. Dal Canto, M., et al., *Cleavage kinetics analysis of human embryos predicts development to blastocyst and implantation.* Reproductive biomedicine online, 2012. **25**(5): p. 474-80.

77. Hlinka, D., et al., *Time-lapse cleavage rating predicts human embryo viability.* Physiol Res, 2012. **61**(5): p. 513-25.

78. Hashimoto, S., et al., *Selection of high-potential embryos by culture in poly(dimethylsiloxane) microwells and time-lapse imaging.* Fertility and sterility, 2012. **97**(2): p. 332-7.

79. Azzarello, A., T. Hoest, and A.L. Mikkelsen, *The impact of pronuclei morphology and dynamicity on live birth outcome after time-lapse culture.* Human Reproduction, 2012. **27**(9): p. 2649-57.

80. Rubio, I., et al., *Limited implantation success of direct-cleaved human zygotes: a time-lapse study.* Fertility and sterility, 2012. **98**(6): p. 1458-63.

81. Meseguer, M., et al., *Embryo incubation and selection in a time-lapse monitoring system improves pregnancy outcome compared with a standard incubator: a retrospective cohort study.* Fertility and sterility, 2012. **98**(6): p. 1481-9 e10.

82. Stensen, M.H., et al., *Fragmentation of human cleavage-stage embryos is related to the progression through meiotic and mitotic cell cycles.* Fertility and sterility, 2015. **103**(2): p. 374-81 e4.

83. Liu, Y., et al., *Prevalence, consequence, and significance of reverse cleavage by human embryos viewed with the use of the Embryoscope time-lapse video system.* Fertility and sterility, 2014. **102**(5): p. 1295-1300 e2.

84. Liu, Y., et al., *Clinical significance of intercellular contact at the four-cell stage of human embryos, and the use of abnormal cleavage patterns to identify embryos with low implantation potential: a time-lapse study.* Fertility and sterility, 2015.

85. Pribenszky, C., et al., *Prediction of in-vitro developmental competence of early cleavage-stage mouse embryos with compact time-lapse equipment.* Reproductive biomedicine online, 2010. **20**(3): p. 371-9.

86. Sugimura, S., et al., *Promising system for selecting healthy in vitro-fertilized embryos in cattle.* PLoS One, 2012. **7**(5): p. e36627.

87. Burruel, V., et al., *Abnormal early cleavage events predict early embryo demise: sperm oxidative stress and early abnormal cleavage.* Scientific reports, 2014. **4**: p. 6598.

88. Campbell, A., et al., *Modelling a risk classification of aneuploidy in human embryos using non-invasive morphokinetics.* Reproductive biomedicine online, 2013. **26**(5): p. 477-85.

89. Basile, N., et al., *Increasing the probability of selecting chromosomally normal embryos by time-lapse morphokinetics analysis.* Fertility and sterility, 2014. **101**(3): p. 699-704.

90. Yang, Z., et al., *Selection of competent blastocysts for transfer by combining time-lapse monitoring and array CGH testing for patients undergoing preimplantation genetic screening: a prospective study with sibling oocytes.* BMC medical genomics, 2014. **7**: p. 38.

91. Vera-Rodriguez, M., et al., *Prediction model for aneuploidy in early human embryo development revealed by single-cell analysis.* Nat Commun, 2015. **6**: p. 7601.

92. Campbell, A., et al., *Modelling a risk classification of aneuploidy in human embryos using non-invasive morphokinetics.* Reprod Biomed Online, 2013. **26**(5): p. 477-85.

93. Kroener, L., et al., *The effect of timing of embryonic progression on chromosomal abnormality.* Fertility and sterility, 2012. **98**(4): p. 876-80.

94. Yang, Z., et al., *Selection of competent blastocysts for transfer by combining time-lapse monitoring and array CGH testing for patients undergoing preimplantation genetic screening: a prospective study with sibling oocytes.* BMC Med Genomics, 2014. **7**: p. 38.

95. Basile, N., et al., *Increasing the probability of selecting chromosomally normal embryos by time-lapse morphokinetics analysis.* Fertil Steril, 2014. **101**(3): p. 699-704.

96. Rienzi, L., et al., *No evidence of association between blastocyst aneuploidy and morphokinetic assessment in a selected population of poor-prognosis patients: a longitudinal cohort study.* Reprod Biomed Online, 2015. **30**(1): p. 57-66.

97. Stensen, M.H., et al., *Fragmentation of human cleavage-stage embryos is related to the progression through meiotic and mitotic cell cycles.* Fertil Steril, 2015. **103**(2): p. 374-81 e4.

98. Vera-Rodriguez, M., et al., *Prediction model for aneuploidy in early human embryo development revealed by single-cell analysis.* Nature communications, 2015. **6**: p. 7601.

99. Kirkegaard, K., et al., *Time-lapse parameters as predictors of blastocyst development and pregnancy outcome in embryos from good prognosis patients: a prospective cohort study.* Human Reproduction, 2013. **28**(10): p. 2643-51.

100. Conaghan, J., et al., *Improving embryo selection using a computer-automated time-lapse image analysis test plus day 3 morphology: results from a prospective multicenter trial.* Fertility and sterility, 2013. **100**(2): p. 412-9 e5.

101. Athayde Wirka, K., et al., *Atypical embryo phenotypes identified by time-lapse microscopy: high prevalence and association with embryo development.* Fertility and sterility, 2014. **101**(6): p. 1637-48 e1-5.

102. Kaser, D.J. and C. Racowsky, *Clinical outcomes following selection of human preimplantation embryos with time-lapse monitoring: a systematic review.* Human Reproduction Update, 2014. **20**(5): p. 617-31.

103. Rubio, I., et al., *Clinical validation of embryo culture and selection by morphokinetic analysis: a randomized, controlled trial of the EmbryoScope.* Fertility and sterility, 2014.

104. Liu, Y., et al., *Time-lapse videography of human oocytes following intracytoplasmic sperm injection: events up to the first cleavage division.* Reproductive biology, 2014. **14**(4): p. 249-56.

105. Campbell, A., et al., *Retrospective analysis of outcomes after IVF using an aneuploidy risk model derived from time-lapse imaging without PGS.* Reprod Biomed Online, 2013. **27**(2): p. 140-6.

106. VerMilyea, M.D., et al., *Computer-automated time-lapse analysis results correlate with embryo implantation and clinical pregnancy: a blinded, multi-centre study.* Reproductive biomedicine online, 2014. **29**(6): p. 729-36.

107. Molder, A., et al., *Semiautomated analysis of embryoscope images: Using localized variance of image intensity to detect embryo developmental stages.* Cytometry. Part A : the journal of the International Society for Analytical Cytology, 2015. **87**(2): p. 119-28.

108. Chavez, S.L., et al., *Dynamic blastomere behaviour reflects human embryo ploidy by the four-cell stage.* Nat Commun, 2012. **3**: p. 1251.

109. Chow, J.F., et al., *Array comparative genomic hybridization analyses of all blastomeres of a cohort of embryos from young IVF patients revealed significant contribution of mitotic errors to embryo mosaicism at the cleavage stage.* Reprod Biol Endocrinol, 2014. **12**: p. 105.

110. Vanneste, E., et al., *What next for preimplantation genetic screening? High mitotic chromosome instability rate provides the biological basis for the low success rate.* Hum Reprod, 2009. **24**(11): p. 2679-82.

111. Hassold, T. and P. Hunt, *To err (meiotically) is human: the genesis of human aneuploidy.* Nature reviews. Genetics, 2001. **2**(4): p. 280-91.

112. MacDonald, M., et al., *The origin of 47,XXY and 47,XXX aneuploidy: heterogeneous mechanisms and role of aberrant recombination.* Hum Mol Genet, 1994. **3**(8): p. 1365-71.

113. Koehler, K.E., et al., *Recombination and nondisjunction in humans and flies.* Hum Mol Genet, 1996. **5 Spec No**: p. 1495-504.

114. Lamb, N.E., S.L. Sherman, and T.J. Hassold, *Effect of meiotic recombination on the production of aneuploid gametes in humans.* Cytogenet Genome Res, 2005. **111**(3-4): p. 250-5.

115. Sherman, S.L., N.E. Lamb, and E. Feingold, *Relationship of recombination patterns and maternal age among non-disjoined chromosomes 21.* Biochem Soc Trans, 2006. **34**(Pt 4): p. 578-80.

116. Handyside, A.H., *Molecular origin of female meiotic aneuploidies.* Biochim Biophys Acta, 2012. **1822**(12): p. 1913-20.

117. Munne, S., et al., *Embryo morphology, developmental rates, and maternal age are correlated with chromosome abnormalities.* Fertility and sterility, 1995. **64**(2): p. 382-91.

118. Nagaoka, S.I., T.J. Hassold, and P.A. Hunt, *Human aneuploidy: mechanisms and new insights into an age-old problem.* Nature reviews. Genetics, 2012. **13**(7): p. 493-504.

119. Munne, S., *Chromosome abnormalities and their relationship to morphology and development of human embryos.* Reprod Biomed Online, 2006. **12**(2): p. 234-53.

120. Munne, S., et al., *Maternal age, morphology, development and chromosome abnormalities in over 6000 cleavage-stage embryos.* Reprod Biomed Online, 2007. **14**(5): p. 628-34.

121. Silber, S., et al., *Chromosomal abnormalities in embryos derived from testicular sperm extraction.* Fertility and sterility, 2003. **79**(1): p. 30-8.

122. Munne, S., et al., *Chromosome mosaicism in cleavage-stage human embryos: evidence of a maternal age effect.* Reprod Biomed Online, 2002. **4**(3): p. 223-32.

123. Braude, P., V. Bolton, and S. Moore, *Human gene expression first occurs between the four- and eight-cell stages of preimplantation development.* Nature, 1988. **332**(6163): p. 459-61.

124. Tachibana, M., et al., *Human embryonic stem cells derived by somatic cell nuclear transfer.* Cell, 2013. **153**(6): p. 1228-38.

125. Harrison, R.H., et al., *Lack of cell cycle checkpoints in human cleavage stage embryos revealed by a clonal pattern of chromosomal mosaicism analysed by sequential multicolour FISH.* Zygote, 2000. **8**(3): p. 217-24.

126. Los, F.J., D. Van Opstal, and C. van den Berg, *The development of cytogenetically normal, abnormal and mosaic embryos: a theoretical model.* Hum Reprod Update, 2004. **10**(1): p. 79-94.

127. Mantikou, E., et al., *Molecular origin of mitotic aneuploidies in preimplantation embryos.* Biochim Biophys Acta, 2012. **1822**(12): p. 1921-30.

128. Li, L., P. Zheng, and J. Dean, *Maternal control of early mouse development.* Development, 2010. **137**(6): p. 859-70.

129. Derijck, A.A., et al., *gammaH2AX signalling during sperm chromatin remodelling in the mouse zygote.* DNA Repair (Amst), 2006. **5**(8): p. 959-71.

130. Roest, H.P., et al., *The ubiquitin-conjugating DNA repair enzyme HR6A is a maternal factor essential for early embryonic development in mice.* Mol Cell Biol, 2004. **24**(12): p. 5485-95.

131. Ramos, S.B., et al., *The CCCH tandem zinc-finger protein Zfp36l2 is crucial for female fertility and early embryonic development.* Development, 2004. **131**(19): p. 4883-93.

132. Tsukamoto, S., et al., *Autophagy is essential for preimplantation development of mouse embryos.* Science, 2008. **321**(5885): p. 117-20.

133. Li, L., B. Baibakov, and J. Dean, *A subcortical maternal complex essential for preimplantation mouse embryogenesis.* Developmental Cell, 2008. **15**(3): p. 416-25.

134. Yurttas, P., et al., *Role for PADI6 and the cytoplasmic lattices in ribosomal storage in oocytes and translational control in the early mouse embryo.* Development, 2008. **135**(15): p. 2627-36.

135. Zheng, P. and J. Dean, *Role of Filia, a maternal effect gene, in maintaining euploidy during cleavage-stage mouse embryogenesis.* Proceedings of the National Academy of Sciences of the United States of America, 2009. **106**(18): p. 7473-8.

136. Yu, X.J., et al., *The subcortical maternal complex controls symmetric division of mouse zygotes by regulating F-actin dynamics.* Nat Commun, 2014. **5**: p. 4887.

137. Akoury, E., et al., *NLRP7 and KHDC3L, the two maternal-effect proteins responsible for recurrent hydatidiform moles, co-localize to the oocyte cytoskeleton.* Hum Reprod, 2015. **30**(1): p. 159-69.

138. Ohsugi, M., et al., *Maternally derived FILIA-MATER complex localizes asymmetrically in cleavage-stage mouse embryos.* Development, 2008. **135**(2): p. 259-69.

139. Pierre, A., et al., *Atypical structure and phylogenomic evolution of the new eutherian oocyte- and embryo-expressed KHDC1/DPPA5/ECAT1/OOEP gene family.* Genomics, 2007. **90**(5): p. 583-94.

140. Ko, M.A., et al., *Plk4 haploinsufficiency causes mitotic infidelity and carcinogenesis.* Nat Genet, 2005. **37**(8): p. 883-8.

141. Keefe, D.L., et al., *Mitochondrial deoxyribonucleic acid deletions in oocytes and reproductive aging in women.* Fertil Steril, 1995. **64**(3): p. 577-83.

142. Van Blerkom, J., P.W. Davis, and J. Lee, *ATP content of human oocytes and developmental potential and outcome after in-vitro fertilization and embryo transfer.* Hum Reprod, 1995. **10**(2): p. 415-24.

143. Wilding, M., et al., *Mitochondrial aggregation patterns and activity in human oocytes and preimplantation embryos.* Hum Reprod, 2001. **16**(5): p. 909-17.

144. Picton, H.M., et al., *Association between amino acid turnover and chromosome aneuploidy during human preimplantation embryo development in vitro.* Mol Hum Reprod, 2010. **16**(8): p. 557-69.

145. Ben-Meir, A., et al., *Coenzyme Q10 restores oocyte mitochondrial function and fertility during reproductive aging.* Aging Cell, 2015. **14**(5): p. 887-95.

146. Eichenlaub-Ritter, U., et al., *Spindles, mitochondria and redox potential in ageing oocytes.* Reprod Biomed Online, 2004. **8**(1): p. 45-58.

147. Takeuchi, T., et al., *Effect of treating induced mitochondrial damage on embryonic development and epigenesis.* Biol Reprod, 2005. **72**(3): p. 584-92.

148. Chiaratti, M.R., et al., *Ooplast-mediated developmental rescue of bovine oocytes exposed to ethidium bromide.* Reprod Biomed Online, 2011. **22**(2): p. 172-83.

149. Vanneste, E., et al., *What next for preimplantation genetic screening? High mitotic chromosome instability rate provides the biological basis for the low success rate.* Human reproduction, 2009. **24**(11): p. 2679-82.

150. Yoon, S.Y., et al., *Human sperm devoid of PLC, zeta 1 fail to induce Ca(2+) release and are unable to initiate the first step of embryo development.* J Clin Invest, 2008. **118**(11): p. 3671-81.

151. Whitaker, M., *Calcium at fertilization and in early development.* Physiol Rev, 2006. **86**(1): p. 25-88.

152. Sathananthan, A.H., et al., *Centrioles in the beginning of human development.* Proceedings of the National Academy of Sciences of the United States of America, 1991. **88**(11): p. 4806-10.

153. Palermo, G., S. Munne, and J. Cohen, *The human zygote inherits its mitotic potential from the male gamete.* Human reproduction, 1994. **9**(7): p. 1220-5.

154. Schatten, G., C. Simerly, and H. Schatten, *Maternal inheritance of centrosomes in mammals? Studies on parthenogenesis and polyspermy in mice.* Proceedings of the National Academy of Sciences of the United States of America, 1991. **88**(15): p. 6785-9.

155. Courtois, A., et al., *The transition from meiotic to mitotic spindle assembly is gradual during early mammalian development.* J Cell Biol, 2012. **198**(3): p. 357-70.

156. Lightfoot, D.A., et al., *The fate of mosaic aneuploid embryos during mouse development.* Developmental biology, 2006. **289**(2): p. 384-94.

157. Palermo, G.D., L.T. Colombero, and Z. Rosenwaks, *The human sperm centrosome is responsible for normal syngamy and early embryonic development.* Rev Reprod, 1997. **2**(1): p. 19-27.

158. Sathananthan, A.H., et al., *From oogonia to mature oocytes: inactivation of the maternal centrosome in humans.* Microsc Res Tech, 2006. **69**(6): p. 396-407.

159. Rawe, V.Y., et al., *A pathology of the sperm centriole responsible for defective sperm aster formation, syngamy and cleavage.* Hum Reprod, 2002. **17**(9): p. 2344-9.

160. Obasaju, M., et al., *Sperm quality may adversely affect the chromosome constitution of embryos that result from intracytoplasmic sperm injection.* Fertil Steril, 1999. **72**(6): p. 1113-5.

161. Lin, G., et al., *A highly homozygous and parthenogenetic human embryonic stem cell line derived from a one-pronuclear oocyte following in vitro fertilization procedure.* Cell Res, 2007. **17**(12): p. 999-1007.

162. Sritanaudomchai, H., et al., *Discovery of a novel imprinted gene by transcriptional analysis of parthenogenetic embryonic stem cells.* Hum Reprod, 2010. **25**(8): p. 1927-41.

163. Leeb, M., et al., *Germline potential of parthenogenetic haploid mouse embryonic stem cells.* Development, 2012. **139**(18): p. 3301-5.

164. Elling, U., et al., *Forward and reverse genetics through derivation of haploid mouse embryonic stem cells.* Cell Stem Cell, 2011. **9**(6): p. 563-74.

165. Paull, D., et al., *Nuclear genome transfer in human oocytes eliminates mitochondrial DNA variants.* Nature, 2013. **493**(7434): p. 632-7.

166. Daughtry, B. and S. Mitalipov, *Concise review: parthenote stem cells for regenerative medicine: genetic, epigenetic, and developmental features.* Stem Cells Transl Med, 2014. **3**(3): p. 290-8.

167. Brevini, T.A., et al., *Centrosome amplification and chromosomal instability in human and animal parthenogenetic cell lines.* Stem Cell Rev, 2012. **8**(4): p. 1076-87.

168. Brevini, T.A., et al., *Cell lines derived from human parthenogenetic embryos can display aberrant centriole distribution and altered expression levels of mitotic spindle check-point transcripts.* Stem Cell Rev, 2009. **5**(4): p. 340-52.

169. Liu, Q., et al., *Karyotype characterization of in vivo- and in vitro-derived porcine parthenogenetic cell lines.* PLoS One, 2014. **9**(5): p. e97974.

170. Combelles, C.M., et al., *Cellular and genetic analysis of oocytes and embryos in a human case of spontaneous oocyte activation.* Hum Reprod, 2011. **26**(3): p. 545-52.

171. Angell, R., *First-meiotic-division nondisjunction in human oocytes.* Am J Hum Genet, 1997. **61**(1): p. 23-32.

172. Wei, Y., et al., *Spindle assembly checkpoint regulates mitotic cell cycle progression during preimplantation embryo development.* PLoS One, 2011. **6**(6): p. e21557.

173. Gregan, J., et al., *Merotelic kinetochore attachment: causes and effects.* Trends in cell biology, 2011. **21**(6): p. 374-81.

174. Lane, S.I., Y. Yun, and K.T. Jones, *Timing of anaphase-promoting complex activation in mouse oocytes is predicted by microtubule-kinetochore attachment but not by bivalent alignment or tension.* Development, 2012. **139**(11): p. 1947-55.

175. Kitajima, T.S., M. Ohsugi, and J. Ellenberg, *Complete kinetochore tracking reveals error-prone homologous chromosome biorientation in mammalian oocytes.* Cell, 2011. **146**(4): p. 568-81.

176. Howe, K. and G. FitzHarris, *Recent insights into spindle function in mammalian oocytes and early embryos.* Biology of reproduction, 2013. **89**(3): p. 71.

177. Daphnis, D.D., et al., *Analysis of the evolution of chromosome abnormalities in human embryos from Day 3 to 5 using CGH and FISH.* Mol Hum Reprod, 2008. **14**(2): p. 117-25.

178. Katz-Jaffe, M.G., A.O. Trounson, and D.S. Cram, *Chromosome 21 mosaic human preimplantation embryos predominantly arise from diploid conceptions.* Fertil Steril, 2005. **84**(3): p. 634-43.

179. Coonen, E., et al., *Anaphase lagging mainly explains chromosomal mosaicism in human preimplantation embryos.* Human reproduction, 2004. **19**(2): p. 316-24.

180. Kuliev, A. and Y. Verlinsky, *Meiotic and mitotic nondisjunction: lessons from preimplantation genetic diagnosis.* Hum Reprod Update, 2004. **10**(5): p. 401-7.

181. Pellestor, F., et al., *Mechanisms of non-disjunction in human female meiosis: the co-existence of two modes of malsegregation evidenced by the karyotyping of 1397 in-vitro unfertilized oocytes.* Hum Reprod, 2002. **17**(8): p. 2134-45.

182. Kiessling, A.A., et al., *Genome-wide microarray evidence that 8-cell human blastomeres over-express cell cycle drivers and under-express checkpoints.* Journal of assisted reproduction and genetics, 2010. **27**(6): p. 265-76.

183. Dobson, A.T., et al., *The unique transcriptome through day 3 of human preimplantation development.* Human molecular genetics, 2004. **13**(14): p. 1461-70.

184. Munne, S., et al., *Self-correction of chromosomally abnormal embryos in culture and implications for stem cell production.* Fertil Steril, 2005. **84**(5): p. 1328-34.

185. Barbash-Hazan, S., et al., *Preimplantation aneuploid embryos undergo self-correction in correlation with their developmental potential.* Fertil Steril, 2009. **92**(3): p. 890-6.

186. Alikani, M., et al., *Human embryo fragmentation in vitro and its implications for pregnancy and implantation.* Fertility and sterility, 1999. **71**(5): p. 836-42.

187. Antczak, M. and J. Van Blerkom, *Temporal and spatial aspects of fragmentation in early human embryos: possible effects on developmental competence and*

association with the differential elimination of regulatory proteins from polarized domains. Human reproduction, 1999. **14**(2): p. 429-47.

188. Sugimura, S., et al., *Time-lapse cinematography-compatible polystyrene-based microwell culture system: a novel tool for tracking the development of individual bovine embryos.* Biology of reproduction, 2010. **83**(6): p. 970-8.

189. Enders, A.C., A.G. Hendrickx, and P.E. Binkerd, *Abnormal development of blastocysts and blastomeres in the rhesus monkey.* Biology of reproduction, 1982. **26**(2): p. 353-66.

190. Buster, J.E., et al., *Biologic and morphologic development of donated human ova recovered by nonsurgical uterine lavage.* American journal of obstetrics and gynecology, 1985. **153**(2): p. 211-7.

191. Pereda, J. and H.B. Croxatto, *Ultrastructure of a seven-cell human embryo.* Biology of reproduction, 1978. **18**(3): p. 481-9.

192. Hardy, K., *Apoptosis in the human embryo.* Reviews of reproduction, 1999. **4**(3): p. 125-34.

193. Hardy, K., et al., *From cell death to embryo arrest: mathematical models of human preimplantation embryo development.* Proceedings of the National Academy of Sciences of the United States of America, 2001. **98**(4): p. 1655-60.

194. Xu, J., et al., *The incidence of cytoplasmic fragmentation in mouse embryos in vitro is not affected by inhibition of caspase activity.* Fertility and sterility, 2001. **75**(5): p. 986-91.

195. Van Blerkom, J., P. Davis, and S. Alexander, *A microscopic and biochemical study of fragmentation phenotypes in stage-appropriate human embryos.* Human reproduction, 2001. **16**(4): p. 719-29.

196. Yang, H.W., et al., *Detection of reactive oxygen species (ROS) and apoptosis in human fragmented embryos.* Hum Reprod, 1998. **13**(4): p. 998-1002.

197. Jurisicova, A., S. Varmuza, and R.F. Casper, *Programmed cell death and human embryo fragmentation.* Mol Hum Reprod, 1996. **2**(2): p. 93-8.

198. Pellestor, F., et al., *Relationship between morphology and chromosomal constitution in human preimplantation embryo.* Mol Reprod Dev, 1994. **39**(2): p. 141-6.

199. Giorgetti, C., et al., *Embryo score to predict implantation after in-vitro fertilization: based on 957 single embryo transfers.* Hum Reprod, 1995. **10**(9): p. 2427-31.

200. Ebner, T., et al., *Embryo fragmentation in vitro and its impact on treatment and pregnancy outcome.* Fertil Steril, 2001. **76**(2): p. 281-5.

201. Ziebe, S., et al., *Embryo morphology or cleavage stage: how to select the best embryos for transfer after in-vitro fertilization.* Hum Reprod, 1997. **12**(7): p. 1545-9.

202. Edwards, R.G., et al., *Factors influencing the success of in vitro fertilization for alleviating human infertility.* Journal of in vitro fertilization and embryo transfer : IVF, 1984. **1**(1): p. 3-23.

203. Pelinck, M.J., et al., *Embryo quality and impact of specific embryo characteristics on ongoing implantation in unselected embryos derived from modified natural cycle in vitro fertilization.* Fertility and sterility, 2010. **94**(2): p. 527-34.

204. Hoover, L., et al., *Evaluation of a new embryo-grading system to predict pregnancy rates following in vitro fertilization.* Gynecol Obstet Invest, 1995. **40**(3): p. 151-7.

205. Keltz, M.D., et al., *Predictors of embryo fragmentation and outcome after fragment removal in in vitro fertilization.* Fertility and sterility, 2006. **86**(2): p. 321-4.

206. Eftekhari-Yazdi, P., et al., *Effect of fragment removal on blastocyst formation and quality of human embryos.* Reproductive biomedicine online, 2006. **13**(6): p. 823-32.

207. Crasta, K., et al., *DNA breaks and chromosome pulverization from errors in mitosis.* Nature, 2012. **482**(7383): p. 53-8.

208. Hoffelder, D.R., et al., *Resolution of anaphase bridges in cancer cells.* Chromosoma, 2004. **112**(8): p. 389-97.

209. Terradas, M., et al., *DNA lesions sequestered in micronuclei induce a local defective-damage response.* DNA repair, 2009. **8**(10): p. 1225-34.

210. Xu, B., et al., *Replication stress induces micronuclei comprising of aggregated DNA double-strand breaks.* PLoS One, 2011. **6**(4): p. e18618.

211. Stephens, P.J., et al., *Massive genomic rearrangement acquired in a single catastrophic event during cancer development.* Cell, 2011. **144**(1): p. 27-40.

212. Pellestor, F., et al., *Chromothripsis: potential origin in gametogenesis and preimplantation cell divisions. A review.* Fertility and sterility, 2014. **102**(6): p. 1785-96.

213. Pellestor, F., *Chromothripsis: how does such a catastrophic event impact human reproduction?* Human Reproduction, 2014. **29**(3): p. 388-93.

214. Loup, V., et al., *Combined FISH and PRINS sperm analysis of complex chromosome rearrangement t(1;19;13): an approach facilitating PGD.* Mol Hum Reprod, 2010. **16**(2): p. 111-6.

215. Kloosterman, W.P., et al., *Chromothripsis as a mechanism driving complex de novo structural rearrangements in the germline.* Hum Mol Genet, 2011. **20**(10): p. 1916-24.

216. Hatch, E.M., et al., *Catastrophic nuclear envelope collapse in cancer cell micronuclei.* Cell, 2013. **154**(1): p. 47-60.

217. Ford, J.H., C.J. Schultz, and A.T. Correll, *Chromosome elimination in micronuclei: a common cause of hypoploidy.* Am J Hum Genet, 1988. **43**(5): p. 733-40.

218. Norppa, H. and G.C. Falck, *What do human micronuclei contain?* Mutagenesis, 2003. **18**(3): p. 221-33.

219. Fenech, M., et al., *Molecular mechanisms of micronucleus, nucleoplasmic bridge and nuclear bud formation in mammalian and human cells.* Mutagenesis, 2011. **26**(1): p. 125-32.

220. Prados, F.J., et al., *The cleavage stage embryo.* Hum Reprod, 2012. **27 Suppl 1**: p. i50-71.

221. Chavez, S.L., et al., *Comparison of epigenetic mediator expression and function in mouse and human embryonic blastomeres.* Human molecular genetics, 2014. **23**(18): p. 4970-84.

222. Alikani, M.S., S.; Cohen, J., *Human Embryo Morphology and Developmental Capacity*, in *Assessment of Mammalian Embryo Quality*, M.B. Ann Van Soom, Editor. 2002, Springer Netherlands: Netherlands. p. 1-31.

223. Van Soom, A., et al., *Assessment of mammalian embryo quality: what can we learn from embryo morphology?* Reprod Biomed Online, 2003. **7**(6): p. 664-70.

224. Lindner, G.M. and R.W. Wright, Jr., *Bovine embryo morphology and evaluation.* Theriogenology, 1983. **20**(4): p. 407-16.

225. Calarco, P.G. and R.A. Pedersen, *Ultrastructural observations of lethal yellow (Ay/Ay) mouse embryos.* J Embryol Exp Morphol, 1976. **35**(1): p. 73-80.

226. Magli, M.C., et al., *Chromosome mosaicism in day 3 aneuploid embryos that develop to morphologically normal blastocysts in vitro.* Hum Reprod, 2000. **15**(8): p. 1781-6.

227. Thompson, S.L. and D.A. Compton, *Chromosome missegregation in human cells arises through specific types of kinetochore-microtubule attachment errors.* Proceedings of the National Academy of Sciences of the United States of America, 2011. **108**(44): p. 17974-8.

228. Huang, Y., et al., *Lagging chromosomes entrapped in micronuclei are not 'lost' by cells.* Cell research, 2012. **22**(5): p. 932-5.

229. Kalousek, D.K. and F.J. Dill, *Chromosomal mosaicism confined to the placenta in human conceptions.* Science, 1983. **221**(4611): p. 665-7.

230. Fragouli, E., et al., *Cytogenetic analysis of human blastocysts with the use of FISH, CGH and aCGH: scientific data and technical evaluation.* Human Reproduction, 2011. **26**(2): p. 480-90.

231. Liu, J., et al., *DNA microarray reveals that high proportions of human blastocysts from women of advanced maternal age are aneuploid and mosaic.* Biology of Reproduction, 2012. **87**(6): p. 148.

232. Fragouli, E., et al., *Comprehensive molecular cytogenetic analysis of the human blastocyst stage.* Human reproduction, 2008. **23**(11): p. 2596-608.

233. Evsikov, S. and Y. Verlinsky, *Mosaicism in the inner cell mass of human blastocysts.* Hum Reprod, 1998. **13**(11): p. 3151-5.

234. Mottla, G.L., et al., *Lineage tracing demonstrates that blastomeres of early cleavage-stage human pre-embryos contribute to both trophectoderm and inner cell mass.* Hum Reprod, 1995. **10**(2): p. 384-91.

235. Magli, M.C., et al., *Chromosome mosaicism in day 3 aneuploid embryos that develop to morphologically normal blastocysts in vitro.* Human reproduction, 2000. **15**(8): p. 1781-6.

236. Capalbo, A., et al., *FISH reanalysis of inner cell mass and trophectoderm samples of previously array-CGH screened blastocysts shows high accuracy of diagnosis and no major diagnostic impact of mosaicism at the blastocyst stage.* Human reproduction, 2013.

237. Johnson, D.S., et al., *Comprehensive analysis of karyotypic mosaicism between trophectoderm and inner cell mass.* Molecular human reproduction, 2010. **16**(12): p. 944-9.

238. Derhaag, J.G., et al., *Chromosomally abnormal cells are not selected for the extra-embryonic compartment of the human preimplantation embryo at the blastocyst stage.* Hum Reprod, 2003. **18**(12): p. 2565-74.

239. Kalousek, D.K. and M. Vekemans, *Confined placental mosaicism.* J Med Genet, 1996. **33**(7): p. 529-33.

240. Goldberg, J.D. and M.M. Wohlferd, *Incidence and outcome of chromosomal mosaicism found at the time of chorionic villus sampling.* Am J Obstet Gynecol, 1997. **176**(6): p. 1349-52; discussion 1352-3.

241. Phillips, O.P., et al., *Risk of fetal mosaicism when placental mosaicism is diagnosed by chorionic villus sampling.* Am J Obstet Gynecol, 1996. **174**(3): p. 850-5.

242. Ledbetter, D.H., et al., *Cytogenetic results from the U.S. Collaborative Study on CVS.* Prenat Diagn, 1992. **12**(5): p. 317-45.

243. Clouston, H.J., et al., *Detection of mosaic and non-mosaic chromosome abnormalities in 6- to 8-day old human blastocysts.* Hum Genet, 1997. **101**(1): p. 30-6.

244. Greco, E., M.G. Minasi, and F. Fiorentino, *Healthy Babies after Intrauterine Transfer of Mosaic Aneuploid Blastocysts.* N Engl J Med, 2015. **373**(21): p. 2089-90.

245. Fragouli, E., et al., *Analysis of implantation and ongoing pregnancy rates following the transfer of mosaic diploid-aneuploid blastocysts.* Hum Genet, 2017. **136**(7): p. 805-819.

246. Bond, D.C., A, in *Aneuploidy: The Origins and Causes of Aneuploidy in Experimental Organisms*. 1983, Oxford University Press: Oxford. p. 86-91.

247. Lee, E., et al., *The clinical effectiveness of preimplantation genetic diagnosis for aneuploidy in all 24 chromosomes (PGD-A): systematic review.* Hum Reprod, 2015. **30**(2): p. 473-83.

248. Battaglia, D.E., et al., *Influence of maternal age on meiotic spindle assembly in oocytes from naturally cycling women.* Hum Reprod, 1996. **11**(10): p. 2217-22.

249. Hassold, T. and P. Hunt, *To err (meiotically) is human: the genesis of human aneuploidy.* Nat Rev Genet, 2001. **2**(4): p. 280-91.

250. Stouffer, R.L. and M.B. Zelinski-Wooten, *Overriding follicle selection in controlled ovarian stimulation protocols: quality vs quantity.* Reprod Biol Endocrinol, 2004. **2**: p. 32.

251. Wolf, D.P., et al., *In vitro fertilization-embryo transfer in nonhuman primates: the technique and its applications.* Mol Reprod Dev, 1990. **27**(3): p. 261-80.

252. Lanzendorf, S.E., et al., *Collection and quality of rhesus monkey semen.* Mol Reprod Dev, 1990. **25**(1): p. 61-6.

253. Vitak, S.A., et al., *Sequencing thousands of single-cell genomes with combinatorial indexing.* Nat Methods, 2017.

254. Krueger, F., S.R. Andrews, and C.S. Osborne, *Large scale loss of data in low-diversity illumina sequencing libraries can be recovered by deferred cluster calling.* PLoS One, 2011. **6**(1): p. e16607.

255. Chen, C., et al., *Software for pre-processing Illumina next-generation sequencing short read sequences.* Source code for biology and medicine, 2014. **9**: p. 8.

256. Zimin, A.V., et al., *A new rhesus macaque assembly and annotation for next-generation sequencing analyses.* Biology direct, 2014. **9**(1): p. 20.

257. Salavert Torres, J., et al., *Using GPUs for the exact alignment of short-read genetic sequences by means of the Burrows-Wheeler transform.* IEEE/ACM transactions on computational biology and bioinformatics / IEEE, ACM, 2012. **9**(4): p. 1245-56.

258. Tarailo-Graovac, M. and N. Chen, *Using RepeatMasker to identify repetitive elements in genomic sequences.* Current protocols in bioinformatics / editoral board, Andreas D. Baxevanis ... [et al.], 2009. **Chapter 4**: p. Unit 4 10.

259. Ramirez-Gonzalez, R.H., et al., *Bio-samtools: Ruby bindings for SAMtools, a library for accessing BAM files containing high-throughput sequence alignments.* Source code for biology and medicine, 2012. **7**(1): p. 6.

260. Olshen, A.B., et al., *Circular binary segmentation for the analysis of array-based DNA copy number data.* Biostatistics, 2004. **5**(4): p. 557-72.

261. Knouse, K.A., J. Wu, and A. Amon, *Assessment of megabase-scale somatic copy number variation using single-cell sequencing.* Genome Res, 2016. **26**(3): p. 376-84.

262. Ventura, M., et al., *Evolutionary formation of new centromeres in macaque.* Science, 2007. **316**(5822): p. 243-6.

263. Van der Auwera, G.A., et al., *From FastQ data to high confidence variant calls: the Genome Analysis Toolkit best practices pipeline.* Curr Protoc Bioinformatics, 2013. **43**: p. 11 10 1-33.

264. McKenna, A., et al., *The Genome Analysis Toolkit: a MapReduce framework for analyzing next-generation DNA sequencing data.* Genome Res, 2010. **20**(9): p. 1297-303.

265. Bolger, A.M., M. Lohse, and B. Usadel, *Trimmomatic: a flexible trimmer for Illumina sequence data.* Bioinformatics, 2014. **30**(15): p. 2114-20.

266. Li, H. and R. Durbin, *Fast and accurate long-read alignment with Burrows-Wheeler transform.* Bioinformatics, 2010. **26**(5): p. 589-95.

267. Smit, A., R. Hubley, and P. Green, *RepeatMasker Open-4.0*. 2013-2015.

268. Nelson, E.K., et al., *LabKey Server: an open source platform for scientific data integration, analysis and collaboration.* BMC Bioinformatics, 2011. **12**: p. 71.

269. Ruiz-Herrera, A., *Chromosomal Rearrangements in Primates*, in *eLS*. 2001, John Wiley & Sons, Ltd.

270. Rogers, J., et al., *An initial genetic linkage map of the rhesus macaque (Macaca mulatta) genome using human microsatellite loci.* Genomics, 2006. **87**(1): p. 30-8.

271. Wienberg, J., et al., *Homologies in human and Macaca fuscata chromosomes revealed by in situ suppression hybridization with human chromosome specific DNA libraries.* Chromosoma, 1992. **101**(5-6): p. 265-70.

272. Schmerler, S. and G.M. Wessel, *Polar bodies--more a lack of understanding than a lack of respect.* Mol Reprod Dev, 2011. **78**(1): p. 3-8.

273. Rabinowitz, M., et al., *Origins and rates of aneuploidy in human blastomeres.* Fertil Steril, 2012. **97**(2): p. 395-401.

274. Battaglia, D.E., N.A. Klein, and M.R. Soules, *Changes in centrosomal domains during meiotic maturation in the human oocyte.* Mol Hum Reprod, 1996. **2**(11): p. 845-51.

275. Gisselsson, D., et al., *Generation of trisomies in cancer cells by multipolar mitosis and incomplete cytokinesis.* Proc Natl Acad Sci U S A, 2010. **107**(47): p. 20489-93.

276. Somigliana, E., et al., *Age-related infertility and unexplained infertility: an intricate clinical dilemma.* Hum Reprod, 2016. **31**(7): p. 1390-6.

277. Rowell, T.E., *Behaviour and Female Reproductive Cycles of Rhesus Macaques.* J Reprod Fertil, 1963. **6**: p. 193-203.

278. Flach, G., et al., *The transition from maternal to embryonic control in the 2-cell mouse embryo.* EMBO J, 1982. **1**(6): p. 681-6.

279. Schramm, R.D. and B.D. Bavister, *Onset of nucleolar and extranucleolar transcription and expression of fibrillarin in macaque embryos developing in vitro.* Biol Reprod, 1999. **60**(3): p. 721-8.

280. Alper, M.M., et al., *To blastocyst or not to blastocyst? That is the question.* Hum Reprod, 2001. **16**(4): p. 617-9.

281. Maxwell, S.M., et al., *Why do euploid embryos miscarry? A case-control study comparing the rate of aneuploidy within presumed euploid embryos that resulted in miscarriage or live birth using next-generation sequencing.* Fertil Steril, 2016. **106**(6): p. 1414-1419 e5.

282. Chamayou, S., et al., *The use of morphokinetic parameters to select all embryos with full capacity to implant.* J Assist Reprod Genet, 2013. **30**(5): p. 703-10.

283. Sathananthan, A.H., et al., *Centrioles in the beginning of human development.* Proc Natl Acad Sci U S A, 1991. **88**(11): p. 4806-10.

284. Schatten, G., C. Simerly, and H. Schatten, *Maternal inheritance of centrosomes in mammals? Studies on parthenogenesis and polyspermy in mice.* Proc Natl Acad Sci U S A, 1991. **88**(15): p. 6785-9.

285. Kalatova, B., et al., *Tripolar mitosis in human cells and embryos: occurrence, pathophysiology and medical implications.* Acta Histochem, 2015. **117**(1): p. 111-25.

286. Antczak, M. and J. Van Blerkom, *Temporal and spatial aspects of fragmentation in early human embryos: possible effects on developmental competence and association with the differential elimination of regulatory proteins from polarized domains.* Hum Reprod, 1999. **14**(2): p. 429-47.

287. Alikani, M., et al., *Human embryo fragmentation in vitro and its implications for pregnancy and implantation.* Fertil Steril, 1999. **71**(5): p. 836-42.

288. Hardy, K., et al., *From cell death to embryo arrest: mathematical models of human preimplantation embryo development.* Proc Natl Acad Sci U S A, 2001. **98**(4): p. 1655-60.

289. Xu, J., et al., *The incidence of cytoplasmic fragmentation in mouse embryos in vitro is not affected by inhibition of caspase activity.* Fertil Steril, 2001. **75**(5): p. 986-91.

290. Buster, J.E., et al., *Biologic and morphologic development of donated human ova recovered by nonsurgical uterine lavage.* Am J Obstet Gynecol, 1985. **153**(2): p. 211-7.

291. Pereda, J. and H.B. Croxatto, *Ultrastructure of a seven-cell human embryo.* Biol Reprod, 1978. **18**(3): p. 481-9.

292. Wu, D.H., et al., *Age does not influence the effect of embryo fragmentation on successful blastocyst development.* Fertil Steril, 2011. **95**(8): p. 2778-80.

293. Pelinck, M.J., et al., *Embryo quality and impact of specific embryo characteristics on ongoing implantation in unselected embryos derived from modified natural cycle in vitro fertilization.* Fertil Steril, 2010. **94**(2): p. 527-34.

294. Guerif, F., et al., *Limited value of morphological assessment at days 1 and 2 to predict blastocyst development potential: a prospective study based on 4042 embryos.* Hum Reprod, 2007. **22**(7): p. 1973-81.

295. Dozortsev, D., et al., *The impact of cellular fragmentation induced experimentally at different stages of mouse preimplantation development.* Hum Reprod, 1998. **13**(5): p. 1307-11.

296. Alikani, M., F. Olivennes, and J. Cohen, *Microsurgical correction of partially degenerate mouse embryos promotes hatching and restores their viability.* Hum Reprod, 1993. **8**(10): p. 1723-8.

297. Keltz, M.D., et al., *Predictors of embryo fragmentation and outcome after fragment removal in in vitro fertilization.* Fertil Steril, 2006. **86**(2): p. 321-4.

298. Hnida, C., E. Engenheiro, and S. Ziebe, *Computer-controlled, multilevel, morphometric analysis of blastomere size as biomarker of fragmentation and multinuclearity in human embryos.* Hum Reprod, 2004. **19**(2): p. 288-93.

299. Alikani, M., T. Schimmel, and S.M. Willadsen, *Cytoplasmic fragmentation in activated eggs occurs in the cytokinetic phase of the cell cycle, in lieu of normal cytokinesis, and in response to cytoskeletal disorder.* Mol Hum Reprod, 2005. **11**(5): p. 335-44.

300. Van Blerkom, J., P. Davis, and S. Alexander, *A microscopic and biochemical study of fragmentation phenotypes in stage-appropriate human embryos.* Hum Reprod, 2001. **16**(4): p. 719-29.

301. Hawes, S.M., Y. Gie Chung, and K.E. Latham, *Genetic and epigenetic factors affecting blastomere fragmentation in two-cell stage mouse embryos.* Biol Reprod, 2001. **65**(4): p. 1050-6.

302. Stubblefield, E. and M. Pershouse, *Direct formation of microcells from mitotic cells for use in chromosome transfer.* Somat Cell Mol Genet, 1992. **18**(6): p. 485-91.

303. Smith, G.F., M.A. Ridler, and J.A. Faunch, *Action of cytochalasin B on cultured human lymphocytes.* Nature, 1967. **216**(5120): p. 1134-5.

304. Mori, Y., et al., *Extrusion of nuclei of murine suspension culture cells with microtubule poisons.* Exp Cell Res, 1984. **153**(2): p. 574-80.

305. Wright, W.E. and L. Hayflick, *Formation of anucleate and multinucleate cells in normal and SV 40 transformed WI-38 by cytochalasin B.* Exp Cell Res, 1972. **74**(1): p. 187-94.

306. Fournier, R.E., *A general high-efficiency procedure for production of microcell hybrids.* Proc Natl Acad Sci U S A, 1981. **78**(10): p. 6349-53.

307. Li, R. and D.F. Albertini, *The road to maturation: somatic cell interaction and self-organization of the mammalian oocyte.* Nat Rev Mol Cell Biol, 2013. **14**(3): p. 141-52.

308. Sun, Q.Y. and H. Schatten, *Regulation of dynamic events by microfilaments during oocyte maturation and fertilization.* Reproduction, 2006. **131**(2): p. 193-205.

309. Longo, F.J. and D.Y. Chen, *Development of cortical polarity in mouse eggs: involvement of the meiotic apparatus.* Dev Biol, 1985. **107**(2): p. 382-94.

310. Pellestor, F., et al., *Direct assessment of the rate of chromosomal abnormalities in grade IV human embryos produced by in-vitro fertilization procedure.* Hum Reprod, 1994. **9**(2): p. 293-302.

311. Marquez, C., et al., *Chromosome abnormalities in 1255 cleavage-stage human embryos.* Reprod Biomed Online, 2000. **1**(1): p. 17-26.

312. Magli, M.C., L. Gianaroli, and A.P. Ferraretti, *Chromosomal abnormalities in embryos.* Mol Cell Endocrinol, 2001. **183 Suppl 1**: p. S29-34.

313. Zhang, C.Z., et al., *Chromothripsis from DNA damage in micronuclei.* Nature, 2015. **522**(7555): p. 179-84.

314. Hardarson, T., et al., *Internalization of cellular fragments in a human embryo: time-lapse recordings.* Reprod Biomed Online, 2002. **5**(1): p. 36-8.

315. Vazquez-Diez, C., et al., *Micronucleus formation causes perpetual unilateral chromosome inheritance in mouse embryos.* Proc Natl Acad Sci U S A, 2016. **113**(3): p. 626-31.

316. Winston, N.J. and M.H. Johnson, *Can the mouse embryo provide a good model for the study of abnormal cellular development seen in human embryos?* Hum Reprod, 1992. **7**(9): p. 1291-6.

317. Chavez, S.L., et al., *Comparison of epigenetic mediator expression and function in mouse and human embryonic blastomeres.* Hum Mol Genet, 2014. **23**(18): p. 4970-84.

318. Munne, S., et al., *Diagnosis of major chromosome aneuploidies in human preimplantation embryos.* Hum Reprod, 1993. **8**(12): p. 2185-91.

319. Gleicher, N., et al., *Accuracy of preimplantation genetic screening (PGS) is compromised by degree of mosaicism of human embryos.* Reprod Biol Endocrinol, 2016. **14**(1): p. 54.

320. Mackenzie, K.J., et al., *cGAS surveillance of micronuclei links genome instability to innate immunity.* Nature, 2017.

321. Santaguida, S., et al., *Chromosome Mis-segregation Generates Cell-Cycle-Arrested Cells with Complex Karyotypes that Are Eliminated by the Immune System.* Dev Cell, 2017. **41**(6): p. 638-651 e5.

322. Schindelin, J., et al., *Fiji: an open-source platform for biological-image analysis.* Nat Methods, 2012. **9**(7): p. 676-82.

323. Cimini, D., et al., *Merotelic kinetochore orientation versus chromosome mono-orientation in the origin of lagging chromosomes in human primary cells.* J Cell Sci, 2002. **115**(Pt 3): p. 507-15.

324. Cimini, D., et al., *Merotelic kinetochore orientation is a major mechanism of aneuploidy in mitotic mammalian tissue cells.* J Cell Biol, 2001. **153**(3): p. 517-27.

325. Rogakou, E.P., et al., *DNA double-stranded breaks induce histone H2AX phosphorylation on serine 139.* J Biol Chem, 1998. **273**(10): p. 5858-68.

326. Terradas, M., et al., *DNA lesions sequestered in micronuclei induce a local defective-damage response.* DNA Repair (Amst), 2009. **8**(10): p. 1225-34.

327. Gordon, D.J., B. Resio, and D. Pellman, *Causes and consequences of aneuploidy in cancer.* Nat Rev Genet, 2012. **13**(3): p. 189-203.

328. Coonen, E., et al., *Anaphase lagging mainly explains chromosomal mosaicism in human preimplantation embryos.* Hum Reprod, 2004. **19**(2): p. 316-24.

329. Racowsky, C., et al., *Standardization of grading embryo morphology.* Fertil Steril, 2010. **94**(3): p. 1152-3.

330. Luke, B., et al., *Using the Society for Assisted Reproductive Technology Clinic Outcome System morphological measures to predict live birth after assisted reproductive technology.* Fertil Steril, 2014. **102**(5): p. 1338-44.

331. Scott, R.T., Jr., et al., *Cleavage-stage biopsy significantly impairs human embryonic implantation potential while blastocyst biopsy does not: a randomized and paired clinical trial.* Fertil Steril, 2013. **100**(3): p. 624-30.

332. Chawla, M., et al., *Morphokinetic analysis of cleavage stage embryos and its relationship to aneuploidy in a retrospective time-lapse imaging study.* J Assist Reprod Genet, 2015. **32**(1): p. 69-75.

333. Sugimura, S., et al., *Time-lapse cinematography-compatible polystyrene-based microwell culture system: a novel tool for tracking the development of individual bovine embryos.* Biol Reprod, 2010. **83**(6): p. 970-8.

334. Sugimura, S., T. Akai, and K. Imai, *Selection of viable in vitro-fertilized bovine embryos using time-lapse monitoring in microwell culture dishes.* J Reprod Dev, 2017.

335. Weinerman, R., et al., *Morphokinetic Evaluation of Embryo Development in a Mouse Model: Functional and Molecular Correlates.* Biol Reprod, 2016. **94**(4): p. 84.

336. Burruel, V., et al., *Abnormal early cleavage events predict early embryo demise: sperm oxidative stress and early abnormal cleavage.* Sci Rep, 2014. **4**: p. 6598.

337. Diamond, M.P., et al., *Using the Eeva Test adjunctively to traditional day 3 morphology is informative for consistent embryo assessment within a panel of*

embryologists with diverse experience. J Assist Reprod Genet, 2015. **32**(1): p. 61-8.

338. Staessen, C., et al., *Preimplantation genetic screening does not improve delivery rate in women under the age of 36 following single-embryo transfer.* Human Reproduction, 2008. **23**(12): p. 2818-25.

339. Hardarson, T., et al., *Preimplantation genetic screening in women of advanced maternal age caused a decrease in clinical pregnancy rate: a randomized controlled trial.* Human Reproduction, 2008. **23**(12): p. 2806-12.

340. Scott, R.T., Jr., et al., *Blastocyst biopsy with comprehensive chromosome screening and fresh embryo transfer significantly increases in vitro fertilization implantation and delivery rates: a randomized controlled trial.* Fertil Steril, 2013. **100**(3): p. 697-703.

341. Scott, R.T., Jr., et al., *Comprehensive chromosome screening is highly predictive of the reproductive potential of human embryos: a prospective, blinded, nonselection study.* Fertil Steril, 2012. **97**(4): p. 870-5.

342. Schoolcraft, W.B., et al., *Live birth outcome with trophectoderm biopsy, blastocyst vitrification, and single-nucleotide polymorphism microarray-based comprehensive chromosome screening in infertile patients.* Fertil Steril, 2011. **96**(3): p. 638-40.

343. Gleicher, N., V.A. Kushnir, and D.H. Barad, *Preimplantation genetic screening (PGS) still in search of a clinical application: a systematic review.* Reprod Biol Endocrinol, 2014. **12**: p. 22.

344. Harton, G.L., et al., *Diminished effect of maternal age on implantation after preimplantation genetic diagnosis with array comparative genomic hybridization.* Fertil Steril, 2013. **100**(6): p. 1695-703.

345. Shapiro, B.S., et al., *Evidence of impaired endometrial receptivity after ovarian stimulation for in vitro fertilization: a prospective randomized trial comparing fresh and frozen-thawed embryo transfer in normal responders.* Fertil Steril, 2011. **96**(2): p. 344-8.

346. Haouzi, D., et al., *Gene expression profile of human endometrial receptivity: comparison between natural and stimulated cycles for the same patients.* Hum Reprod, 2009. **24**(6): p. 1436-45.

347. Balakier, H., et al., *Impact of multinucleated blastomeres on embryo developmental competence, morphokinetics, and aneuploidy.* Fertil Steril, 2016. **106**(3): p. 608-614 e2.

348. Shenfield, F., et al., *I. The moral status of the pre-implantation embryo.* Hum Reprod, 2001. **16**(5): p. 1046-8.

349. Ethics, E.T.F.o., et al., *ESHRE Task Force on Ethics and Law 12: oocyte donation for non-reproductive purposes.* Hum Reprod, 2007. **22**(5): p. 1210-3.

350. Tatham, B.G., et al., *Centrifugation of bovine oocytes for nuclear micromanipulation and sperm microinjection.* Hum Reprod, 1996. **11**(7): p. 1499-503.

351. Notter, D.R., *The importance of genetic diversity in livestock populations of the future.* J Anim Sci, 1999. **77**(1): p. 61-9.

352. Hawley, R.S., J.A. Frazier, and R. Rasooly, *Separation anxiety: the etiology of nondisjunction in flies and people.* Hum Mol Genet, 1994. **3**(9): p. 1521-8.

353. Wolstenholme, J. and R.R. Angell, *Maternal age and trisomy--a unifying mechanism of formation.* Chromosoma, 2000. **109**(7): p. 435-8.

354. Liu, L. and D.L. Keefe, *Defective cohesin is associated with age-dependent misaligned chromosomes in oocytes.* Reprod Biomed Online, 2008. **16**(1): p. 103-12.

355. Pan, H., et al., *Age-associated increase in aneuploidy and changes in gene expression in mouse eggs.* Dev Biol, 2008. **316**(2): p. 397-407.

356. Somfai, T., et al., *Relationship between the length of cell cycles, cleavage pattern and developmental competence in bovine embryos generated by in vitro fertilization or parthenogenesis.* J Reprod Dev, 2010. **56**(2): p. 200-7.

357. Chen, M., et al., *Does time-lapse imaging have favorable results for embryo incubation and selection compared with conventional methods in clinical in vitro fertilization? A meta-analysis and systematic review of randomized controlled trials.* PLoS One, 2017. **12**(6): p. e0178720.

358. Savage, P., et al., *Partial molar pregnancy after intracytoplasmic sperm injection occurring as a result of diploid sperm usage.* J Assist Reprod Genet, 2013. **30**(6): p. 761-4.

359. Hamanoue, H., et al., *Complete hydatidiform mole and normal live birth following intracytoplasmic sperm injection.* J Hum Genet, 2006. **51**(5): p. 477-9.

360. Yamada, M., et al., *Genetic Drift Can Compromise Mitochondrial Replacement by Nuclear Transfer in Human Oocytes.* Cell Stem Cell, 2016. **18**(6): p. 749-54.

361. Lukinavicius, G., et al., *SiR-Hoechst is a far-red DNA stain for live-cell nanoscopy.* Nat Commun, 2015. **6**: p. 8497.

362. Munne, S., et al., *Detailed investigation into the cytogenetic constitution and pregnancy outcome of replacing mosaic blastocysts detected with the use of high-resolution next-generation sequencing.* Fertil Steril, 2017. **108**(1): p. 62-71 e8.

363. Marin, D., R.T. Scott, Jr., and N.R. Treff, *Preimplantation embryonic mosaicism: origin, consequences and the reliability of comprehensive chromosome screening.* Curr Opin Obstet Gynecol, 2017. **29**(3): p. 168-174.

364. Capalbo, A., et al., *FISH reanalysis of inner cell mass and trophectoderm samples of previously array-CGH screened blastocysts shows high accuracy of diagnosis*

and no major diagnostic impact of mosaicism at the blastocyst stage. Hum Reprod, 2013. **28**(8): p. 2298-307.

365. Liu, J., et al., *DNA microarray reveals that high proportions of human blastocysts from women of advanced maternal age are aneuploid and mosaic.* Biol Reprod, 2012. **87**(6): p. 148.